THE UNIVERSITY OF CALGARY

TRANSMURAL PRESSURE-DIMENSION RELATIONSHIPS OF THE RIGHT ATRIUM AND VENTRICLE

by

Douglas Ross Hamilton

A THESIS

SUBMITTED TO THE FACULTY OF GRADUATE STUDIES

IN PARTIAL FULFILMENT OF THE REQUIREMENTS FOR

THE DEGREE OF DOCTOR OF PHILOSOPHY

DEPARTMENT OF MEDICAL SCIENCE

CALGARY, ALBERTA

JUNE 1991

© Douglas R. Hamilton

National Library of Canada
Bibliothèque nationale du Canada

Canadian Theses Service
Service des thèses canadiennes

Ottawa, Canada
K1A 0N4

The author has granted an irrevocable non-exclusive licence allowing the National Library of Canada to reproduce, loan, distribute or sell copies of his/her thesis by any means and in any form or format, making this thesis available to interested persons.

The author retains ownership of the copyright in his/her thesis. Neither the thesis nor substantial extracts from it may be printed or otherwise reproduced without his/her permission.

L'auteur a accordé une licence irrévocable et non exclusive permettant à la Bibliothèque nationale du Canada de reproduire, prêter, distribuer ou vendre des copies de sa thèse de quelque manière et sous quelque forme que ce soit pour mettre des exemplaires de cette thèse à la disposition des personnes intéressées.

L'auteur conserve la propriété du droit d'auteur qui protège sa thèse. Ni la thèse ni des extraits substantiels de celle-ci ne doivent être imprimés ou autrement reproduits sans son autorisation.

ISBN 0-315-71142-6

Canada

THE UNIVERSITY OF CALGARY

FACULTY OF GRADUATE STUDIES

The undersigned certify that they have read, and recommend to the Faculty of Graduate Studies for acceptance, a thesis entitled "Transmural Pressure-Dimension Relationships of the Right Atrium and Ventricle" by Douglas R. Hamilton in partial fulfilment of the requirements for the degree of Doctor of Philosophy.

Supervisor
Doctor J.V. Tyberg
Medicine and Medical
Physiology

Doctor H.E.D.J. ter Keurs
Medicine and Medical
Physiology

Doctor W. A. Whitelaw
Medicine

Doctor B. M. Nigg
Physical Education

Doctor J. W. Covell
External Examiner
University of California, San Diego

June 24,1991

Abstract

Although it is generally agreed that ventricular transmural pressure is the best clinical indicator of cardiac preload, this appreciation has been compromised by the confusion in the literature as to the magnitude and method of measurement of pericardial constraint. The topics covered in this dissertation have one common theme, 'pericardial constraint of the heart'.

Chapter 1 is a historical perspective on the understanding of pericardial physiology. Chapter 2 defines some of the nomenclature and concepts of pericardial constraint used in following chapters. The dynamic response of the pericardial balloon used in the CVR labs of the University of Calgary was found to be limited only by the 2nd order frequency response of the catheters used to connect it to an external strain-gauge pressure transducer. The CVR balloon integrates loads, not homogenously distributed over its active surface area, giving the equivalent mean stress. The CVR high-fidelity pericardial balloon has frequency response characteristics which are superior to the standard CVR pericardial balloon and this new technology will allow the physiologist to measure systolic transmural pressure with an intact pericardium with a bandwidth of 200 Hz.

Chapter 3 uses the concepts of Chapter 2 to measure the transmural pressure of the right side of the heart. Chapter 3 determines the transmural pressure-dimension relationship of the right atrium (RA) and right ventricle (RV)

before and after pericardiectomy in six open-chest dogs. RA and RV transmural pressure was also measured on humans undergoing coronary artery bypass surgery. Results indicate that diastolic pericardial constraint accounts for: [1] 95% of the RA cavitary pressure in the dog and 89% in humans and [2] 85% of the RV cavitary pressure in the dog and 78% in humans. Chapter 4 uses the pericardial balloon to measure pericardial pressure over the right atrium and ventricle during the whole cardiac cycle. Results suggests that the relation of the pericardium to the RA must allow effective constraint in systole even though the RV pericardium is momentarily slack. Chapter 5 also exploits the advances in the CVR high-fidelity pericardial balloon technology which permits the measurement of pericardial pressure over the whole cardiac cycle. To determine the work performed on the RV free-wall by the pericardium, 6 open-chest dogs were instrumented with a high-fidelity pericardial balloon over the RV free wall. Results suggest that the LV "contributes" to RV performance, via a pericardial mechanism. In conclusion, the pericardium contributes from 1/6 to 1/5 of the total work being imparted to the blood by the RV free-wall under normal physiological conditions. Chapter 6 describes the measurement of pericardial pressure over the RV and LV of humans. Results from the six patients confirm a linear relationship between right and left pericardial pressure (slope = 0.968, intercept = -0.436 and correlation coefficient = 0.996) over a range of CVP from 2 to 18 mm Hg.

Acknowledgements

I find myself writing this part of my thesis last... only a couple of hours before it is due. It is difficult to describe the emotions I feel at this time because the last one and a half decades has seen me accomplish a number of things I never dreamed I would or could do.

In the late 1970's, during my first few years of university education in engineering, I was informally exposed to the life sciences by some of my friends who attended medical school. After spending many hours perusing their medical textbooks, I discovered physiology to be an area of science that I could no longer ignore. Accordingly, with a lot of fast talking, I managed to convince the head of the Department of Physiology to allow a 3rd year electrical engineer, who did not even have grade 10 biology under his belt, to enrol in Medicine 411, a physiology course taught to 1st year medical students. The reader need not be surprised to learn that the computer marking my final exam did not spend much time to accomplish the task (a problem which has followed me since grade one), but considering that I didn't know what a living cell was when I started the course, a marginal passing grade seemed to satisfy me nonetheless. I obtained my bachelors degree in electrical engineering May 1980 and completed my bio-medical research designing surgical laser systems for my masters degree in electrical engineering in May 1983 (my thesis was completed 1 year later ... a couple of

hours before the deadline).

I found myself on May 7, 1983, in a room attending Dr. John Tyberg, Dr. Eldon Smith, and Dr. Wayne Giles in an interview for a job to install and manage a network of mainframe computers for the Cardiovascular Research Group. These three gentlemen, for reasons yet to be made available to me, reached the conclusion that I was up to the task and hired me one week later. My previous experiences in medical research had left me with the impression that the medical community regarded engineers as people that had to be tolerated and not respected. That one week in my life in May 1983 was one of mixed emotion, as I toiled over whether I should take the job or not. I owe much of where I am now to these three gentlemen. They helped me make the right decision.

John Tyberg, in his very own patient and quiet manner, taught me how to 'slow down' and 'organize my thoughts', mind you, he still hasn't taught me to speell. He is always very composed in the face of adversity and is never at a loss to produce, from memory, a famous or infamous quote which is always appropriate for the occasion. I initially found John sometimes difficult to communicate with, probably due to my boisterous manner. He once told me that I was a bull that carried my own china shop around with me. I now find that I can discuss almost anything with him:

> "Friendship is the inexpressible comfort of being with someone, having not to weigh thoughts nor measure words."
>
> George Eliot.

Dr. Eldon Smith has always been supportive of my academic and professional ambitions. The fact that he wrote letters of reference, to several medical schools, across the nation, on my behalf for four years, is testimony to that fact.

Dr. Wayne Giles has taught me more about politics and procedure than a lifetime in parliament could possibly provide. Wayne, never once second guessed my judgement when I asked for an extra whats-it or thing-a-ma-bob. He blindly gave me his trust and I always worked hard to make sure he would not regret giving it.

Dr. Henk ter Keurs was a positive influence on my decision to apply for medical school. I was inviting myself to entertain the thought that there was no place in medicine for engineers. Henk showed me, through his sophisticated technical knowledge of instrumentation, that I was wrong.

Gerry Groves holds a special place in my heart as person who would unselfishly give 110% of his time and ask for nothing in return. I cannot begin to imagine a way of repaying this debt. He has always being supportive in my times of need and an honest and objective source of criticism when occasions required it. Gerry always assumes goodness in anybody he meets, and his friendly nature brings out the best in everyone who is fortunate to make his acquaintance.

Cheryl Pawlak's surgical expertise and patience with the 'Hami

protocols' contributed greatly to their success. I will continue to purchase 'lemons' so that she may never be without a 'Hami car story' for her friends and teammates.

Dr. Nairne Scott-Douglas has proven to be a steady supporter of my research in the lab and I respect his valued advice and opinion. It is a curious twist of fate that we both obtained our PhD in the same lab, went to the same medical school, and now will participate in the same residency program in Internal Medicine. Narine has taught me that some aspects of life need not be tackled and tamed, but rather the natural ebb and flow of destiny can be changed in more subtle ways. I have a feeling that the currents of chance that provided the opportunity for us to meet, will also make us lifelong friends.

Dale Bergman was hired directly out of university, during my earlier years of employment, to help me with instrumentation and computing commitments with the Cardiovascular Research Group. He quickly proved to be capable of learning faster than I could teach and has accelerated past me in the technical knowledge of computers and computing. He has always been a person I could drink several beers and talk 'kbaud' with, and never be wanting for parity.

Dr. Rosa Dani is a person whose patience I have tested numerous times and she has never complained once. I am truly amazed by her industry and sense of duty. Rosa helped me analyze the majority of the 900 megabytes of analyzed data generated for this dissertation and I am truly

grateful for her contributions.

I would also like to thank Dr. William Whitelaw and Dr. Benno Nigg for their valued contributions and criticisms during my candidacy and Dr. James Covell for agreeing to being a member of my doctorate thesis defense committee.

There are a number of people I wish to acknowledge for the time they have spent 'bashing ideas about' with me. They are Dr. Israel Belenkie, Dr. Peter Backx, Gwyneth de Vries, Dr. Hank Duff, Dr. Chris Eagle, Dr. Gabrielle Horne, Dr. Teri Keiser, Dr. Greg Powell, Keith Robinson, Dr. Roy Semlacher, Terry Shaw, Gregory Smith, Dr. James Stone, Dr. Mouhieddin Traboulsi, Dr. Peter de Tombe, Dr. Yu-Di Wang and Dr. Peter Wilkes.

Finally, I would like to thank my family. My father for impressing upon me at an early age the importance of education. My success in Engineering and Medicine is partly due to the his teaching me, at an early age, to always think 'What if...'. I think the only person who really appreciated my scientific bent as a child was my mother. She put up with numerous species of pets, which were often found in places in the house they shouldn't have been. My brothers, Waldo (James), Orb (Robert) and Pooh (Patrick), have been very supportive of my decision to make medicine part of my life and I thank them for being so.

I would also like to thank my Aunty Lou, who gave me my first medical textbook.... Reader's Digest.

And finally, I would like to thank my wife, Kathy, who has tolerated my crazy schedule and the upside-down lifestyle it has created. There are very few people in this world who could live with someone who goes to medical school, gets a PhD and builds aircraft production equipment for the Boeing Corporation at the same time. I hope, now that all these commitments are completed, I can reciprocate, and let her aspire toward those things in life she sacrificed to allow me to pursue these endeavors.

Dedication

This thesis is dedicated to:

Dr. Robert Jarvik,

.....a man of vision

and to

Dr. Barney Clark
Mr. William Schroeder
Mr. Murray Haydon
Mr. Jack Burcham
Mr. Leif Stenberg

..... men of courage.

TABLE OF CONTENTS

APPROVAL PAGE ii

ABSTRACT iii

ACKNOWLEDGEMENTS v

DEDICATION xi

TABLE OF CONTENTS xii

LIST OF TABLES xv

LIST OF FIGURES xvi

CHAPTER I

Historical Perspective Of Pericardial Physiology 1

CHAPTER II

Measurement Of Epicardial Radial Stress

Introduction 8
Calibration of the CVR Balloon 18
Unstressed Volume Determination of the CVR Balloon 19
CVR Balloon Static Linearity Using the CVR Calibrator 20
The Effect of Non-Uniform Loads on the CVR Balloon 23
Dynamic Response of the CVR Pericardial Balloon 24
The CVR High-Fidelity Pericardial Balloon 27
Conclusions 29
Figures 30

CHAPTER III

Right Atrial And Right Ventricular Transmural Pressure In The Human And Transmural Pressure-Dimension Relationships In The Dog: Effects Of The Pericardium

Introduction 55
Rationale 57

Methods - Animal 58
Methods - Human 61
Data Analysis - Animal Studies 65
Data Analysis - Human Studies 70
Results - Animal Studies 71
Results - Human Studies 73
Discussions 74
Conclusions 79
Tables 81
Figures 91

CHAPTER IV

High Fidelity Measurement Of Right Atrial And Ventricular Pericardial Pressure Over The Whole Cardiac Cycle

Introduction 113
Rationale 114
Methods 115
Protocol 117
Data Analysis 118
Results 118
Conclusions 122
Figures 123

CHAPTER V

Positive Work Is Transmitted On Segments Of The Right Ventricle Via The Overlying Pericardium In Dogs

Introduction 135
Rationale 137
Methods 137
Protocol 140
Data Analysis 140
Results 141
Conclusions 146
Tables 147
Figures 149

CHAPTER VI

An Intra-Operative Study Of The Relationship Between Left and Right Pericardial Pressures

Introduction 155
Methods 157
Data Analysis 160
Results 161
Conclusions 162
Tables 163
Figures 165

CONCLUSIONS 173

BIBLIOGRAPHY 179

LIST OF TABLES

Table 3.1 81
Patient Data

Table 3.2 82
Change in Percent Strain After Pericardietomy

Table 3.3 83
Change in Cavitary Pressure Figure 3 After Pericardiectomy

Table 3.4 84
Linear Regression Coeffients for Human RV Data

Table 3.5 85
Pressures at CVP=5,10 and 15 mm Hg.

Table 3.6 86
Pressure Intercepts Using Various Regression Techniques

Table 3.7 88
3-Parameter Exponential Equation

Table 3.8 89
Logarithmic Equation

Table 3.9 90
Cubic Equation

Table 5.1 147
Work Performed by Pericardium and Myocardium

Table 5.2 148
Ratio of Pericardial to Cavitary Work at Various Mean Right Atrial Pressures

Table 6.1 163
Patient Data

Table 6.2 164
Regression Coefficents of Pprv vs Pplv

LIST OF FIGURES

Figure 2.1 30
Stresses on the Pericardium

Figure 2.2 31
Effect of Changes in Balloon Height to Reference Height

Figure 2.3 32
Comparision of the Transmural Pressures Calculated Using Air-Filled and Liquid-Filled Balloons

Figure 2.4 33
The CVR Pericardial Balloon

Figure 2.5 34
Mould used to make the CVR Pericardial Balloon

Figure 2.6 35
Laplacian Pressure on a Curved Surface

Figure 2.7 36
Determination of Unstressed Volume of the CVR Balloon

Figure 2.8 37
Typical CVR Balloon Operating Room Calibration Curve

Figure 2.9 38
Calibrator Chamber Pressure vs Pericardial Ballon Pressure

Figure 2.10 39
Stresses Delivered to a Balloon Using a Thin Membrane

Figure 2.11 40
Non-Uniform Loading Characteristics of the CVR Balloon

Figure 2.12 41
CVR Balloon Non-Uniform Loading Characteristics

Figure 2.13 42
Frequency Response of a 100 cm. 7F Catheter

Figure 2.14 43
Frequency Response of a Standard CVR Balloon

Figure 2.15 44
Phase Response of Standard CVR Balloon

Figure 2.16 45
Frequency Response of High-Fidelity CVR Balloon

Figure 2.17 46
Sweeped Frequency Response of the High Fidelity Balloon

Figure 2.18 47
Comparision of the Standard CVR Pericardial Balloon to the High Fidelity CVR Balloon in the Calculation of Transmural Pressure

Figure 2.19 48
Comparision of the Standard CVR Pericardial Balloon to the High Fidelity CVR Balloon in the Pericardial Space With Catheter Motion-Induced Artifacts

Figure 2.20 49
Transmural Pressure Dimension-Loop of the Left Ventricular During an Inferior Vena Cava Occlusion Using a CVR High-Fidelity Pericardial Balloon

Figure 2.21 50
High Gain Plot of a Transmural Pressure-Dimension Loop During Inferior Vena Cava Occlusion Using a CVR High-Fidelity Pericardial Balloon

Figure 2.22 51
CVR Static Balloon Calibrator-Drawing #1

Figure 2.23 52
CVR Static Balloon Calibrator-Drawing #2

Figure 2.24 53
CVR Static Balloon Calibrator-Drawing #3

Figure 2.25 54
CVR Dynamic Balloon Calibrator

Figure 3.1 91
RV and RA Pressure vs Dimension Data and Percent Strain For Dog 1

Figure 3.2 92
RV and RA Pressure vs Percent Strain For Dog 1

Figure 3.3 93
RV and RA Pressure vs Percent Strain for Dog 2

Figure 3.4 94
RV and RA Pressure vs Percent Stain For Dog 3

Figure 3.5 95
RV and RA Pressure vs Percent Strain For Dog 4

Figure 3.6 96
RV and RA Pressure vs Percent Strain For Dog 5

Figure 3.7 97
RV and RA Pressure vs Percent Strain For Dog 6

Figure 3.8 98
A Schematic Representation of the Estimation of Cavitary Strain Increase Following Percardiectomy

Figure 3.9 99
Increase in Strain Calculated at Intracavitary Pressures of 5,10,and 15 mm Hg for Individual Dogs

Figure 3.10 100
A Schematic Representation of the Calculation of the Decrease in Intracavitary Pressure upon Pericardiectomy Measured at the same Strain

Figure 3.11 101
RV Cavitary Pressure vs RV Pericardial Pressure With a Balloon

Figure 3.12 102
RA Intracavitary Pressure vs RA Pericardial Pressure Measured with a Balloon

Figure 3.13 103
Plot of Pooled Data for all Dogs of RV and RA Transmural Pressure vs Percent Strain

Figure 3.14 104
Plot of Pooled Data for all Dogs of RV and RA Transmural Pressure vs Percent Strain

Figure 3.15 105
Plot of Pooled Data for Six Patients of RA Transmural and RA Pericardial Pressure vs CVP

Figure 3.16 106
The Raw Data and Linear Regression for Patients 1 to 4 With RV End-Diastolic Pressure, RV Pericardial Pressure, and RV Transmural Pressure

Figure 3.17 107
The Raw Data and Linear Regression for Patients 5 to 7 with RV End-Diastolic Pressure, RV Pericardial Pressure and RV Transmural Pressure

Figure 3.18 108
Time-Domain Plot of RV Cavitary Pressure, Central Venous Pressure, RA Pericardial Pressure, Calculated RA Transmural Pressure and the EKG for Temporal Reference

Figure 3.19 109
Cubic and Exponential Regression Curves for the RV.

Figure 3.20 110
Cubic and Exponential Regression Curves for the RA.

Figure 3.21 111
Examples of Regression Equations Which Vastly Differ

Figure 3.22 112
Logarithmic Regression Curves for the RA and RV

Figure 4.1 123
Time Domain Plot Showing Diastolic and Systolic Delineators

Figure 4.2 124
Time Domain Plot of RA Cavitary Pressure, RV Cavitary Pressure, RA Pericardial Pressure, RV Pericardial Pressure, RV Free Wall Segment Length, and RA Appendage Dimension

Figure 4.3 125
Dog 1 RA Pericardial Pressure vs RV Pericardial Pressure

Figure 4.4 126
Dog 2 RA Pericardial Pressure vs RV Pericardial Pressure

Figure 4.5 127
Dog 3 RA Pericardial Pressure vs RV Pericardial Pressure

Figure 4.6 128
Dog 4 RA Pericardial Pressure vs RV Pericardial Pressure

Figure 4.7 129
Dog 5 RA Pericardial Pressure vs RV Pericardial Pressure

Figure 4.8 130
Dog 1 Time-Domain Plot

Figure 4.9 131
Dog 3 Time-Domain Plot

Figure 4.10 132
Maximum A-V Regional Difference vs Pra

Figure 4.11 133
Dog 3 Maximum Regional Difference vs Pra

Figure 4.12 134
Change in Pericardial Pressure vs RA Cavitary Pressure

Figure 5.1 149
RV Pressure-Dimension Loop for Dog 5

Figure 5.2 150
Time Domain Plot of Pressures and Dimension in Figure 5.1

Figure 5.3 151
Pressure-Dimension Loops for an Infarcted Right Ventricle

Figure 5.4 152
Time-Domain Plot of Pressures and Dimension for Figure 5.3

Figure 5.5 153
Right Atrial Pressure-Dimension Relationships

Figure 5.6 154
Atrial Transmural Pressure-Dimension Loop

Figure 6.1 165
Pprv vs Pplv for Patient #1

Figure 6.2 166
Pprv vs Pplv for Patient #2

Figure 6.3 167
Pprv vs Pplv for Patient #3

Figure 6.4 168
Pprv vs Pplv for Patient #4

Figure 6.5 169
Pprv vs Pplv for Patient #5

Figure 6.6 170
Pprv vs Pplv for Patient #6

Figure 6.7 171
Pprv vs Pplv Pooled Data of All Patients

Figure 6.8 172
Pplv vs Prv Pooled Data of All Patients

Chapter 1

Historical Perspective of Pericardial Physiology

The function of the pericardium has been a topic of debate since antiquity. The anatomical significance of the pericardium was revealed to the ancients through animal and human sacrifices and battlefield observations.

> "The Bible (Deuteronomy 10:16; Jeremiah 4:4) admonishes the evil people among the Israelites to 'circumcise the foreskin of the heart'. The Dead Sea Scrolls (circa 1 AD) describe the Wicked Priest as one who 'did not circumcise the foreskin of the heart ' (Habbakuk 2:16)."(1)

Hippocrates noted that the normal pericardium "is a smooth mantle surrounding the heart and containing a small amount of urine."(1). Much was learned from the battlefield. Galen noted that the pericardium could protect the heart and that pericardial wounds could be lethal and that a patient could die later. The fact that such a traumatized patient was found to "be of sound mind which is testimony that the heart is not the seat of the mind".(1) According to Galen the vascular bed consisted of the arterial system, including the left heart, which carried "vital spirits" to the organs, and the hepato-venous system which formed blood out of ingested food and the veins transported it to the periphery. Both system were connected by pores in the septum of the heart. This concept was strongly accepted until the seventeenth century.

Aristotle's conception that the heart was the "central abode of life and

the soul", made many physicians reluctant to approach it during the Middle Ages. After the Middle Ages dissections and vivisection became widespread in the interests of medicine and science. Initially, these non-Galenic and non-Aristotelian approaches to medicine were considered heretical. Vesalius described the normal anatomy of the pericardium:

> " The entire heart is covered with a certain membranous involucrum, to which it is joint at no point. This involucrum is much more ample than the heart and is moistened by an aqueous humour. (1)"

William Harvey presented his revolutionary doctrine on the circulation of the blood during the seventeenth century, which was an enlightening period in the area of hemodynamic physiology. Robert Boyle, a famous chemist in that century, asked Harvey, "What were the things that had induc'd him to think of a Circulation of the Blood?", Boyle was quoted as to Harvey's reply:

> "He answer'd me, that when he took notice that the Valves in the Veins of so many several parts of the Body, were so plac'd that they gave free passage to the Blood Towards the Heart, but oppos'd the passage of the Venal Blood the Contrary way: He was to imagine, that so Provident as a Cause as Nature had not so Plac'd so many Valves without Design: and no Design seem'd more probable, than That, since the Blood could not well, because of the interposing, Valves, be Sent by the Veins, to the Limbs; it should be Sent through the Arteries, and Return through the Veins, whose Valves did not oppose its course that way. "(2)

Harvey was quoted to say the following about the pericardium upon reading Chapter 19, verse 34 of the Gospel of St. John in which he read that when Christ's side was pierced on the Cross by the Centurion's lance "came thereout blood and water":

> I think it to have been made by nature to prevent the heart from becoming completely dry. So the wounds of Christ exuded water along with blood."(3)

One of the most significant physiological observations regarding the pericardium during the seventeenth century was by Richard Lower who noted the following about cardiac tamponade and constrictive pericarditis:

> "With regard to this, the covering of the heart, let it be said, it cannot have its function described by one term, for it serves to keep the heart moist to protect it from injuries;... when too much water accumulates in it, injury of the heart results and when such (i.e. fluid) is lacking, it adheres closely to the heart, even on all side of it; since it is also attached to the diaphragm it is inevitable that the motion of the heart is combined and united with it... this must be regarded as a great impediment and inconvenience... Just as the heart labours when affected by disease within, so it does when oppressed from without by disease of its covering. So it happens that when that same covering of the heart is filled with an effusion and the walls are compressed with water on every side, so that they cannot dilate to receive blood; then truly the pulse diminishes until at length it is suppressed by even more water, when syncope, and death itself follows. Just as the accumulation of too much water harms the heart, so too does trouble come when the heart and the pericardium become everywhere adherent." (1).

A number of clinical observations regarding the anatomy of pericardial disease were made by Giovanni Morgagni in the eighteenth century, recognizing the importance of the rate of filling in cases of traumatic hemopericardium and therefore advocated the use of pericardiocentesis (3).

The nineteenth century saw further investigation in the clinical aspects of pericardial pathology by Jean Nicholas Corvisart, Napoleon's favourite physician, who distinguished the various forms of pericarditis and differentiated them from pericardial effusions (3). This century also saw the development of

instrumentation necessary to make more complex physiological measurements. Carl von Ludwig invented the kymograph, the first serviceable apparatus to measure blood pressure, the blood flowmeter and the plethysmograph. This enabled him to be the first to record the movement of an isolated heart, perfused with an artificial nutrient fluid (2). Adolf Fick devoted thirty years toward the understanding of the physiology of muscular contraction. He demonstrated the relationships between fibre length and the strength of contraction. His simple principle; the total oxygen absorbed per minute, divided by the uptake of oxygen into the blood per minute, (i.e. the arterio-venous oxygen difference) gives the total blood flow through the lungs is the basis for all presently used dilution techniques used to measure cardiac output. The late nineteenth century saw the work of Otto Frank who published a paper on "The dynamics of the heart muscle". Limitations in the mercury manometer, invented by von Ludwig, caused Frank to invent the spring manometer and volume recorder. These inventions allowed him to produce the first pressure-volume diagram of the heart. He postulated that the inotropic effect of any agent should be revealed by the shift of the curve of isometric maxima to higher or lower pressure. He was able to predict the stroke volume at various diastolic cavitary pressures at fixed afterloads. This was later confirmed in warm blooded animal by Ernest Starling who went one step further and correlated this with cavitary dimension and volume.

The late nineteenth and early twentieth century saw the realization that

the pericardium affects the preload of the heart and that its constraining effect might be significant in normal and pathological states. Simple anatomical observations regarding the right side of the heart and the nature of the pericardium were made by Barnard (4), who performed simple experiments on cat pericardium to illustrate its non-distensible and constraining nature on the heart in diastole. Kuno also demonstrated that the pericardium served a protective role in limiting the dilatation of the heart and that removing it could increase cardiac output and arterial pressure. The work of Starling and Frank made it readily apparent that preload was a very important parameter in cardiac dynamics and the constraining effects of the pericardium could not be ignored. In order to apply the Frank-Starling Law in the anlysis of pericardial performance, one must calculate the transmural pressure and, therefore, measure the pericardial "pressure". In 1955 Katz (5) wrote:

> "Even the use of end-diastolic pressure as an index of end-diastolic volume is not justified ..... Furthermore, if the expansion of the heart is limited, for example by the pericardium, changes in end-diastolic pressure lose much of their meaning in terms of change of end-diastolic volume."(5)

Kenner and Wood (6), in 1966, used liquid-filled catheters to measure pericardial constraint during occlusions of the pulmonary artery. They found that the increases in right atrial pressure are not followed by increases in pericardial pressure. In our view, these physiological conclusions were erroneously arrived at because inappropriate measuring techniques were used. The data obtained from the use of flat balloons in the pericardial space

by Holt et al (7) were compromised due to the correction of the balloon data so that it measured the same as open-end catheters. Morgan et al (8), in 1965, used flat balloons in the pleural space and a modified "pericardial catheter" which under some circumstances would emulate the behaviour of a flat balloon. As time progressed the use of flat flexible balloons became more common in the literature, however, Spodick (9), in 1983, published several statements which compelled the author to make pericardial constraint the focus of this dissertation:

1.) the pericardium is "a fluid-filled chamber at slightly subatmospheric pressure".

2.) "At normal cavitary pressures, pericardial transmural pressure is 0, because pericardial pressure is almost equal to and varies with pleural pressure"

3.) "the normally negative pericardial pressure produces a distending pressure that is higher than intracavitary pressure"

Misconceptions such as these about the magnitude of pericardial constraint have been responsible for the publication of papers of such widely varying and inconsistent understanding of the physiology of ventricular preload that the medical community has been reticent to accept anybody's pericardial data as valid. Experimental attempts to quantify the constraining effects of the pericardium on the heart may also have been ignored by the medical community because pericardial pressure is an entity which cannot not be easily determined at the bedside.

The study of pericardial mechanics in the CVR lab at the University of Calgary began as a search to understand the apparent changes in left ventricular compliance mediated by vasodilating drugs. Presently, the CVR lab has expanded its research to include myocardial function, arterial, venous and splanchnic vascular mechanics, and heart-lung interaction.

This dissertation is written to help settle the controversy regarding end-diastolic pericardial pressure and its role in determining the preload of the heart. The author hopes that the advances in pericardial constraint measuring techniques, documented in this thesis, will increase the medical community's understanding of the pericardium.

Chapter 2

Measurement of Epicardial Radial Stress

Introduction

It is the author's hypothesis that designing a high fidelity ,flat ,flexible balloon will open up new horizons in biological stress measurement. The pericardial balloon currently being used in the Cardiovascular Research (CVR) Labs at the University of Calgary has been a valuable tool in revealing many important fundamental aspects of cardiac physiology; in particular of ventricular preload and diastolic function. Recent advances in the design of this flat flexible stress transducer have enabled the author to investigate the systolic aspects of pericardial constraint. This chapter is written to acquaint the reader with presently used epicardial radial stress measuring techniques and the characteristics of the new CVR high-fidelity pericardial balloon. Throughout this document epicardial radial stress may also be referred to as "pericardial pressure". The reasons for this will become clear upon reading this chapter.

The heart is surrounded by a thin fibro-collagenous sac called the pericardium which over a short period of time may be considered to be a non-yielding entity (10,7) when stressed. This mean that small changes in pericardial volume will create large changes in pericardial pressure when the

pericardial volume is greater than its unstressed volume. Scalar terms such as "pressure" have been used to describe the stresses the pericardium imposes upon the epicardial surface. If one considers the tangential stress (shear stress) at the surface of these two structures to be negligible, then the resultant radial stress might be considered to be scalar in nature since the total vector stress will be normal to both surfaces, emulating fluid behaviour over small elemental areas (Figure 2.1). The same situation can exist if sufficient fluid is present in the pericardial space such that the epicardium and pericardium are separated hydrostatically. Under these circumstances the measurement of the hydrostatic pressure through the use of an open lumen catheter system requires that the thickness of the fluid layer be large and/or the catheter small enough to maintain an undisturbed system of stresses. It has been shown that open ended catheters do not accurately measure the radial stress being imposed on the epicardium by the pericardium unless an adequate volume of pericardial fluid is present (11) and the amount of pericardial fluid required for this may not always be physiological. The accurate measurement of cavitary pressure (endocardial radial stress) and pericardial pressure (epicardial radial stress) is essential for the calculation of transmural pressure (transmural radial stress). The measurement of cavitary pressure is easily obtained using the transcutaneous insertion technique of open-ended or micro strain-gauge tipped cardiac catheters. However, the accurate measurement of the magnitude and direction of the stresses being transferred between two opposing, readily

deformable serous membranes, such as those found in the pericardial space, is complicated by the physical disturbance created on these tissues by present transducer technology (12). The creation of a void to accommodate the introduction of a transducer, between what was previously two contiguous surfaces, may cause deformations which would re-distribute elastic forces in a manner such that those stresses being experienced by the transducer are not the same as those which existed before its introduction (12). An open ended catheter may create a potential space such that the catheter itself is responsible for the transmission of stress between two surfaces and the fluid pressure in the surrounding area is only that which is required to fill the void created by the catheter. The use of a fluid-filled thin flat balloon ensures that the transmission of stress between the two deformable surfaces can only be accomplished if the medium in the balloon is also stressed. This assumes that the inside surfaces of the flat balloon are adequately separated by a medium capable of transmitting hydrostatic pressure (air, water, oil, etc..) to its external lumen. Convenient methods used to verify the accuracy of these balloons used for the purposes of measuring pericardial pressure have usually involved the comparison of cavitary pressure-volume relationships before and after pericardiectomy.

Many researchers have attempted to measure the normal stresses transferred between two opposing serous tissues, such as the lung or pericardium, by introducing a fluid layer between them and then measuring the

pressure developed in the fluid. The liquid, once injected, may not always remain static and may not necessarily keep the two opposing surfaces completely separated over the area occupied by the transducer. In some instances there is indeed a liquid layer between two serous membranes but under most circumstances it is so small that pressure measurements are difficult, especially when both tissues are deformable and move relative to each other (12,13,14,15,16). The determination of pleural and pericardial pressure has presented researchers with all of these problems and many methods have been proposed to solve them. The presence of two separate types of stress have been postulated to account for the differences in stress measured by the various pressure measuring techniques in the pleural space. The combined action of "liquid pressure" and a "contact stress" have been proposed to account for the total integrated stress being transferred between these two surfaces (17-23). The separation of normal surface stress into liquid pressure plus contact stress was probably born through the inability of technology to measure the stress normal to a surface under these conditions. However, in the pleural space, these surfaces are indeed separated by a very thin layer of fluid (8 to 25 μm). Therefore, the proper measurement of liquid pressure in this environment would yield correct estimations of the local stress being imparted on the opposing surfaces when those two surfaces are not moving relative to each other (12,13). The author is not aware of any study that attempts to directly determine the regional thickness of the liquid layer in the pericardial

space. This might be due to the inherent technical problems such an endeavour would present. The measurement of pleural pressure has been made easier using the rib-capsule technique (24-26). This has only been possible due to the presence of a rigid structure (ie, rib), to provide a stable platform where one serous surface can be used as the nonmoving entity and therefore facilitate the convenient placement of a pressure measuring device. Without this anatomical platform, the measurement of liquid pressure in fluid layers as small as 8 to 25 μm might prove to be nearly impossible. Therefore, present transducer technology can only non-invasively measure the stress normal to two contiguous serous membranes when the surfaces in question are separated by a fluid layer and when these two surfaces are situated anatomically such that the placement of such transducers will not disturb the environment to be measured. This raises the question; "How does one measure pericardial pressure where no such anatomical platforms exist for placement of our liquid pressure measuring transducers?" The thickness of the fluid layer separating the two surfaces in the pericardial space is indeterminate to such a degree that open ended catheters may not measure the liquid pressure at all (11). Since liquid pressure cannot always be measured under these circumstances and given that all other methods of stress measurement will disturb the system of stresses we are attempting to measure, a transducer must be used which will at least minimize these disturbances in the pericardial space. As stated before, the thickness of the fluid layer between the two opposing serous surfaces may

be unknown, therefore, the transducer response must be independent of the amount of fluid present. Since these surfaces move relative to each other, are readily deformable and probably curved, the transducer must be very thin and flexible. To give a reasonable estimate of average stress, such a transducer must obviously have an area of contact that will be quite large compared to microscopic changes in the surface topography of the biological tissue it is in contact with.

Validation of the methods and devices used for the measurement of epicardial radial stress and pleural pressure has been the topic of some debate in cardiovascular and pulmonary physiology for many decades (7,8,12,14,27-51). In particular, the approximate magnitude of end-diastolic pericardial pressure is still being debated to the present, due to varying measurement techniques (52-56). Small flat balloons have been employed by many researchers as epicardial radial stress transducers which do not succumb to the inherit limitations of open-ended or micro strain-gauge tipped catheters. The shape of these balloons is such that they reduce, as much as possible, the artifacts created by their presence in the pericardial space. Since some form of physical intervention is required to measure this epicardial stress, a properly constructed flat balloon might be employed to couple and simultaneously measure the stresses between the epicardial and endo-pericardial surfaces. The types of flat balloons that have been successfully used to measure epicardial radial stress with the ultimate intention of calculating myocardial

transmural stress can be broken down into two categories:

1) liquid-filled flat balloons

2) gas-filled flat balloons

The liquid filled balloon contains a fluid which is incompressible and thus represents a high mechanical impedance to the system of stresses being measured. Others have suggested that, because the CVR balloon contains water instead of air, the incompressibility of water will cause some distortion of the interface between two serous membranes causing the balloon to overestimate pericardial pressure (52,53,57). The fact that the balloon is relatively incompressible means that very little work is dissipated in the device unlike a compressible air filled balloon. Whether this is significant remains to be seen. We have not found any significant differences in the calibration of air or liquid filled balloons when calibrated using the procedures described in this paper or by McMahon et al (58). The inherent limitation of the liquid-filled balloon is that the pressure measuring transducer at the distal end of the catheter, cannot distinguish between the pressure developed inside the balloon and the hydrostatic pressure developed through changes in height of the balloon relative to the transducer zero pressure reference height (Figure 2.2). Additional information as to the physical location of the balloon relative to the zero reference must be provided so the exact pressure developed in the balloon may be calculated. The gas filled balloon will experience changes in internal volume with applied surface stress and this may affect the behaviour of

the balloon due to the compressible nature of air. Nonetheless, pressure developed in the balloon will be transferred through the connecting lumen with no hydrostatic gradient modification and thus present itself, undisturbed by changes in height, to an external pressure measuring transducer. Thus, given that a gas filled balloon can be properly calibrated to give a predictable relationship between external balloon surface stress and internal balloon pressure, it would be a very useful device for measuring the absolute magnitude of the epicardial radial stress. Why then does the author prefer to use liquid-filled balloons?

In most hemodynamic research laboratories pericardial balloons are used ultimately for the purpose of deriving myocardial transmural stress, in particular, the end-diastolic transmural stress. As stated previously, an air filled balloon will present the internal pressure developed in the balloon to an external pressure transducer regardless of the height of the balloon relative to the external transducer's zero pressure reference point. However, how does one obtain the exact measurement of endocardial radial stress at the same location in the heart as the epicardial location of the balloon? The measurement of cavitary pressure is usually measured using an open ended liquid filled lumen referenced to an external zero reference height. In most circumstances, the reference height is taken to be midway up the total height of the cavity in question. In some instances the cavitary pressure is measured using a micro strain-gauge tipped catheter for better fidelity but the mean pressure is usually corrected using a

liquid filled catheter connected to an external strain-gauge pressure transducer. The only way to obtain the exact endocardial radial stress under these circumstances is to measure the height of the endocardial surface relative to the zero reference height of the cavitary pressure. This, of course, is very difficult when the animal is undergoing changes in cavitary, total cardiac and thoracic volume. Any unaccounted shift in the height of the endocardial surface relative to the zero reference height will introduce hydrostatic errors in the transmural stress calculation. A liquid-filled balloon measuring system compensates for these changes in height by modifying the contribution of the hydrostatic gradient in the connecting lumens of both transducer systems. Therefore, while the liquid filled balloon cannot give the exact magnitudes of epicardial radial stress relative to atmospheric pressure, it can be used to derive the exact transmural stress by merely subtracting it from cavitary pressure referenced to the same zero pressure reference height (Figure 2.3). Therefore, the transmural pressure derived from the difference in pericardial pressure measured by a liquid filled balloon and the cavitary pressure measured by a fluid-filled catheter will be independent of the position of the balloon on the myocardium. This is true throughout the whole cardiac cycle. Stated differently, the fluid filled transducer systems cannot give the absolute values for endo and epicardial radial stress but it can provide the difference between these two pressures.

Description of the CVR Pericardial Balloon

The balloon used in the Cardiovascular Research Labs at the University of Calgary is fabricated using a 7 cm by 4 cm flat silastic™ sheet (0.254 mm thick Compound = AR131, Lot Number = 0170, Armet Industries Corporation, Concord Ontario) wrapped around a 14 cm length of medical grade silastic™ tubing (59,60) (1.575 mm ID, 3.175 mm OD, Dow Corning Silastic™ brand tubing, catalog number = 602-285, Lot Number HH085407). The tubing has three 2.0 mm by 1.50 mm holes, spaced 5.00 mm apart, cut into the side of the tubing starting 7.50 mm from the end of the lumen inside the balloon. The silastic™ sheet is then wrapped around the tubing and the opposing surfaces are bonded using silicone adhesive (Figure 2.4). The fabrication procedure has been standardized using a metal mould (Figure 2.5) which allows the balloon to be slightly pressurized during the curing procedure. This method reduces the variation of the internal volume and standardizes the geometry of all balloons used in the CVR lab. The opposing surfaces to be bonded are cured at 50 °C for 24 hours under pressure (the balloon mould is held together using a C-clamp), the balloon is removed from the mould and left to stand at room temperature for 24 hrs. The advantages of using silastic™ sheets and silicon adhesive as the only materials in the CVR balloon are the long shelf life after fabrication, non-reactivity to body tissues, and extreme flexibility and resistance to fatigue (59,60). For most experiments conducted in the CVR lab the balloon is attached to a 100 cm length of 7-French (7-F) angiographic catheter which

is may be shortened to 75 - 60 cm, depending on the application (French = the outside circumference in mm of the catheter).

Calibration of the CVR Pericardial Balloon

The balloon used in the Cardiovascular Research Labs at the University of Calgary is liquid containing and void of air in all conduits leading to a strain-gauge pressure transducer via a 7-F angiographic catheter. Therefore the magnitude of the pressure seen by the pressure transducer will be the sum of the hydrostatic pressure created by differences in height between the balloon and the transducer and the pressure developed in the balloon (see Figure 2.3). This requires that all static calibrations be conducted in a manner such that no changes in height relative to the pressure transducer zero reference height occur. McMahon et al (58) published a calibration method, referenced by many investigators who use flat balloons, to determine linearity between pressure developed in a balloon and the normal stress applied to it. An important point elucidated by this paper was that Laplacian stresses developed by a pressure difference across a curved thin membrane might prevent a balloon from obtaining a linear relationship between external stresses applied normal to it and internal balloon pressure developed (Figure 2.6). As a consequence, the balloon geometry should be designed to prevent Laplacian stresses from developing. In order to minimize the disturbance the balloon creates when placed in such an environment it must be made as thin as possible.

Furthermore, the construction of a testing apparatus to emulate the balloon's environment is difficult since it is this very balloon we are using to determine the characteristics of such an environment. Therefore we dud a series of loading tests to emulate the environment that the balloon would be exposed to when placed in a biological system of stresses, such as those found in the pericardial space. The following characteristics on the CVR pericardial balloon were determined:

1.) Unstressed volume

2.) Static linearity

3.) The effect of non-uniform loads

4.) The dynamic response

5.) The dynamic response of the high-fidelity CVR balloon

Unstressed Volume Determination of the CVR Pericardial Balloon

Unstressed volume of the CVR balloon was measured by filling the balloon with various volumes of water and measuring the internal balloon pressure developed. The balloon was flushed repeatedly to remove all air bubbles and all remaining fluid was withdrawn until a balloon pressure of -5.0 mm Hg relative to atmospheric was developed. This was defined to be zero volume since all collapsible structures would be void of fluid. The strain-gauge pressure transducer (Model P23 Db, Statham-Gould, Oxnard, California) is electrically zeroed to the same height of the balloon and connected via the

previously described 100 cm length of 7-F angiographic catheter, with the balloon lying on a flat surface. Fluid was added to the unstressed balloon in increments to determine the pressure-volume relationship of a standard CVR balloon. Figure 2.7 shows typical data from a CVR balloon showing the unstressed pressure-volume relationship. The graph clearly shows that introducing fluid volumes ranging from 0.5 to 1.0 ml did not develop any significant pressure in the balloon. Another zero volume determination method which, worked well for the hospital operating room where the balloon must be manipulated in a sterile environment, was the removal of all fluid in the balloon until the silastic™ surfaces form a dimple on the side-ports of the silastic™ tubing inside the balloon (this works out to be approximately -10 mm Hg). After the zero volume was established, fluid was added (approximately 0.85 ml). Figure 2.8 shows a typical balloon calibration curve obtained using this technique.

CVR Balloon Static Linearity Using the CVR Static Calibrator

A method of determining pericardial balloon linearity to static loading was published by McMahon et al (58) which requires the use of a 7 litre latex meterological balloon to impart normal stresses onto an air filled balloon transducer placed on a flat surface (Figure 2.10). The results produced by McMahon's paper are consistent with what we have seen in the CVR laboratory; however, the use of a 7-litre balloon is cumbersome and the presence of Laplacian tension in the large balloon may cause some error if the transducer

being calibrated deforms the membrane of the latex balloon. These deformations could create local laplacian stresses which might prevent the complete transmission of the large meterological balloon's internal pressure to the outer surface of the pericardial balloon being tested. To minimize this artifact, we have designed a compact pericardial balloon calibrator fabricated from plexiglass and silicone rubber. The principle behind this particular calibrator embodiment is to provide stresses normal to the balloon transducer surface using a thin, unstressed, very compliant silastic™ membrane. A thin silastic™ membrane (same material used in the fabrication of the CVR balloon) is attached to a plexiglass cylinder (12.7 cm. OD, 11.4 cm. ID) so that it is unstressed but not floppy. The other end of the cylinder is sealed with a plexiglass endplate (15.24 cm. dia, 1.27 cm. thick) (see Figures 2.22 to 2.24). By placing the membrane bearing portion of the cylinder over the balloon transducer lying on a flat surface, the desired testing configuration is achieved. A flat disk (15.24 cm. dia, 1.27 cm. thick) supporting the balloon transducer (balloon support disk) is held against the thin membrane using three brass screws so that the whole assembly can be assembled or disassembled easily. A small trough (3.175 mm. wide) was machined into the balloon support disk, permitting access of the balloon silastic™ tubing (3.175 mm. OD) to the outside of the calibrator. The pressure inside the cylinder can be manipulated through a small air hose coupling. The clear plexiglass used in this apparatus allows the researcher to observe the balloon as it is being tested to ensure proper testing

conditions. The balloon support disk has several small-diameter full thickness holes (1.587 mm dia) throughout its surface to allow air trapped between it and the membrane during assembly to escape. This ensures that the only stress experienced by the balloon is through contact with the silastic™ membrane. Another transducer support disk was fabricated to permit the testing of balloon transducers under conditions of negative pressure, such as those found in the pleural space over the diaphragm or mediastinum, where the rib capsule technique cannot be applied. This balloon calibrator embodiment used to measure negative pressure had one hole in the balloon support disk (see Figures 2.22 to 2.24) which allowed air to escape during the positive pressure testing. These holes were then sealed during peak positive pressurization, and the pressure in the test chamber was reduced to less than atmospheric to expose the balloon to negative stress conditions (Figure 2.9).

The linearity of the CVR liquid containing balloon is dependent on the amount of fluid present in it. In order to determine the volume of fluid required to obtain a 1:1 relationship between applied stress and measured pressure developed inside the balloon, the balloon calibration chamber was employed. Fluid was introduced into the balloon in the same manner described in the unstressed volume determination methods. The balloon was then placed inside the calibration chamber and the air pressure inside the calibrator was increased to apply a membrane stress to the balloon. The pressure inside the balloon was measured using the same methods described in the unstressed pressure-

volume relationship section of this chapter and compared to the pressure introduced in the calibrator pressure chamber (see Figure 2.9). All CVR pericardial balloons required from 0.70 to 0.90 ml of fluid to calibrate linearly with a 1:1 relationship between calibrator chamber pressure and measured balloon pressure.

The Effect of Non Uniform Loads on the CVR Balloon

A bench-top experiment was performed to investigate whether the CVR pericardial balloon would collapse (ie, the two opposing internal surfaces of the balloon touch without a liquid layer interposed between them; see Figure 2.11 C and D) in areas where the greatest stress is applied. The effect of non-homogeneously distributed loads on the CVR balloon were examined by placing weights of different mass and contact area over the upper surface of the balloon while the balloon was resting on a flat surface (Figure 2.11). The Laplacian stresses developed in the upper surface of this balloon must be opposed by the balloon's silastic™ borders or serious deformations may occur. The silastic™ borders of the balloon must be wide enough so they oppose buckling due to this upper membrane tension created by non uniform loads. Identical stresses (ie, force per unit area) over varying fractions of the balloons active contact surface (see Figure 2.4) were applied with blocks of different sizes and weights (see Figure 2.11 A and B). Figure 2.12 shows the results of this test with the balloon pressure being equal to the applied stress times the

ratio of weight area to total balloon area. At ratios less than 25% (with the weight placed in the geometrical centre of the balloon's active contact area) the balloon collapsed and underestimated the applied stress. Figure 2.12 shows that CVR pericardial balloon transducer accurately records the average stress applied over the total balloon surface when the stress is applied over more than 25% of its active contact surface. This bench-top experiment loaded the CVR pericardial balloon in an extremely nonuniform manner. The pericardium should distribute load much more equally.

Dynamic Response of the CVR Pericardial Balloon

The pericardial balloons presently used in the CVR labs at the University of Calgary are connected to 7-F angiography catheters. The frequency response and noise due to motion of these catheters are well known (84,85). The frequency response of these catheters behave typically like over-damped 2nd order systems, with a resonant peak around 25 - 40 Hz. When one considers these inferior frequency response characteristics and the motion induced artifacts that are easily generated from a beating heart, it becomes readily apparent how these pericardial balloons may present serious limitations in measuring epicardial stress. Figure 2.13 gives the frequency response of a typical 100 cm length of a 7-F angiography catheter measured in this lab using a sinusoidal pressure generator (Model WGA-200 multi-function pressure generator, Millar Instruments, Houston, Texas). The response of the 7-F

angiography catheter to a sinusoidal forcing function ranging from 0 to 100 Hz shows a typical 2nd order over-damped response with a peak resonance at approximately 25 Hz (see Figure 2.13).

The author has constructed a dynamic calibration chamber with a high-fidelity speaker (Model SW6025G Alpha Sub-Woofer, Heco-Hennel and Company, Germany), driven by two 100 watt DC-coupled amplifiers in a class B push-pull configuration (Model SM-100, OPAMP Labs, Los Angles, California) which amplifies a sinusoidal input signal (Model 180 LF sweep generator, Wavetek, San Diego, California or Model 625A test oscillator, Hewlett Packard Corporation, Palo Alto, California). The sub-woofer, mounted in a variation of the static balloon calibrator embodiment, imposes a time-varying pressure onto the pericardial balloon (see Figure 2.25) to determine its frequency response and the total harmonic distortion. The chamber pressure created by the sub-woofer is sensed by a micro strain-gauge tipped catheter (Model PR-279 8F Mikro-tip™ catheter pressure transducer, Millar Instruments), placed inside the pressure chamber via a side port. The signal from the sweep generator or test oscillator was compared to that from the chamber pressure sensing catheter using in-house designed and constructed electronic circuits to create an error signal. The error signal was used for negative feedback to the sub-woofer amplifier driving circuits. This sinusoidal pressure generating system kept total harmonic distortion of the chamber pressure waveform to less than 3% over frequencies ranging from 2-200 Hz at peak sinusoidal pressures ranging from

0-20 mm Hg. The calibration chamber was designed to allow for pressurization up to ±60 mm Hg (ie, the mean chamber pressure could be 40 mm Hg and a ±20 mm Hg sinusoidal pressure created by the sub-woofer could be modulated onto that mean chamber pressure) to test for non-linearities and harmonic distortion at higher pressures. The sinusoidal pressure generated in the pressure chamber was transferred to the balloon via a thin silastic™ membrane identical to that used in the CVR static calibrator. To measure the stresses being imposed upon the balloon by the membrane, a load cell (Model P23-BB venous strain-gauge pressure transducer, Statham, Hato Rey, Puerto Rico) was placed under the balloon and flush with the calibrator's balloon support disk surface (see Figure 2.25). There was always a 1:1 relationship between the signal measured by the chamber pressure sensing catheter and the load cell indicating that the membrane was not modifying the time-varying pressure created by the sub-woofer (Figure 2.16).

The frequency and phase response of a CVR balloon is given in Figure 2.14 and 2.15. Notice the typical 2nd order phase-shift at frequencies corresponding to the peak of resonance. This frequency dependent response of the CVR balloon is very similar to the frequency response of the angiographic 7-F catheter, indicating that the major factor which determines frequency response of the balloon-catheter system is the catheter frequency response characteristics.

The CVR High-Fidelity Pericardial Balloon

The author has recently developed a balloon which has a flat frequency response to 200 Hz with no measurable waveform or harmonic distortion introduced through motion of the connecting 7-F angiographic catheter. This increase in fidelity is achieved through the introduction of a 3-F micro strain-gauge tipped catheter (Model PR-249 3F mikro-tip™ catheter pressure transducer) inside the connecting catheter lumen and advancing it to the middle side-port of the silastic™ balloon lumen. This pericardial balloon has a flat frequency response from 0 to 200 Hz. An internal balloon semiconductor strain-gauge catheter such as that described for the high-fidelity CVR balloon, is susceptible to baseline drift which must be corrected for retrospectively. The CVR high-fidelity balloon has a 7-F catheter identical to the conventional CVR balloon, therefore the mean pressure may be accurately measured externally using a conventional strain-gauge pressure transducer. Figure 2.16 shows the frequency response of the CVR high-fidelity balloon compared to the signal received by the pressure transducer at the end of the connecting angiographic catheter. Figure 2.17 shows a time-domain plot comparing the response of the conventional CVR balloon (upper panel) to the high-fidelity CVR balloon (lower panel). The sinusoidal forcing function signal is derived from a sweep generator adjusted to make repetitive frequency runs from 10 to 50 Hz over 6 second intervals. The upper panel shows how the pressures sensed by the balloon at the end of the angiographic catheter are altered by the over-damped 2nd order

resonant behaviour of the catheter. The lower panel shows the frequency response of the CVR high-fidelity balloon exposed to the same forcing function. The reader may observe that the high-fidelity CVR balloon has a completely flat response over the range of frequencies tested.

Another useful feature of the high-fidelity CVR balloon is that it does not sense catheter motion induced artifacts (ie, catheter whip). This is shown in Figure 2.18 which is a time-domain plot comparing LV transmural pressure calculated using standard fluid-filled catheter transducers to that calculated using their high-fidelity counterparts. The reader can see that, at end-diastole, the fluid-filled system is adequate for the determination of transmural pressure, but the high-fidelity transducers can be used to calculate transmural pressure over the whole cardiac cycle. If the fluid-filled catheters are shaken, either by motion of the heart or some other source of vibration, the 'catheter ring' may totally obscure the physiological pressure signal. This is shown rather well in Figure 2.19 where the high-fidelity CVR balloon is not disturbed by extreme catheter motion artifacts. Even though these fluid-filled catheters ring excessively their mean pressure is still unaltered by vibration. Therefore, they can still be used for mean pressure correction of the high-fidelity systems.

This design modification to the CVR pericardial balloon opens up the possibility of measuring pericardial pressure over the whole cardiac cycle. This would allow the determination of transmural pressure over the whole cardiac cycle (see Figures 2.20 and 2.21).

Conclusions

This chapter has shown that a small silastic™ balloon may be calibrated reliably for the purposes of measuring epicardial radial stress (or pericardial pressure). The standard CVR pericardial balloon can be modified with the insertion of a small micro strain-gauge catheter inside the balloon to provide superior frequency response and extremely low catheter motion-induced noise. The high-fidelity CVR pericardial balloon has made it possible to measure pericardial constraint throughout the whole cardiac cycle to a bandwidth of 200 Hz.

Figure 2.1 Stresses on the Pericardium

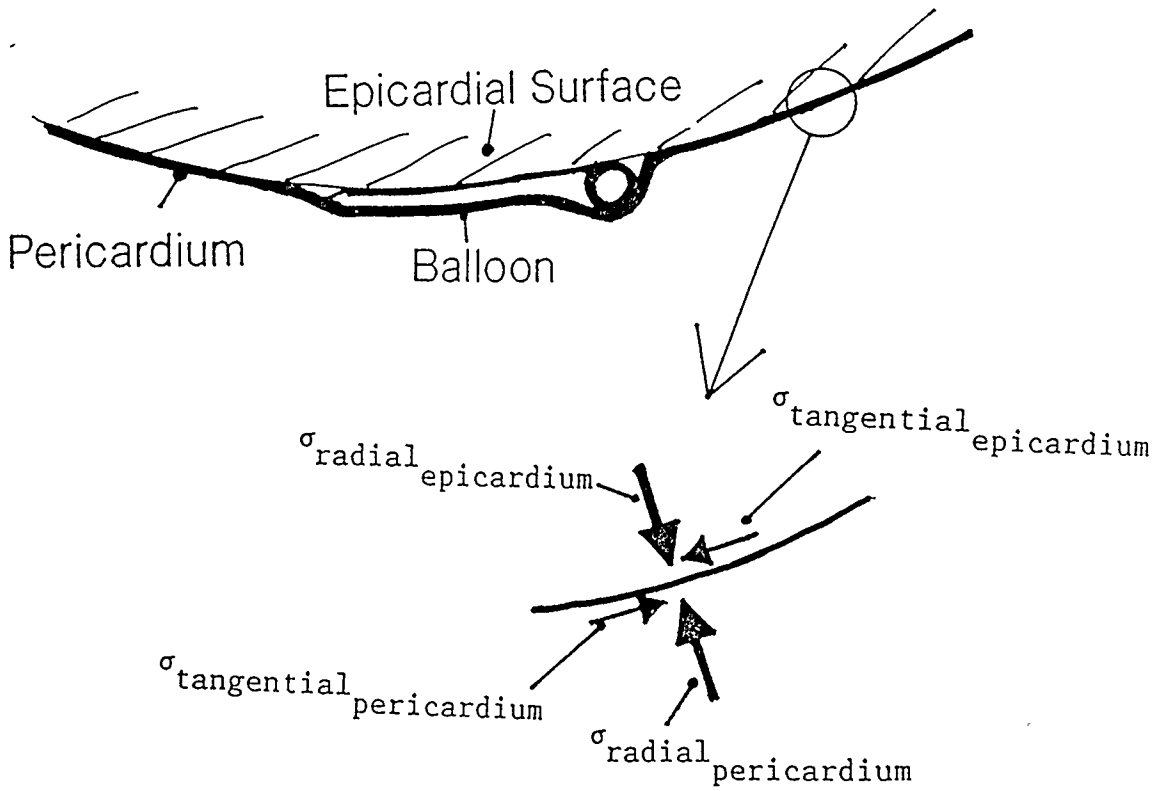

A schematic drawing showing the stresses experienced by the epicardial surface in one plane (another set of stresses would be coming in and out of the page). The motion of the heart relative to the pericardium might develop tangential or shear stresses, but for the purposes of this dissertation we will assume they do not affect the magnitude of the radial stresses to a large degree. This can be considered to be true at end diastole since the heart is not in rapid motion at this time. Comparison of pre- and post-pericardiectomy end-diastolic pressure-dimension relationships also support this assumption.

Figure 2.2 Effect of Changes in Balloon Height to Reference Height

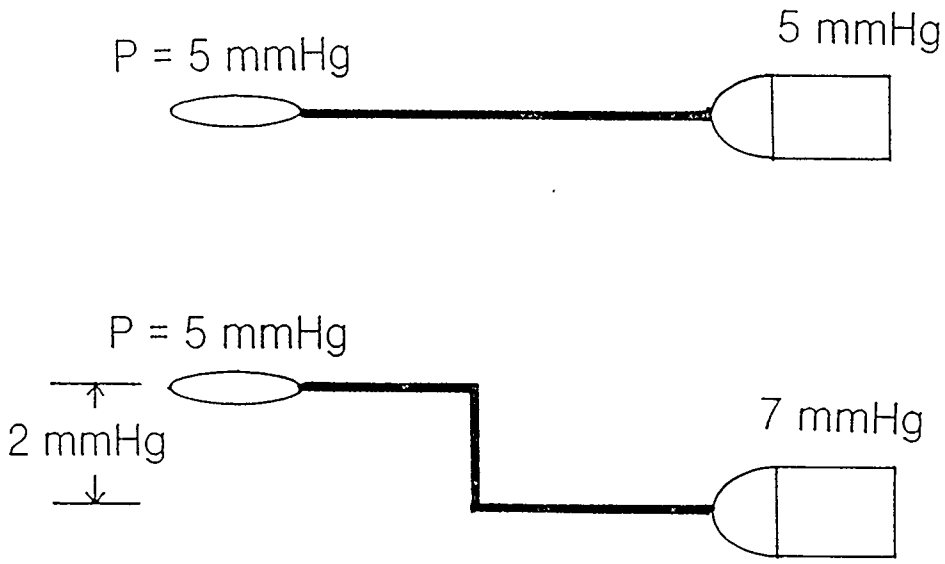

A schematic drawing illustrating the fact that a fluid filled pericardial pressure measuring system will have hydrostatic offsets in its pressure signal if the height of the balloon is different from the height of the zero pressure reference level.

Upper panel — Shows a balloon at the same height as the zero reference level of the pressure transducer. The balloon is experiencing a stress of 5 mm Hg which is sensed at the pressure transducer without hydrostatic modification.

Lower panel — Shows a balloon at a height 2.7 cm (2 mm Hg) higher than the level of the zero reference level of the pressure transducer. The balloon is experiencing a stress of 5 mm Hg but the difference in height is added to the pressure and therefore the pressure transducer sees a 7 mm Hg pressure.

The pressure transducer is unable to distinguish between the pressure experienced by the balloon and the hydrostatic offset created by the balloon being at a height different from the zero pressure reference level of the pressure transducer.

Figure 2.3 Comparison of the Transmural Pressures Calculated Using Air-Filled and Liquid-Filled Balloons

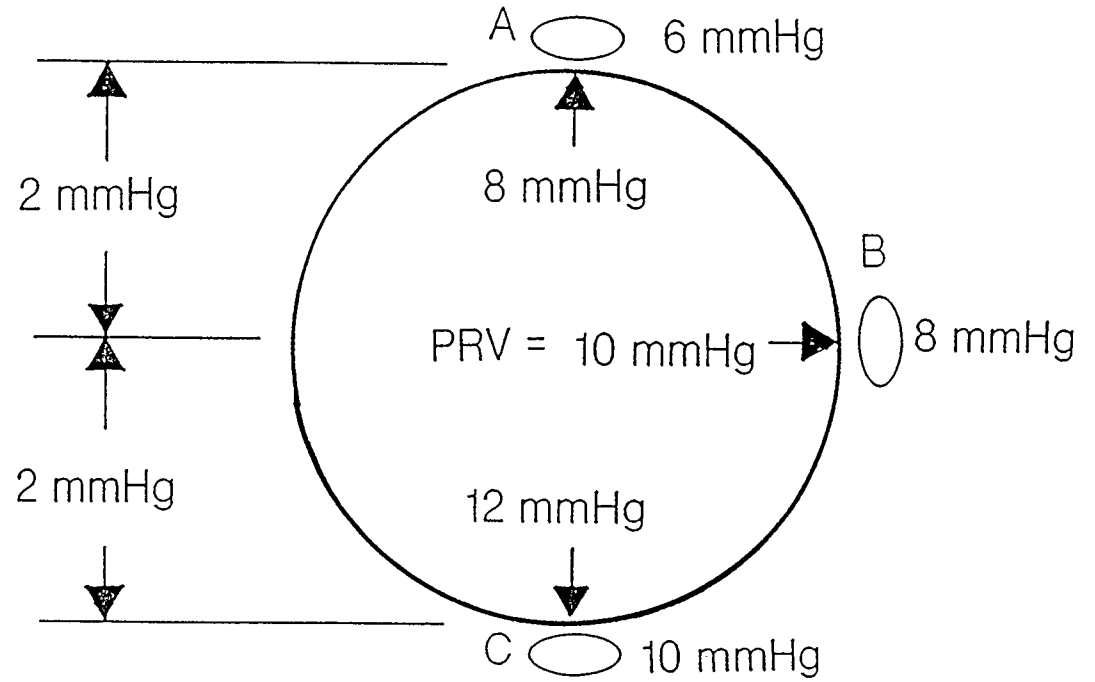

Position	P_{air}	$P_{trans-air}$	P_{liq}	$P_{trans-liq}$
A	6	4	8	2
B	8	2	8	2
C	10	0	8	2

A schematic diagram showing the position of three balloons at different location on the heart (position A, B and C). The endocardial radial stress is shown in the figure to be 8,10 and 12 mm Hg for positions A,B and C, respectively. However, the cavitary pressure is being sensed from a fluid-filled lumen referenced at the mid-cavitary height (ie P_{cav} = 10 mm Hg). If we assume the transmural pressure to be 2 mm Hg at all three positions, then the pressure sensed by a pressure transducer connected to an air-filled balloon is given in the column labelled P_{air}. The calculated transmural pressure using air-filled balloons ($P_{trans-air}$) will only give correct results if the balloon is located at the same zero reference height as the fluid-filled cavitary pressure transducer. The hydrostatic offset created by the fluid-filled balloons provides a hydrostatic offset correction which will give a P_{liq} that, when used with P_{cav}= 10 mm Hg, will give the correct transmural pressure ($P_{trans-liq}$) regardless of the epicardial position of the balloon.

Figure 2.4 The CVR Pericardial Balloon

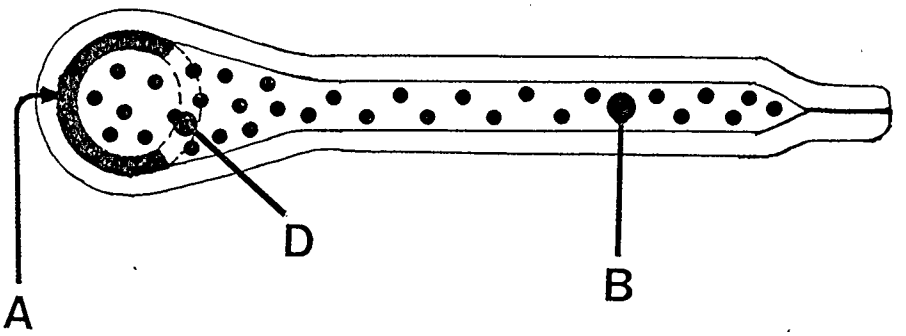

(A) - Silastic™ connecting tubing.

(B) - Active contact area.

(C) - Border to prevent buckling of balloon edges.

(D) - Side ports to communicate active contact area pressure to connecting lumen.

RV balloon dimensions
(y) = 30 mm
(x) = 30 mm
(z) = 5 mm

RA balloon dimensions
(x) = 12 mm
(y) = 14 mm
(z) = 2 mm

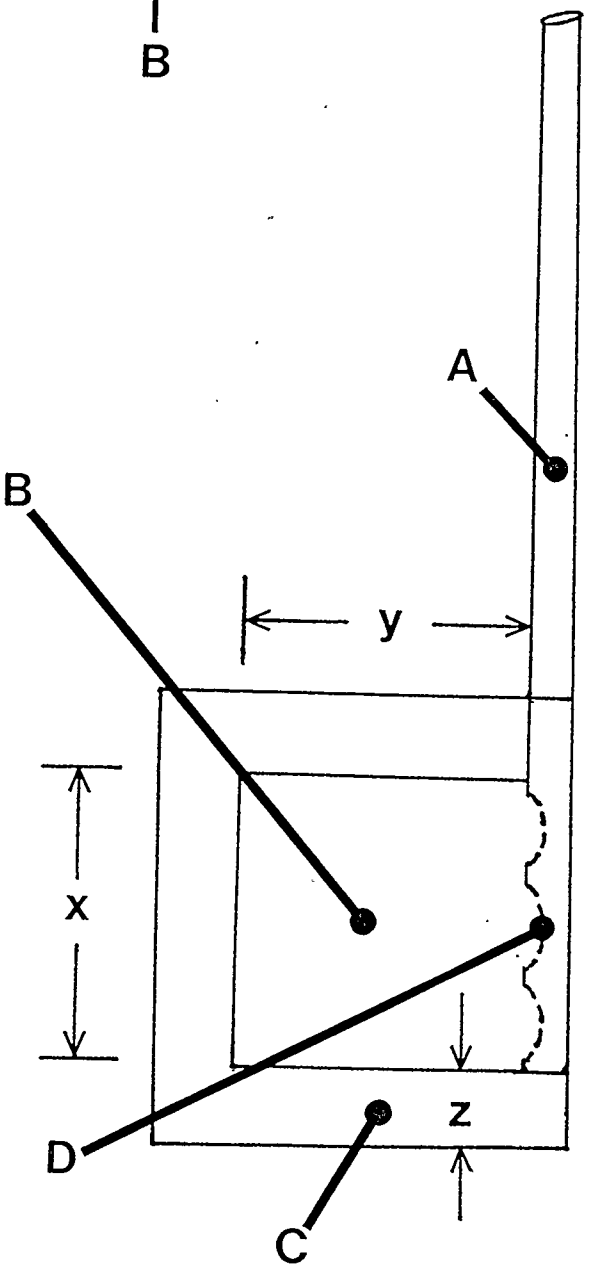

Figure 2.5 Mould used to make the CVR Pericardial Balloon

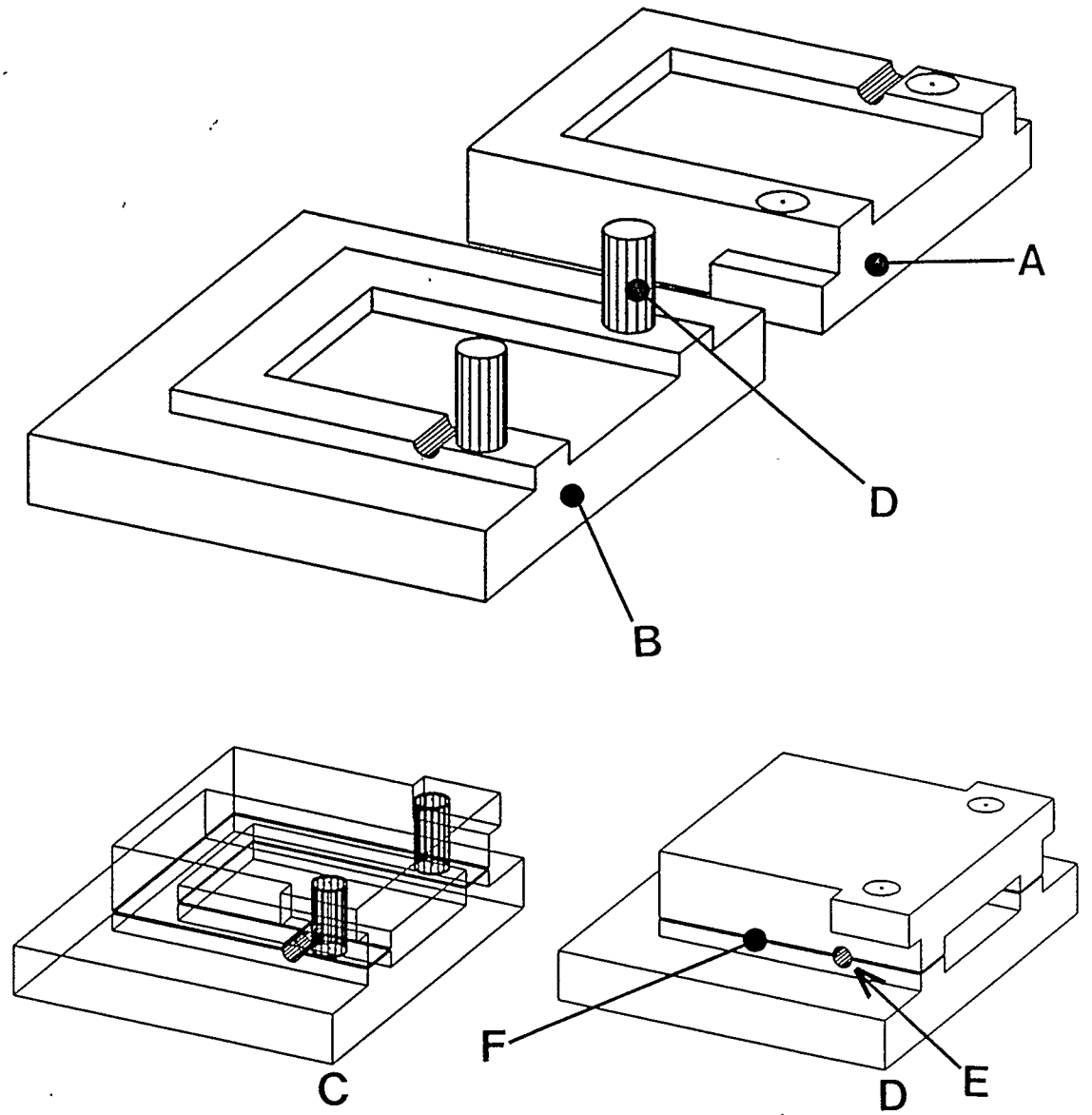

Drawing of the mould used to fabricate the CVR pericardial balloon. The mould consists of two parts which are brought together by the alignment pins (D). A 4 X 7 cm sheet of silastic™ is folded around a silastic™ tube and the upper (A) and lower (B) parts sandwich the silastic™ sheet surfaces together (F). The balloon is bonded together using silastic™ adhesive. The balloon is slightly pressurized during the curing procedure (50 °C for 24 hour). Notice the hole (E) for the silastic™ tubing exiting the side of the assembled mould (C and hidden lines removed D).

Figure 2.6 Laplacian Stresses on a Curved Surface

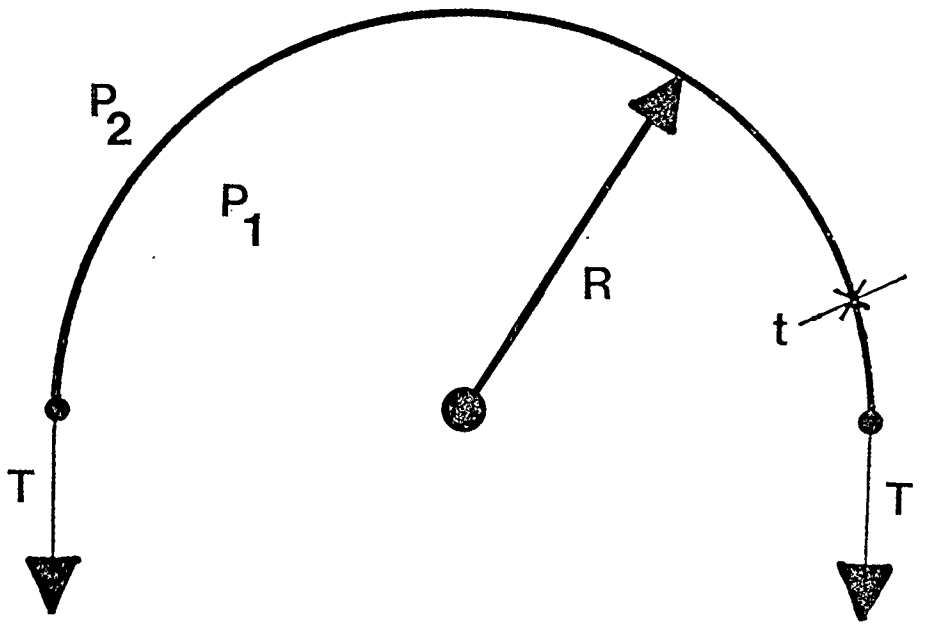

$$\sigma_{membrane} \propto \frac{(\Delta P \cdot R_{curvature})}{t_{membrane}}$$

Drawing of a curved thin membrane with a membrane stress ($\sigma_{membrane}$) or tension (T), which is directly proportional to the pressure difference across it ($\Delta P = P_1 - P_2$) and the radius of curvature ($R_{curvature}$), and inversely proportional to the membrane thickness ($t_{membrane}$).

FIGURE 2.7 Determination of Unstressed Volume of the CVR Balloon

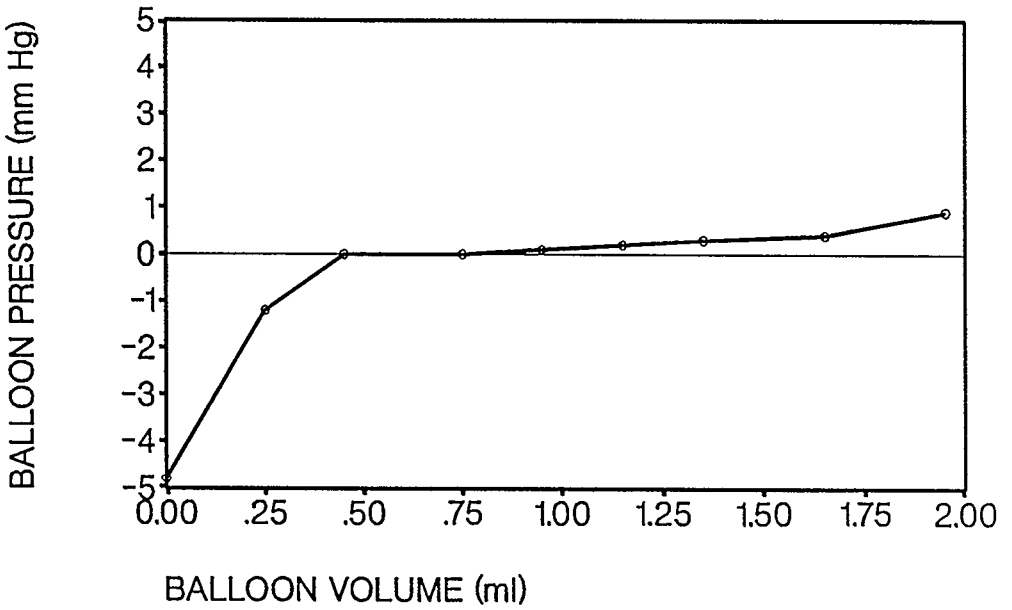

Plot of the pressure developed in an unstressed CVR pericardial balloon with incremental increases in fluid. Notice the pressure is zero for fluid volumes ranging from 0.50 to 1.00 ml. The amount of fluid normally use to calibrate the CVR balloon ranges from 0.70 to 0.90 ml.

Figure 2.8 Typical CVR Balloon Operating Room Calibration Curve

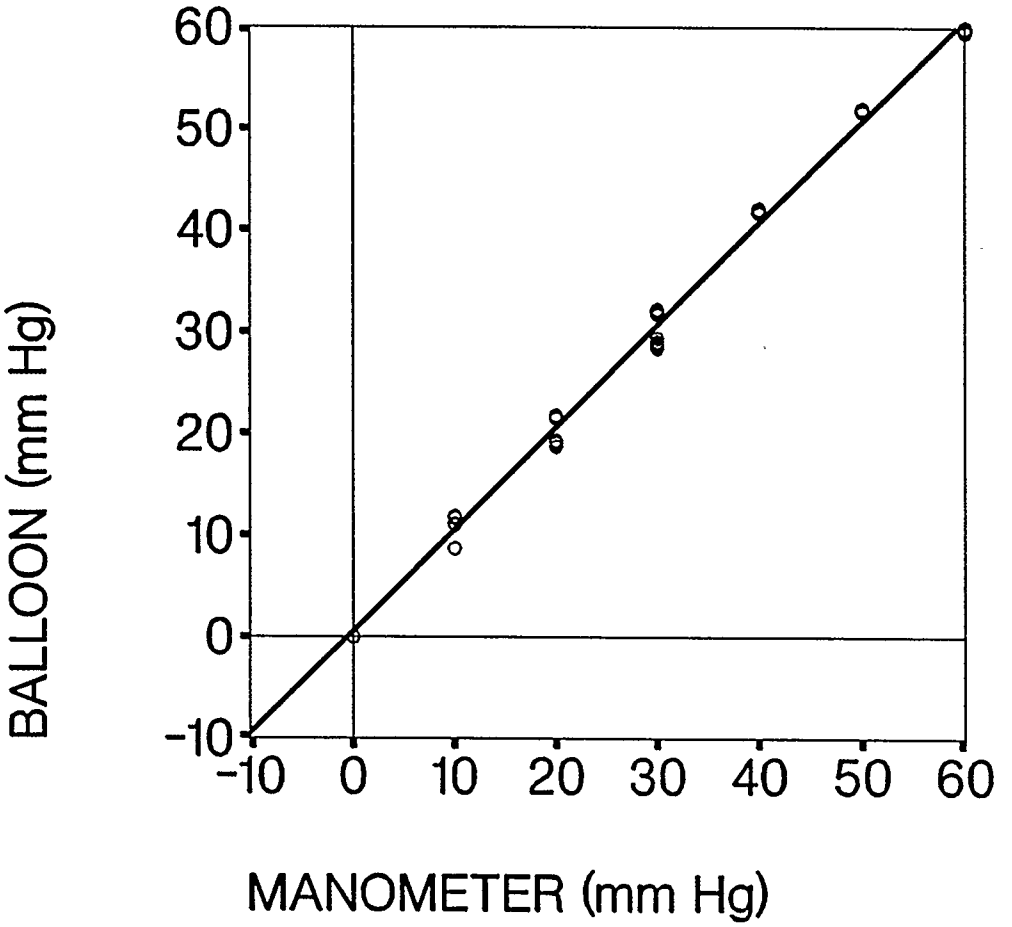

The CVR pericardial balloon was calibrated in the CVR static balloon calibrator using a mercury manometer as the pressure calibration source. All pressure transducers in the operating room were also calibrated with a mercury manometer. The plot shows the linear regression of the data points collected for the balloon calibration. Several data points were collected at each manometer pressure. To preserve sterility, the balloons were calibrated after they had been used in the experiment. This required that the precise amount of fluid to be added to the balloon pre-operatively to minimize errors. The sterile operating room environment can be considered to create a "worst case" situation regarding balloon calibration since the volume fluid required for linearity cannot be confirmed pre-operatively unlike acute animal surgery where the balloon calibration can be confirmed with a manometer or strain-gauge pressure transducer.

Figure 2.9 Calibrator Chamber Pressure vs Pericardial Balloon Pressure

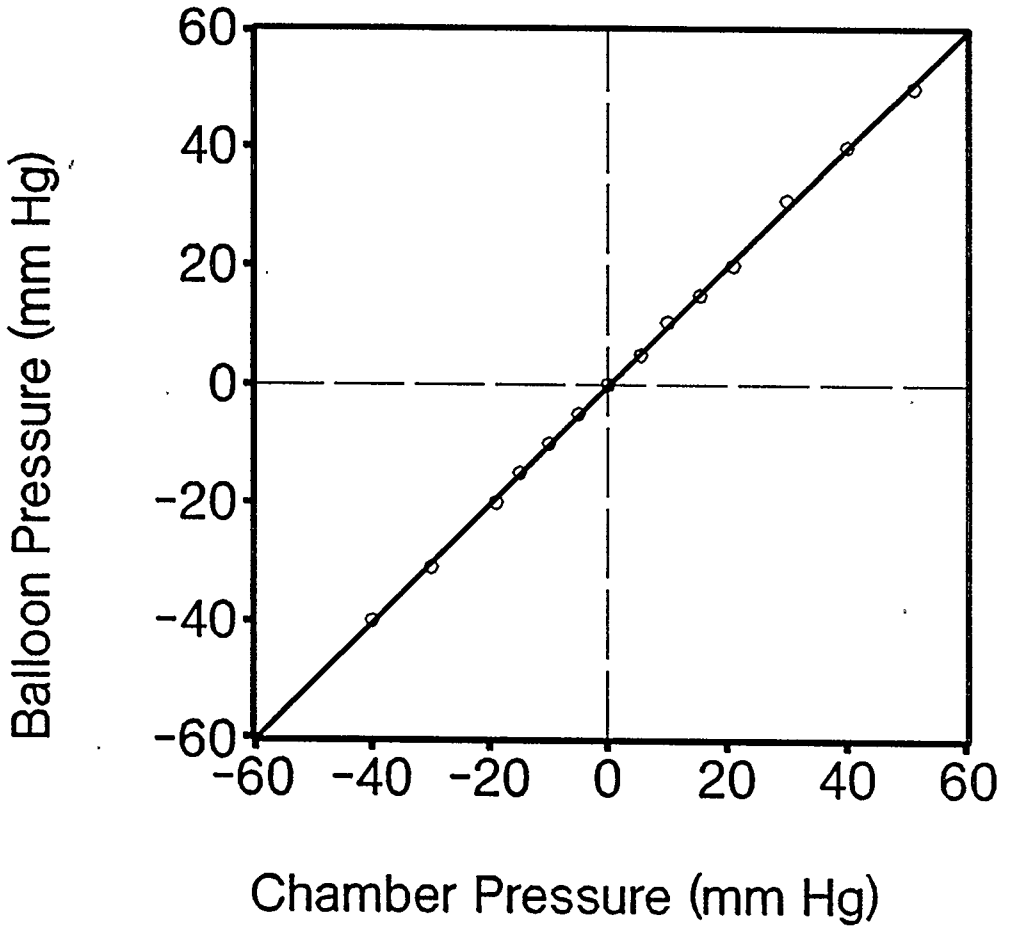

The CVR pericardial balloon was tested for static linearity using the CVR static balloon calibrator. The calibrator chamber pressure was varied from -40 to +50 mm Hg. The measured balloon pressure is plotted against the chamber pressure. A linear regression line illustrates the 1:1 relationship between applied chamber pressure and balloon pressure. The unstressed volume used in this balloon was 0.85 ml and that volume was added to the balloon using the same methods used in the sterile hospital operating room procedures.)

Figure 2.10 Stresses Delivered to a Balloon Using a Thin Membrane

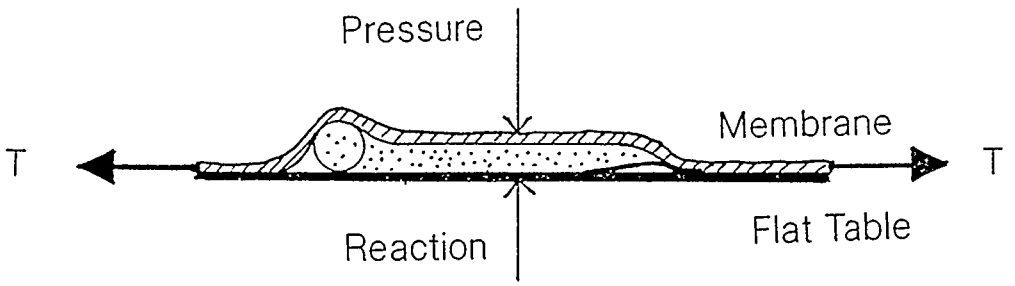

The diagram shows a CVR balloon in cross-section being stressed by a thin membrane. The stresses being delivered to the balloon should be equal to the air pressure applied to the membrane. If the membrane is under tension (T), then laplacian stresses can exist anywhere the membrane is deformed. The fact that the membrane is pressed over the balloon by the chamber pressure predicates that laplacian stresses will exist around the edges of the balloon, furthermore, the balloon will deform under these stresses. The system of stresses being created will be disturbed if the membrane is also under tension. This might happen if a large latex balloon (such as that proposed by McMahon et al) is used to stress the balloon over a flat table. The CVR balloon calibrator is designed to prevent the membrane from developing tension.

Figure 2.11 Non-Uniform Loading Characteristics of the CVR Balloon

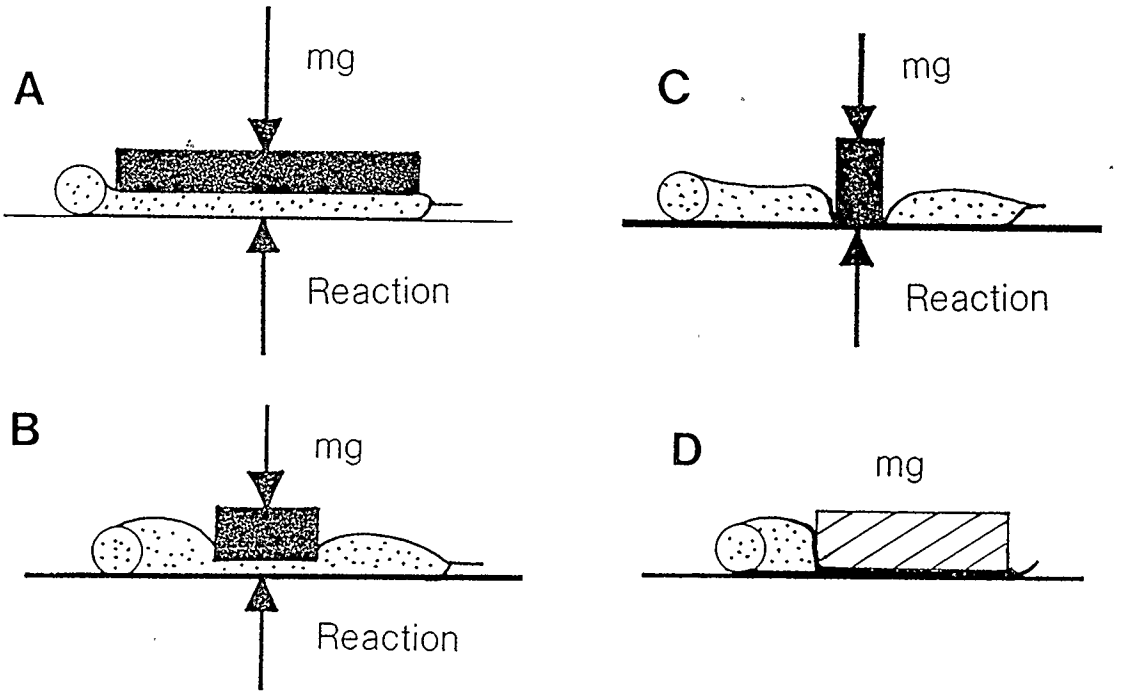

A schematic representation of the type of loading to which the CVR pericardial balloon was exposed to determine its non uniform loading characteristics. The panels labelled A and B show how the balloon behaved when it was loaded such that the loaded area was greater than 25% of the total balloon area (9 cm^2). Panel C shows the loading area to be less than 25% resulting in the upper and lower internal surfaces of the balloon making contact and therefore transferring some or all of the weight to the table without generating any internal balloon fluid pressure. Panel D shows the extreme case of loading where only the distal portion of the balloon is loaded.

Figure 2.12 CVR Balloon Non-Uniform Loading Characteristics

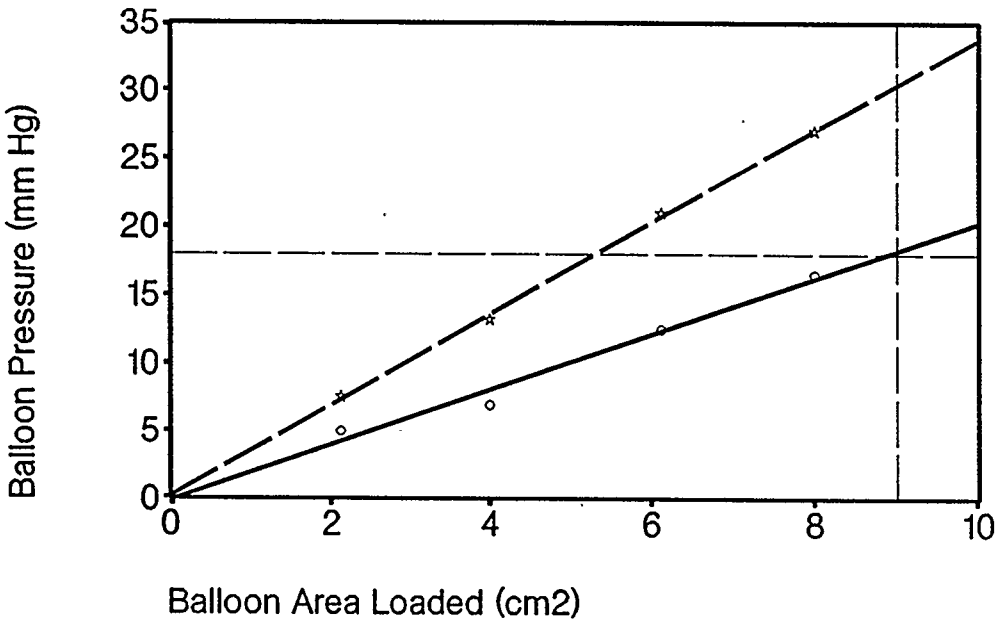

The pressure developed in the CVR pericardial balloon with weights of different mass and contact area applied to the centre of the balloon. The dashed line is the linear regression of the balloon pressure developed by a set of loading weights (stars) equivalent to a stress of 32 mm Hg (43 grams per cm^2) applied to the areas given on the X-axis. The solid line represents loadings weight equivalent to a stress of 18 mm Hg (25 grams per cm^2). A horizontal reference line at a balloon pressure = 18 mm Hg and a vertical reference line at the total balloon active contact area = 9 cm^2 are also plotted.

Figure 2.13 Frequency Response of a 100 cm. 7F Catheter

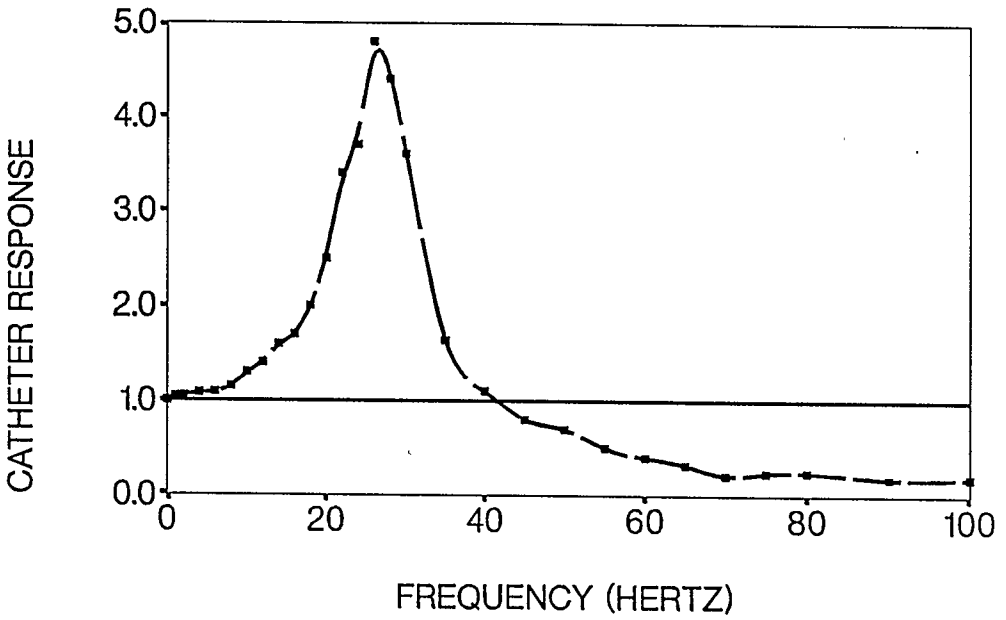

The catheter response (amplitude ratio) of a 100 cm 7-F angiographic catheter (Cordis Corporation, Miami, Florida) plotted against frequency. The catheter response behaves like a over-damped second order system with a resonant peak at approximately 25 Hz.

Figure 2.14 Frequency Response of Standard CVR Balloon

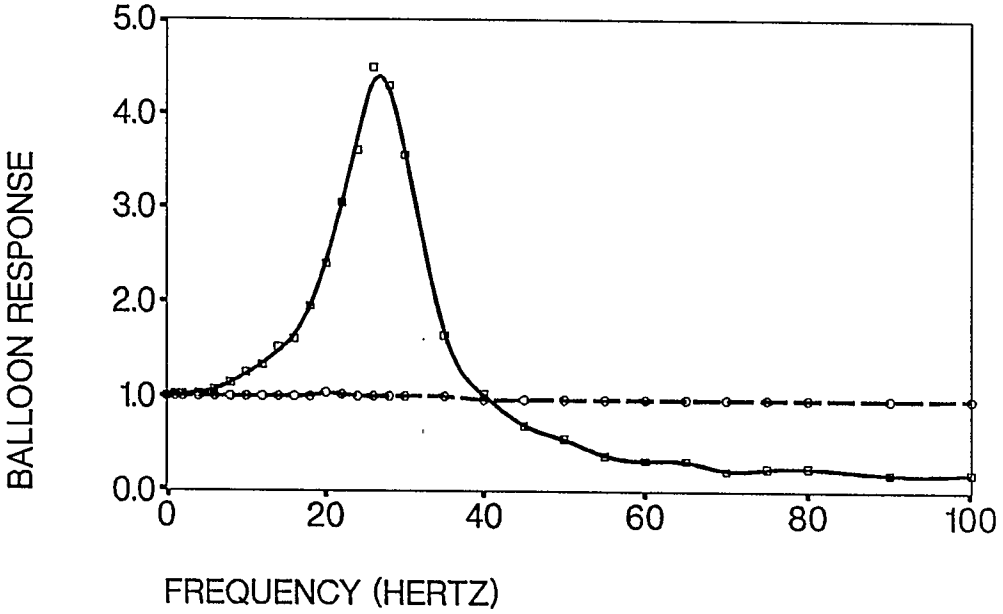

The response of a standard CVR pericardial balloon attached to a 100 cm length 7-F angiographic catheter (solid line, data points = squares) is compared to the measured pressure from the load cell (dashed line, data points = circles) situated under the balloon as it is being stressed. The load cell indicates that the balloon is being exposed to a stress that is equal to the pressure developed in the pressure chamber (which is being sensed with a micro strain-gauge tipped catheter). The balloon response is very similar to the 7F catheter response alone (see Figure 2.13), indicating that the balloon response is mainly due to the transmission characteristics of the catheter.

Figure 2.15 Phase Response of Standard CVR Balloon

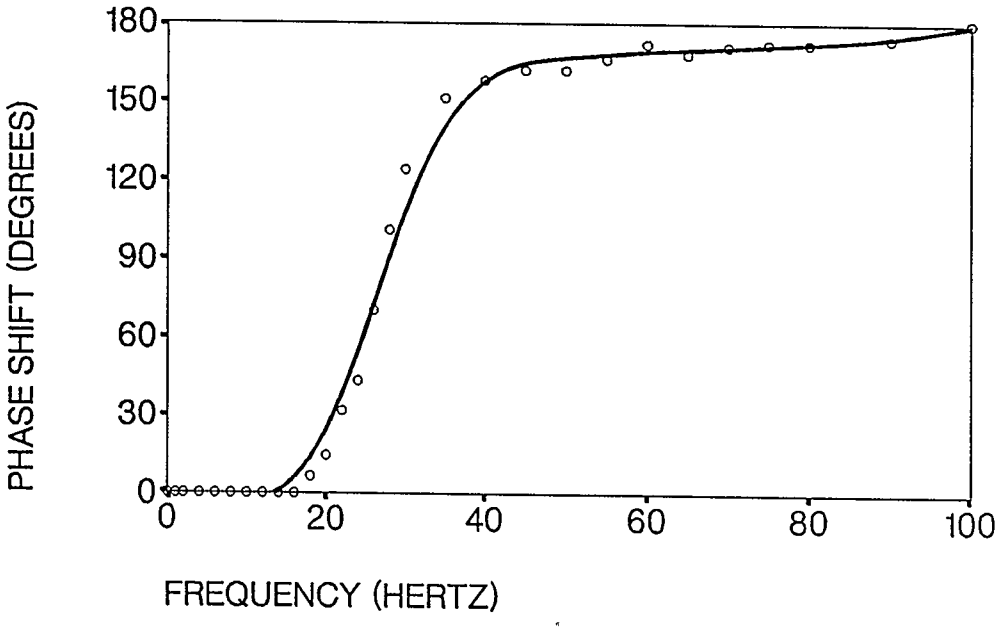

The phase response (degrees) for the CVR pericardial balloon is given with the phase shift from 0 to 180 degrees occurring around the resonant peak (see Figure 2.14) with a phase shift of 90 degrees corresponding to the peak resonance, typical of a 2nd-order resonant system.

Figure 2.16 Frequency Response of High-Fidelity CVR Balloon

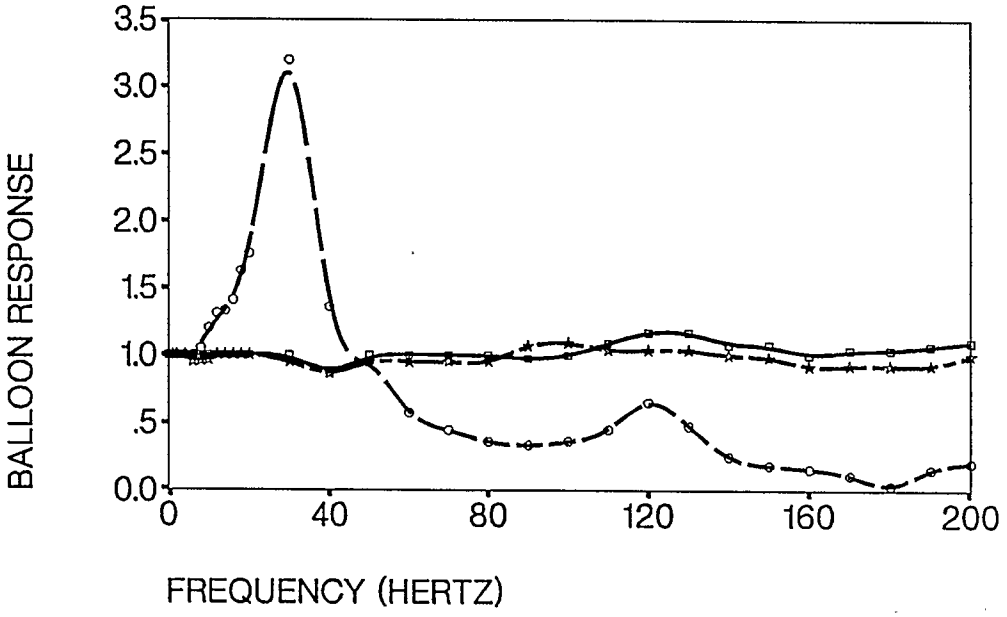

The high-fidelity CVR balloon response (solid line, data points = squares) is compared to the load cell response (dashed line, data points = stars). The load cell and the high-frequency balloon have similarly flat frequency response characteristics up to 200 Hz. The connecting catheter response (dashed line, data points = circles) is similar to the standard CVR balloon response (see Figure 2.14) with the peak resonant balloon response being slightly less. This may be caused by the electrical signal cable for the 3-F micro strain-gauge tipped catheter which runs through the lumen of the connecting 7-F angiographic catheter and perhaps alters its transmission characteristics.

Figure 2.17 Sweeped Frequency Response of the High Fidelity Balloon

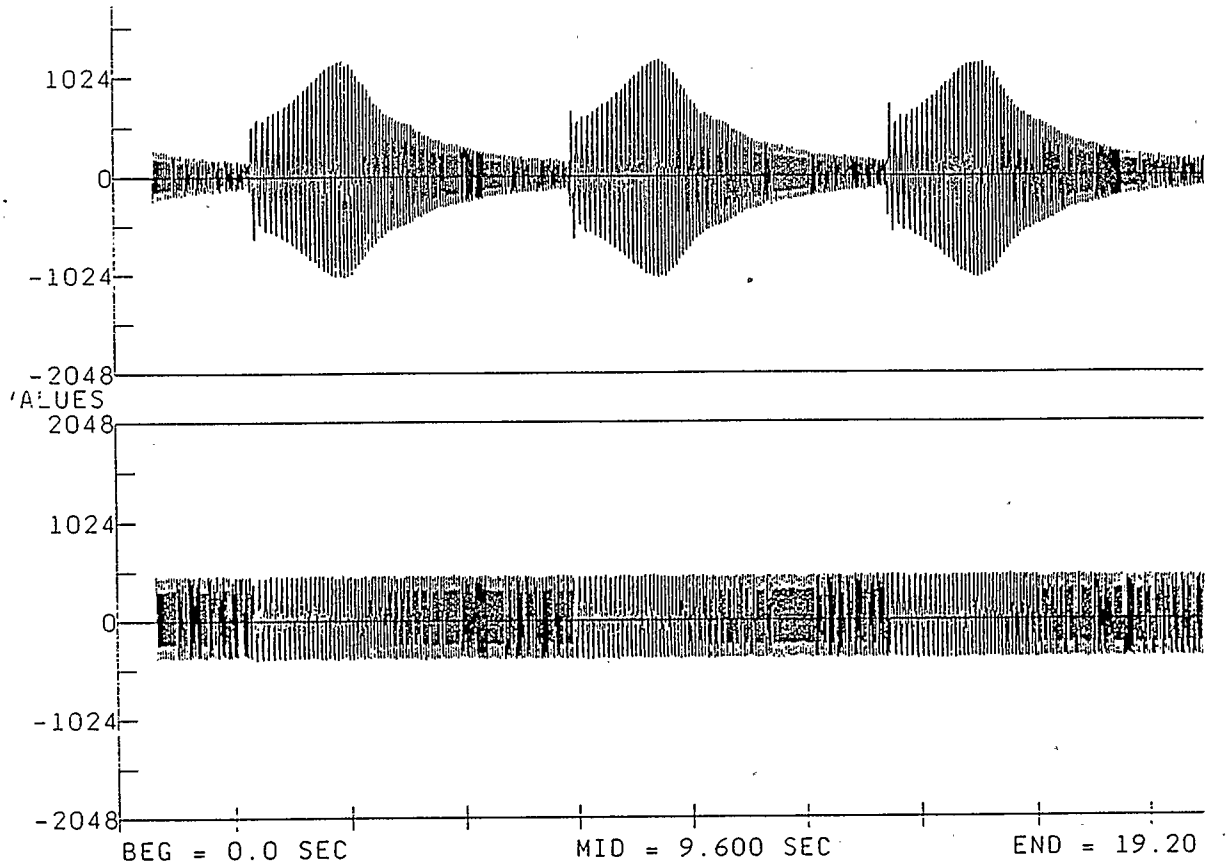

The upper panel shows the time-domain response of the standard CVR balloon when exposed to frequency sweeps ranging from 10 to 50 Hz repeating every 6 seconds. The standard CVR balloon response creates a peak amplitude envelope which is similar to its frequency response plot (see figure 2.14). The lower panel is the time-domain response of the high-fidelity balloon exposed to the same sweeps showing a flat amplitude envelope indicating its superior frequency response characteristics.

Figure 2.18 Comparison of the Standard CVR Pericardial Balloon to the High Fidelity CVR Balloon in the Calculation of Transmural Pressure

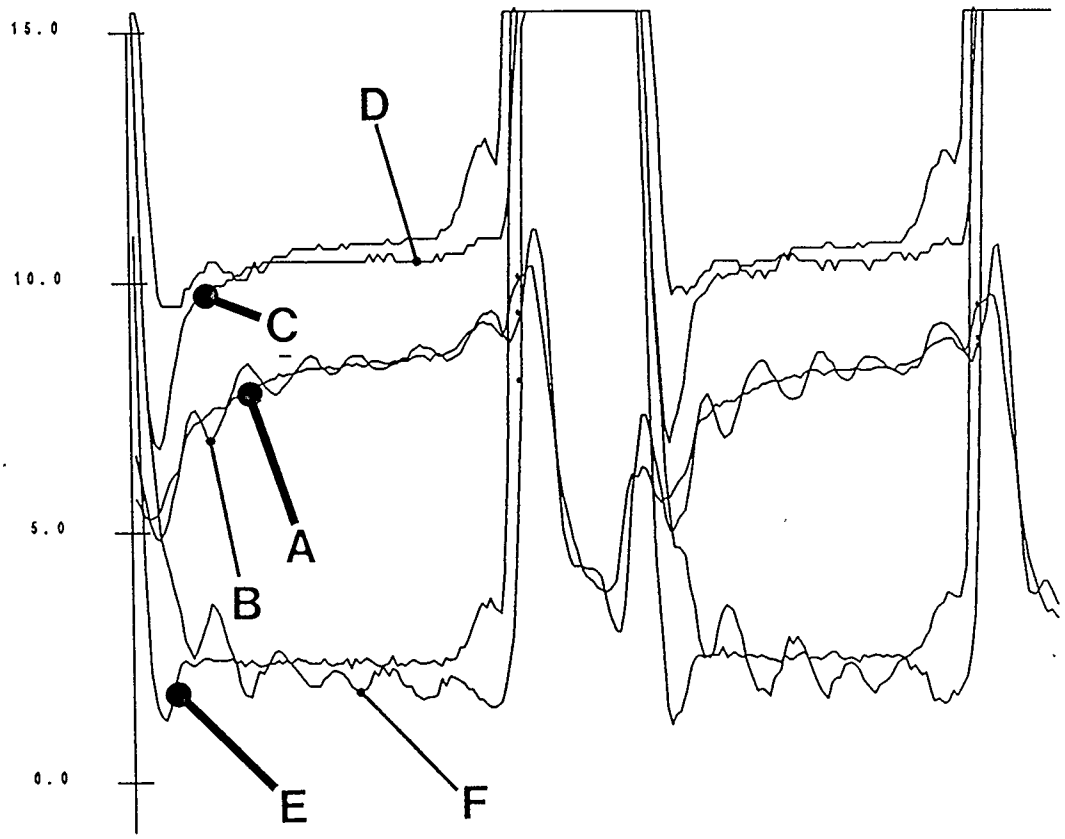

Time-domain plot of the high-fidelity balloon (A), and its connecting catheter (B), intracavitary micro strain-gauge catheter (C) and fluid-filled intracavitary catheter (D) in a dog. The high-fidelity transmural pressure (E) is calculated using the high-fidelity signals (E = A-C). The conventional transmural pressure is calculated using signals from the fluid-filled (F) lumens (F = B-D). Notice the substantial "ring" that occurs in the fluid-filled lumens when compared to their high-fidelity counterparts. However, this ring settles at end diastole, giving rise to similar transmural pressure measurements.

Figure 2.19 Comparison of the Standard CVR Pericardial Balloon to the High Fidelity CVR Balloon in the Pericardial Space With Catheter Motion Induced Artifacts

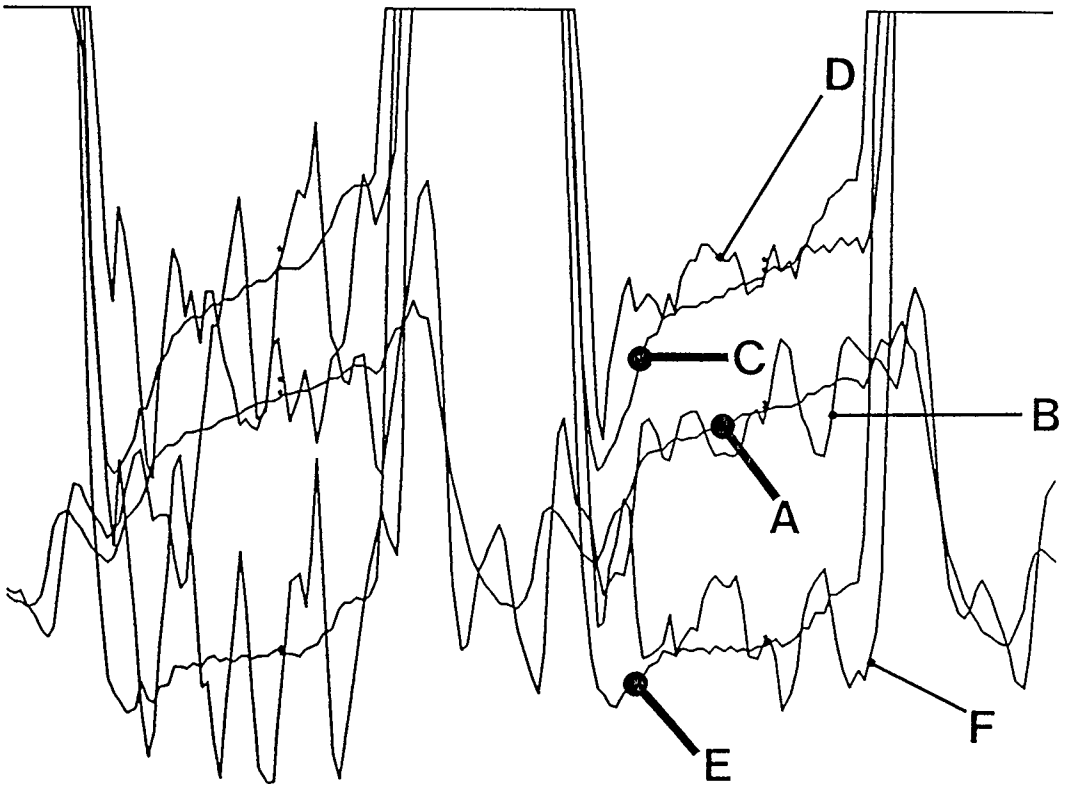

Notice the extreme catheter motion induced ringing that occurs in the fluid-filled lumens when compared to their high-fidelity counterparts. This ring would prevent a researcher from making any transmural pressure measurements if only fluid-filled transducers were used. Time-domain plot of the high-fidelity balloon (A), and its connecting angiography catheter (B), intracavitary micro strain-gauge catheter (C) and fluid-filled intracavitary catheter (D) in a dog. The high-fidelity transmural pressure (E) is calculated using the high-fidelity signals (E = A-C). The conventional transmural pressure is calculated using signals from the fluid-filled (F) lumens (F = B-D).

Figure 2.20 Transmural Pressure Dimension-Loop of the Left Ventricular During an Inferior Vena Cava Occlusion Using a CVR High-Fidelity Pericardial Balloon

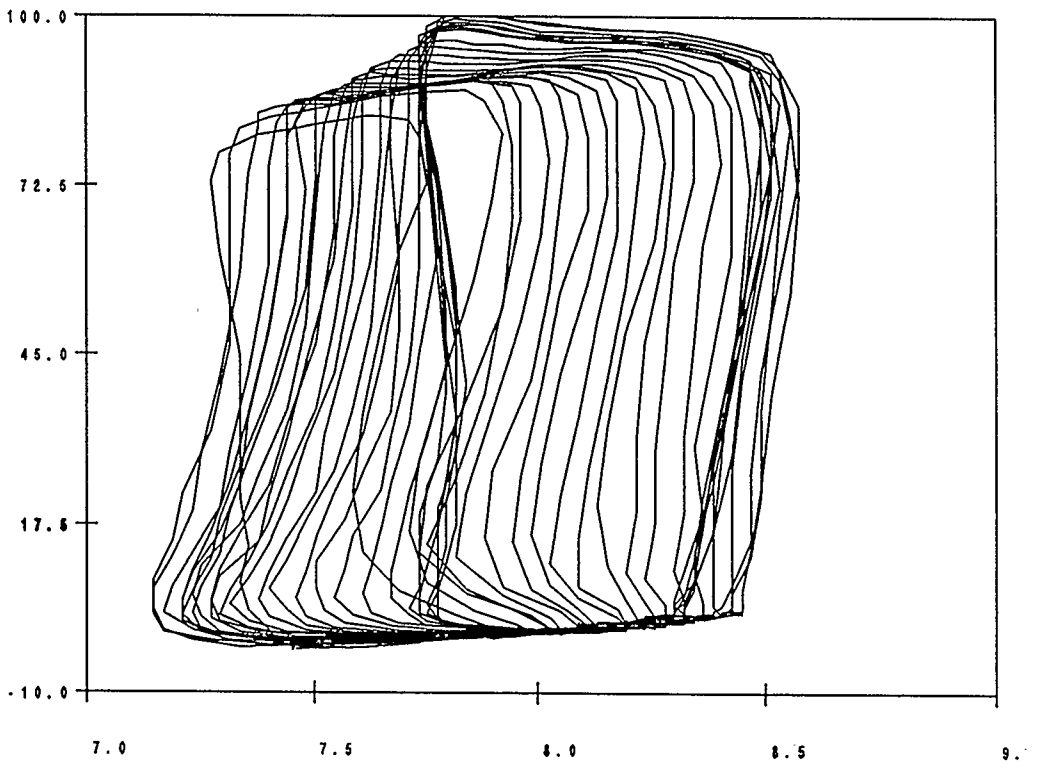

LV transmural pressure-dimension loop (Y axis = pressure, X axis = dimension) obtained using a high-fidelity CVR pericardial balloon. The superior dynamic response of the high-fidelity pericardial balloons allows the researcher to examine transmural function, throughout the whole cardiac cycle, with an intact pericardium. The leftward shift of the transmural pressure-dimension loops during an inferior vena cava occlusion are easily visualized due to the low noise and absent catheter ring which fluid-filled balloon transducer systems would have created.

Figure 2.21 High-Gain Plot of a Transmural Pressure-Dimension Loop During an Inferior Vena Cava Occlusion Using a CVR High-Fidelity Pericardial Balloon

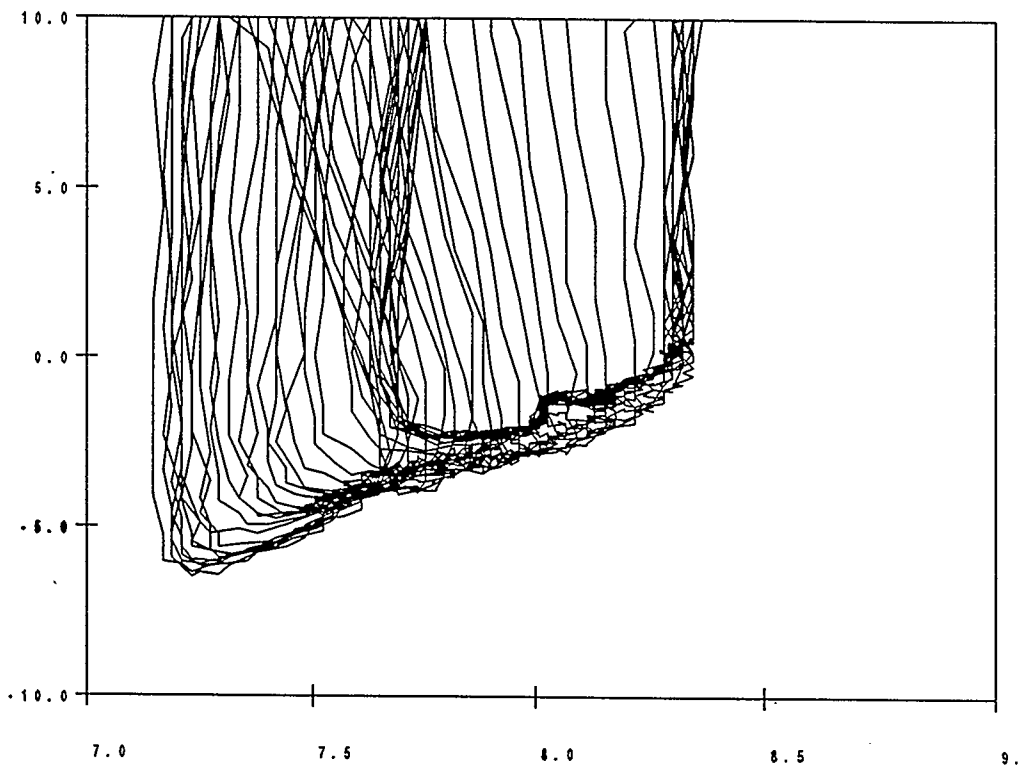

High-gain LV transmural pressure-dimension loop (Y axis = pressure(mm Hg), X axis = LV segment length mm) obtained using a high-fidelity CVR pericardial balloon showing the LV end-systolic transmural pressure becoming substantially negative during an inferior vena cava occlusion. Fluid-filled transducer systems underestimate the magnitude of negative LV transmural pressure developed at end-systole (see Figure 2.18). This is the first time end-systolic negative LV transmural pressure, with a bandwidth of 100 Hz, has been measured in an intact pericardium.

Figure 2.22 CVR Static Balloon Calibrator - Drawing #1

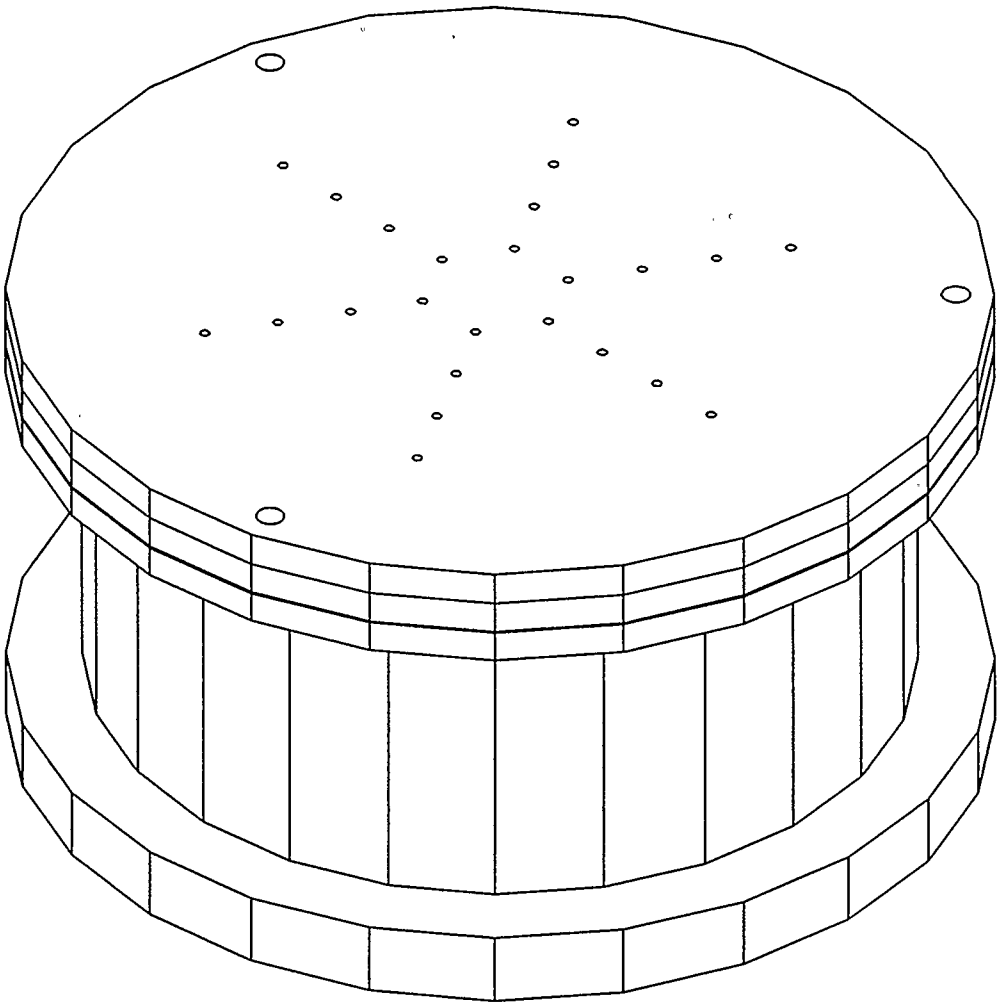

Upper angled view of the CVR static balloon calibrator (actually drawn upside-down to visualize the balloon support plate). Therefore the uppermost structure is the balloon support plate (see next page). The pressure chamber (lower structure) and the membrane support ring (middle structure) hold the thin silastic™ balloon stressing membrane (see exploded diagram - Figure 2.24). Notice the holes in the balloon support disk which allow air trapped between it and the silastic™ membrane to escape. Three bolt holes, which are threaded through the balloon support disk, membrane support ring and the pressure chamber can be seen on the balloon support disk.

Figure 2.23 CVR Static Balloon Calibrator - Drawing #2

Balloon support disk:

[A] showing holes which allow trapped air to escape.

[B] a groove to allow the silastic™ balloon tubing to exit the calibrator.

[C] bolt holes for easy assembly / disassembly.

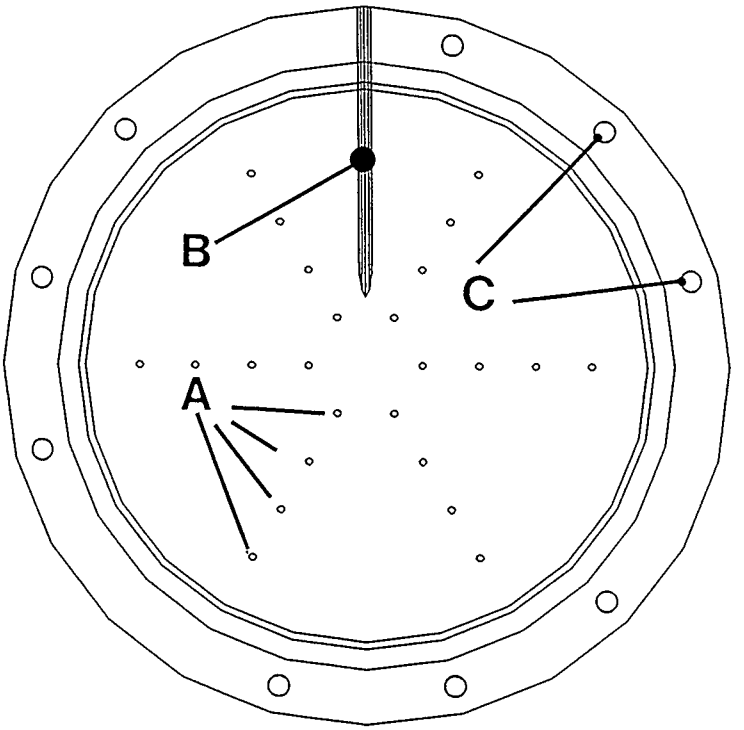

Side view showing (hidden lines not removed) the grove in the balloon support plate which allows the balloon silastic™ tubing to exit the calibrator. Notice the balloon support plate is recessed to lie flush with the stressing membrane. The membrane support ring fits (A) into the balloon support ring (B).

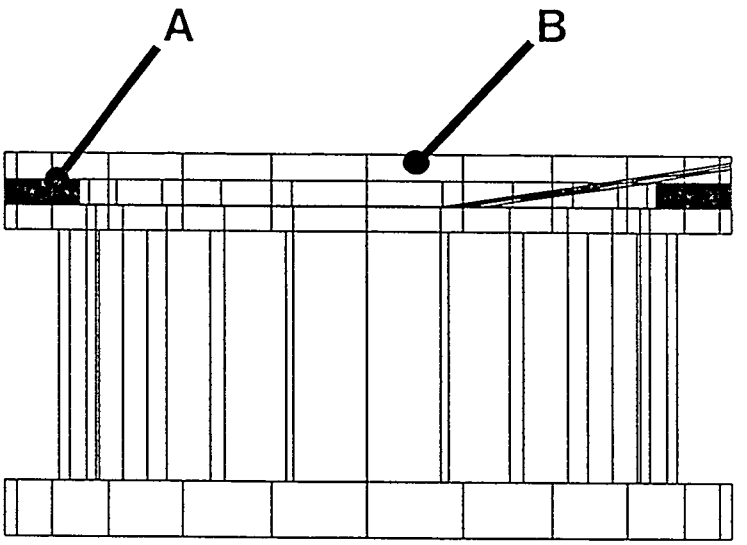

Figure 2.24 CVR Static Balloon Calibrator - Drawing #3

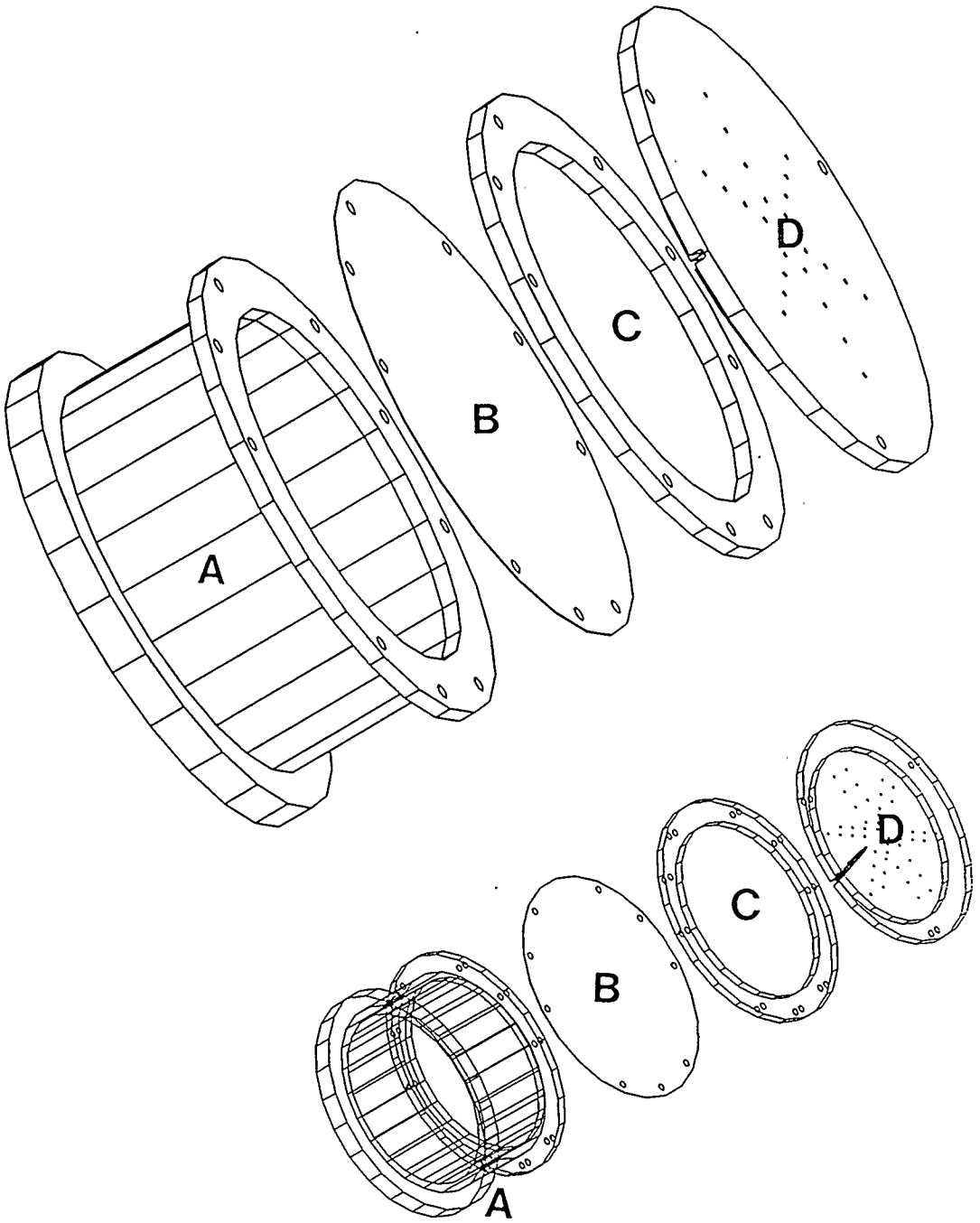

Exploded parts view from two different perspectives (upper = hidden lines removed) showing the pressure chamber (A), silastic™ membrane (B), membrane support ring (C) and the balloon support disk (D).

Figure 2.25 CVR Dynamic Balloon Calibrator

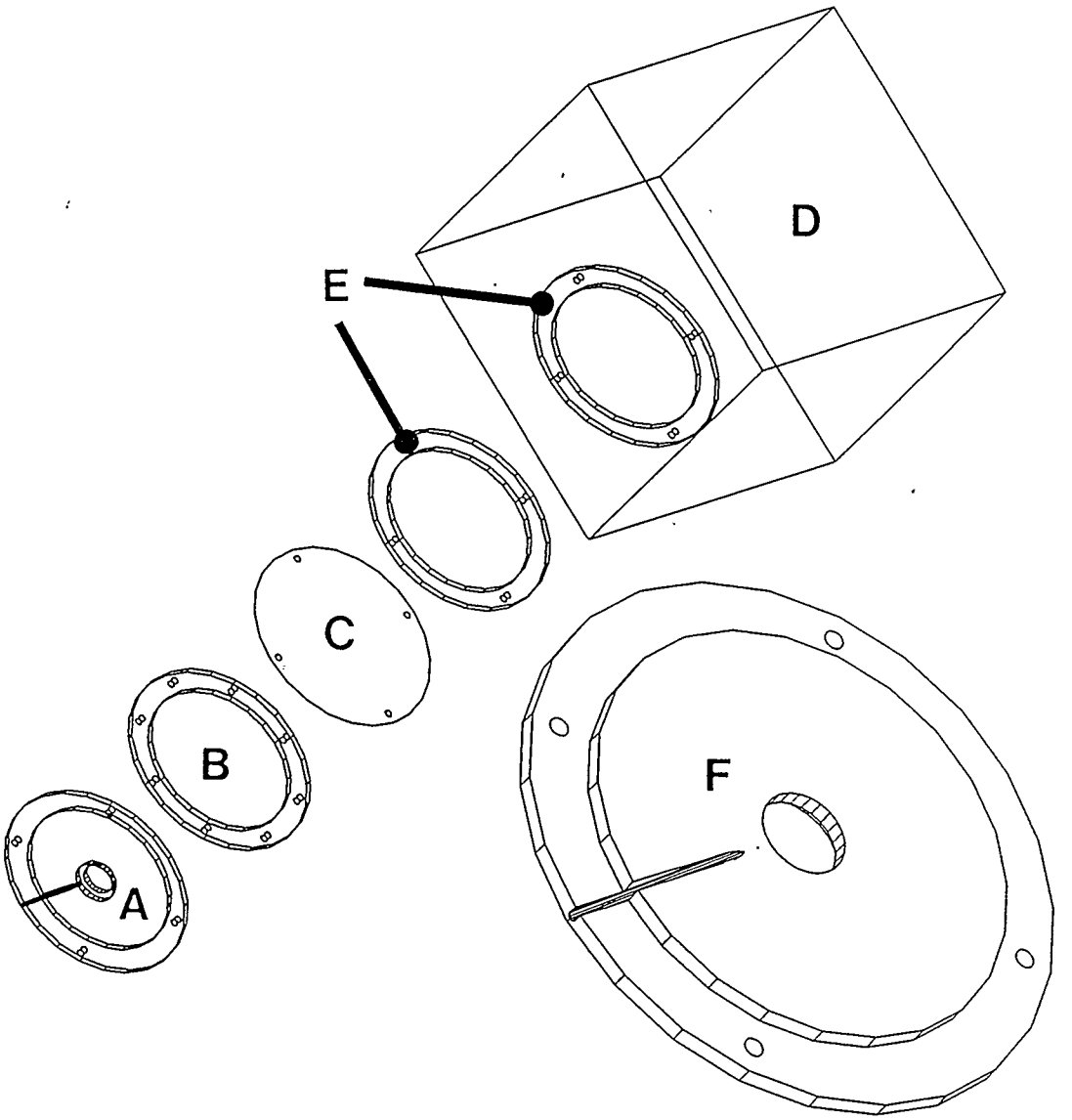

Exploded parts view showing the CVR dynamic balloon calibrator. The assembly is similar to the static balloon calibrator with a balloon support plate (A), membrane support ring (B), silastic™ membrane (C) and a larger pressure chamber (D). A speaker support ring (E) to mount the sub-woofer is bonded to the pressurizing chamber. A larger drawing of the balloon support plate (F) is drawn (lower right), showing the centre mounting hole for the load cell.

Chapter 3

RIGHT ATRIAL AND RIGHT VENTRICULAR TRANSMURAL PRESSURE IN THE HUMAN AND TRANSMURAL PRESSURE-DIMENSION RELATIONSHIPS IN THE DOG: THE EFFECTS OF THE PERICARDIUM

Introduction

The role the pericardium plays in the behaviour of cardiac hemodynamics has stimulated the curiosity of physiologists for many years. The fact that the pericardium can be a significant constraint to the filling of the heart was reported almost a century ago (1898) by Barnard (4). In a simple experiment he isolated and acutely inflated the pericardium of a dog with a bicycle pump to observe that it would not rupture until pressures of approximately 950 to 1330 mm Hg were obtained. Barnard further observed that, while within its pericardium, a cat's heart would hold 12 ml at a filling pressure of 20 cm H_2O and this increased to 23 ml when the pericardium was removed. Upon pericardiectomy he noted that, "this extra quantity of blood is chiefly received by the right auricle and ventricle" (4). From these and other experiments Barnard concluded, "When a relaxed heart is subject to a venous

pressure of from 10 to 20 mm Hg., the pericardium takes the strain and prevents dilatation of the heart beyond a certain point. Thus the mechanical disadvantages of dilated cavities and of a thinned wall are prevented."(4). Barnard's observations that the parietal pericardium exerts a significant stress on the epicardium are undeniable but efforts to measure this constraint directly in the absence of abnormal pericardial effusions have yielded conflicting results (11,27,28,61). The direct measurement of epicardial radial stress (pericardial pressure) has been attempted through the use of open-end catheters (6,8,29,62), air-filled balloons (30,31,57,63) and liquid-filled balloons (7,32,64), inserted into the pericardial space. The magnitude of epicardial radial stress measured by these devices has ranged from zero to nearly the magnitude of the cavitary pressure of the chamber being investigated. As Tyberg et al (65) originally proposed, the magnitude of pericardial constraint may be determined by measuring the fall in cavitary pressure (eg, ΔLVEDP) after pericardiectomy, measured at the same cavitary volume or strain. This method of determining pericardial constraint has been used by many investigators (11,52,53,66). Traboulsi et al (66) found that the magnitude of the right ventricular (RV) transmural pressure measured using liquid-containing balloon transducers over a wide range of physiological end diastolic pressures was slightly above zero and difficult to resolve from zero at lower filling pressures using presently available transducer systems. At the RV strain observed when the pericardium-intact cavitary pressure was 20 mm Hg, the

RV transmural pressure measured with the pericardium removed was only 2-3 mm Hg.

Traboulsi (66) also showed that the RV can undergo very large strains even when exposed to small transmural pressures. Only when the RV strains were extreme did the magnitude of these transmural pressures rise above 5 mm Hg and these were obtained only when the constraint of the pericardium was removed. These results show that the pericardium is primarily responsible for the RV cavitary pressure-volume relationship but do not imply that the right ventricular transmural pressure-volume relationship is flat or has a slope of zero.

Rationale

The fact that the right ventricle (RV) fills during diastole while the right atrium (RV) empties suggests that the effective compliance of the RV is greater than that of the RA, as Nagano and his colleagues demonstrated (67). However, the RA is a thinner structure which would be expected to be more distensible than the RV. Previous studies performed in this laboratory have shown that, when the constraint of the pericardium is properly measured by a balloon transducer (11), pericardial pressure (more precisely, epicardial radial stress) accounts for the substantial difference (at a given chamber dimension) between the cavitary pressure recorded when the pericardium is intact and that recorded after the pericardium has been removed (ΔLVEDP). Since the

RV transmural pressure-volume relation is mostly dependent on the pericardium (66) and that the RA is an even thinner, more distensible structure, it seems reasonable to suggest that the pericardium might also be a major contributor to the RA cavitary pressure-dimension relationship.

Thus, our hypothesis was that it is the effect of the pericardium that makes the effective chamber compliance of the right atrium less than (or, at least, comparable to) that of the RV, even though, the RA is apparently more distensible without the pericardium.

Methods - Animal

After receiving 10 - 20 mg morphine sulfate (i.m.), six mongrel dogs (20-25 Kg.) of both sexes were anaesthetized with 12.5 mg/Kg sodium thiopental. Anaesthesia was maintained with 30 μg/Kg/min fentanyl while ventilation with a 2:1 nitrous oxide:oxygen mixture was delivered by a constant-volume ventilator (Model 607, Harvard Apparatus, Millis, Massachusetts). All dogs received a tidal volume of 15 ml/kg and a positive end-expiratory pressure of 2 cm H_2O was applied. 3 The animals were maintained at 37°C using a circulating-water warming blanket and a constant temperature heating system (Haake Model FE2, Berlin, Germany). The ECG was continuously monitored throughout the experiment.

With the dog in the supine position, a midline sternotomy was performed and 100 to 200 ml of heparinized Ringer's lactate solution were

infused to maintain normal aortic pressure. The left lateral surface of the pericardium was opened using a longitudinal incision, with the ventricles delivered through this incision for purposes of instrumentation. RV free-wall segment length (L_{rv}) and RA appendage diameter (D_{ra}) were measured by sonomicrometry (Triton Technology, San Diego, California) as previously described by Smiseth et al (33). Two flat liquid-containing balloon transducers were attached loosely to the epicardium with single stay sutures; one was positioned over the RV free wall adjacent to the crystals, and the other was positioned cephalad to the sonomicrometer crystals on the RA appendage. The heart was repositioned into the pericardium and the pericardial margins reapproximated using interrupted 3-0 silk sutures spaced 1 cm apart, taking care to avoid compromising pericardial volume. RV and RA cavitary pressures were measured using 8F micromanometer-tipped catheters with reference lumens (Model PR279, Millar Instruments, Houston, Texas) inserted through the internal jugular and femoral veins, respectively. Aortic pressure was measured with an 8-F fluid-filled catheter (Cordis Corporation, Miami, Florida) introduced through the femoral artery. Inferior vena cava and pulmonary arterial pneumatic vascular constrictors were also positioned on all dogs. The RV balloon (3.0 cm x 3.0 cm) was fabricated from Silastic sheets (compound AR131, Lot #0170, Dow Corning Corporation, Midland, Michigan) and attached to a 70-cm 8F cardiac catheter (Cordis Corporation, Miami, Florida). The RA balloon dimensions were 1.2 cm x 1.4 cm with a 20-cm length of

Silastic medical grade tubing (1.0 mm i.d., 2.2 mm o.d., Dow Corning Corporation) connected directly to a pressure transducer (Model P23 Db Statham-Gould, Oxnard, California). A calibration curve for both balloons and transducers was described before and after each experiment using a pressurized chamber which loaded the balloons with a membrane similar to those used by McMahon et al (58,68). No differences between pre- and post-experiment calibration curves were found in any experiment. Each balloon had a 3F micromanometer-tipped catheter (Model PR249, Millar Instruments) positioned internally to provide a high fidelity measurement of balloon pressure. Intra-balloon catheter-tip pressure transducers do not sense the artifacts and oscillations generated from catheter motion and also are free of the frequency-dependent transmission characteristics of fluid-filled tubes. The dynamic response of this high fidelity balloon pressure measuring system is linear with a flat frequency response to 200 Hz (68).

Conditioned signals (Model VR16, Electronics for Medicine, White Plains, New York) were acquired using a computer (Model PDP-11/23 MINC, Digital Equipment Corporation, Maynard, Massachusetts). The analog signals (pressure, dimension and ECG) were scaled using gain and offset amplifiers and then filtered with a 7th order Cauer elliptic lowpass active anti-aliasing filter (cutoff frequency = 100 Hz, 78dB attenuation at floor = 165 Hz, Model 675, Frequency Devices, Haverhill, Massachusetts) before being sampled at 200 Hz using a 12-bit analog-to-digital converter. The digitized data were subse-

quently analyzed on a computer (Model VAX 11/750, Digital Equipment Corporation), using analytical software developed in our laboratory and statistical and graphics software (SPSS Incorporated, Chicago, Illinois).

After preparatory surgery, all animals were stabilized for 1/2 hour before any data were recorded. Mean RA pressure was caused to vary from 0 to 25 mm Hg by adjusting intravascular volume (Ringer's lactate solution was infused or blood removed through a large-bore catheter in an external jugular vein) or by manipulating the inferior vena cava or pulmonary artery vascular pneumatic occluders (In Vivo Metric Systems, Healdsburg, California). Hemodynamic and sonomicrometer measurements were obtained continuously for 1 minute at each volume load state (ie. after each incremental increase of mean RA cavitary pressure), each recording interval beginning with a 20-second control period. The ventilation was interrupted at the end-expiratory position for several cardiac cycles during each recording interval. After reducing mean RA pressure to 4-5 mm Hg by haemorrhage, the pericardium was opened widely to eliminate any external constraint on the right side of the heart. After removal of the pericardium the animal was again allowed to stabilize for 1/2 hour and previous methods were again used to manipulate mean right atrial pressure.

Methods - Human

Seven patients (age 19-76 years) scheduled for elective cardiac surgery

gave informed written consent to participate in this study. The protocol had been previously been reviewed and approved by a joint University-Hospital ethics committee. Patient data are given in Table 3.1. No patient had valvular disease or right ventricular hypertrophy. General anaesthesia was induced with an intravenous combination of 2-7 mg. of midazolam, 500 mcg of sulfenta, and vecuronium bromide (0.08 to 0.10 mg/Kg). Anaesthesia was maintained with: (1) sulfenta (8 mcg/Kg iv), or (2) fentanyl (25 mcg/Kg iv) and isoflurane, or (3) enflurane. A median sternotomy exposed the pericardial sac. One-centimetre horizontal pericardial incision was over the RV. Through this aperture, a previously described 3 cm. X 3 cm., flat, liquid-containing Silastic balloon was inserted and positioned to lie over the RV free wall. A 7.5F Swan Ganz catheter (Model 93A-931H-7.5F Thermodilution Paceport(tm) Catheter with Thromboshield(tm), American Edwards Laboratories, Anasco, Puerto Rico) was also inserted. The pericardial balloons were calibrated before sterilization. Following gas sterilization, the previously determined volume of saline was injected into the balloons after they had been flushed to remove all air. A calibration curve for each balloon was also described after each experiment, using the same methods described in the animal protocol. Post-operatively, all balloons were found to calibrate linearly within 1 mm Hg applied pressure in the balloon calibrator chamber. The volume of saline in the balloon was measured after the experiment and compared to the amount injected pre-operatively to detect inadvertent volume changes.

Stay sutures were placed at the edges of the pericardotomy and secured to the balloon catheters to prevent excessive motion. The Swan-Ganz catheter was used to measure central venous pressure, RV pressure (measured from the RV pacing port), pulmonary arterial and pulmonary capillary wedge pressure. All pressures were measured using disposable semiconductor strain-gauge pressure transducers (Trantec(tm) Disposable Pressure Transducer, American Hospital Supply, Irvine, California) connected to a patient monitoring system (Model 78534C, Hewlett-Packard, Palo Alto, California). All transducers were calibrated using internal calibration signals and then checked post-operatively using a mercury manometer, before being disconnected from the patient monitoring system. Post-operatively all transducers were found to calibrate linearly to 100 mm Hg. Conditioned signals were acquired on a computer (Model 2551 80286/80287 12-MHz personal computer, Compaq Computer Corporation, Houston, Texas) using a 12-bit analog-to-digital converter (Model 2801, Data Translation, Marlboro, Massachusetts). The analog signals were scaled using gain and offset amplifiers and then filtered with a 7th order Cauer elliptic lowpass active anti-aliasing filter (cutoff frequency = 100 Hz, 78dB attenuation at floor = 165 Hz, Model 675, Frequency Devices, Haverhill Massachusetts) before being sampled at 200 Hz. The digitized data were subsequently analyzed on a computer (Model ST-1144A Packard Bell 386X 80386/80387 Personal Computer, Chatsworth, California) , using analytical software developed in our

laboratory (CVSOFT, Odessa Computer Systems Limited, Calgary, Alberta) and statistical and graphics software (SPSS Incorporated, Chicago, Illinois) running on a multi-tasking computer (Model VAX 11/750 Digital Equipment Corporation, VMS version 4.6, operating system).

Before each set of measurements was made the pressure transducers were zeroed at the mid-plane of the left ventricle. Volume loading was achieved by an intravenous infusion of 1-2 litres of Ringer's lactate or normal saline. In two cases, 100 ml of 25% albumin was given in addition to the cystalloid solutions. Depending on the patient's status during the operative procedure the mean central venous pressure was increased 5 - 10 mm Hg from baseline during volume loading. The right sided pericardial balloon was initially placed over the RA to measure RA pericardial pressure (this was not done on patient # 1) and then repositioned over the RV during volume loading. This balloon then remained over the RV throughout the volume loading. When the post-volume load central venous pressure had stabilized at its highest value the balloon was moved back over the RA. This protocol allowed the measurement of RA pericardial pressures at the lowest and highest central venous pressure obtained. The RV pericardial pressure was measured continuously throughout the volume load.

Data Analysis - Animal Studies

Only data collected at end expiration were analyzed. All high fidelity micromanometer-tipped catheter signals were corrected to equal its corresponding pressure recorded via the fluid-filled catheter at end diastole. This correction was performed using software that automatically adjusted the mean pressure of the micromanometer-tipped catheter to equal the mean of its fluid-filled counterpart. This method was completely automatic and therefore eliminated operator input; nonetheless, all pressure tracing corrections were inspected visually to ensure validity, although no adjustments were made. With the pericardium intact, transmural pressure was calculated as cavitary pressure minus pericardial balloon pressure. Upon pericardiectomy and retraction of the lungs, epicardial radial stress was reduced to zero and, therefore, transmural pressure became equal to cavitary pressure.

All data were collected over 60-second intervals. The post-experiment analysis involved the extraction of the last three late-diastolic data points which immediately preceded atrial contraction from the sampled data file (5 milliseconds sampling interval).

The unstressed cavitary dimension was determined to provide a means of comparing the pericardiectomy-effected changes in dimension between both chambers and among all six dogs. Due to the asymptotic behaviour of the RA and RV transmural pressure-dimension relationships (ie, at low transmural pressures, the slope approached zero), the determination of the

unstressed dimensions was difficult and no single type of regression equation seemed satisfactory for the analysis of all animals. Therefore, using transmural pressure-cavitary dimension (X) data before (ie, calculated transmural pressure) and after pericardiectomy, the unstressed cavitary dimension (X_0), for each dog was calculated using three different least-squares regression techniques.

1.) The natural logarithm of the transmural pressure was used as the dependent variable in a linear regression analysis (52):

$$\ln(P_{trans}) = Mx + b$$

The 0.1 mm Hg and 1.0 mm Hg intercept and slope of this linear regression equation were used to determine the unstressed cavitary dimension. This technique could not be employed for data sets which contained negative pressures. (When the transmural pressures approached zero, the noise in the transducer systems occasionally produced individual negative values, even though the statistical mean of several nearby points was zero or slightly positive, see figure 3.22)

2.) A 3-parameter exponential function to determine the unstressed cavitary dimension:

Visual inspection of the raw data points and the corresponding

$$P_{trans} = A * e^{B*x} + C$$

exponential regression line derived for the pressure-dimension relationship of the respective cavity indicated that this regression equation follows the cavitary pressure-dimension relationship quite convincingly. Furthermore, this regression method is capable of handling negative pressure data points (see figure 3.19 and 3.20).

3.) A cubic equation:

$$P_{trans} = A * X^3 + B * X^2 + C * X + D$$

This regression equation was very effective at creating solutions which intersected the P = 0 line and thereby defined the unstressed dimension, but, in some animals, the derived cavitary pressure-dimension relationship did not model the behaviour of a simple elastic vessel (ie, pressure did not always increase monotonically with dimension, see figure 3.21).

For the RV and RA data from each dog, the value of the unstressed dimension defined by each regression equation was compared to the distribution of the pericardium-intact cavitary pressure-dimension data to determine which technique was best. A pericardium-intact cavitary pressure-

dimension relationship was described by connecting the raw data points with straight lines as pressure increased. The unstressed dimension was chosen using the following rules.

1.) If the pericardium-intact cavitary pressure-dimension relationship and the transmural regression curve intersected, the unstressed length was taken to be the point of intersection.

2.) If the pericardium-intact cavitary pressure-dimension relationship and transmural pressure-dimension curve did not intersect but the pericardium-intact cavitary pressure-dimension relationship came within 2 mm Hg of the transmural pressure regression curve, that point (at which the difference was less than 2 mm Hg) was taken as the unstressed length.

3.) If the pericardium-intact cavitary pressure-dimension relationship and transmural pressure-dimension curve did not intersect or approach within 2 mm Hg of each other, then the smallest cavitary dimension measured was taken to be the unstressed dimension.

The raw data for dog1 is displayed in Figure 3.1 with a reference line indicating the chosen unstressed dimension, X_o. The percent strain for each cavity was calculated using the unstressed dimension, X_o, in the following formula:

$$Strain(\%) = \frac{(X - X_0)}{X_0} * 100\%$$

The RA and RV pericardium-intact cavitary pressure and transmural pressure - strain curves for all dogs were compared using two methods:

1) The estimated increase in strain that would have been observed when the pericardium was removed had the cavitary pressures of 5, 10 and 15 mm Hg been maintained. (see Figure 3.8). Strain was determined by linearly interpolating between the pressure values closest to the nominal cavitary pressure.

2) The estimated decrease in cavitary pressure that would have been observed when the pericardium was removed had strain remained constant (ie. ΔEDP) was determined at strains corresponding to cavitary pressures (measured with an intact pericardium) of 5, 10 and 15 mm Hg.(see Figure 3.9). The

decrease in pressure was calculated by linearly interpolating between pericardium-intact intracavitary pressures closest to the nominal pressures (ie, 5, 10 or 15 mm Hg.) and subtracting the transmural pressure at the same strain. The transmural pressure was calculated using the 3-parameter exponential regression equation.

Data Analysis - Human Studies

RV transmural pressure was calculated as RV intracavitary pressure (measured from the pacing port of the Swan-Ganz catheter) minus pericardial balloon pressure. RA transmural pressure was calculated as central venous pressure (measured from the CVP port of the Swan-Ganz catheter) minus pericardial balloon pressure. The pericardial balloon was connected to its respective transducer via a 100-cm length of extension tubing. All data were collected over 60-second intervals. The zero reference level ports of all transducers were all mounted on a rack to ensure that they remained at the same hydrostatic level. The error in each pressure measurement was found to be within ± 1 mm Hg when the automatic balancing and gain adjustment features of the patient monitoring system were calibrated against a mercury manometer. Therefore, the error in the calculated transmural pressures could have been no more than $\pm$ 2 mm Hg. These errors should have been random and should not have affected the mean values of the pooled data.

The post-experiment analysis involved the extraction of last three late-diastolic data points (5 milliseconds sampling interval) immediately preceding atrial contraction. To compensate for the delay introduced by the extension tubing, a correction of 50 milliseconds was use to temporally align the pericardial pressures to those obtained from the Swan-Ganz catheter (the time shift from the various Swan-Ganz ports was negligible for the purposes of this study). Any significant motion-induced oscillations in the pressure tracings were filtered using a 101-term, finite impulse response, linear phase digital lowpass, time-corrected filter (breakpoint = 20 Hz, attenuation of 80 db in 5 Hz, Remez exchange algorithm, Signal Technology Incorporated, Santa Barbara, California).

Results

Animal Studies

The results from the six animals consistently showed large changes in the chamber pressure-dimension relationships upon the removal of the pericardium (see Figures 3.1 to 3.7). The transmural pressure of both chambers was calculated using the difference between cavitary pressure and pericardial pressure when the pericardium was intact. Transmural pressure was equal to the intracavitary pressure after the pericardium had been removed, assuming no constraint by other structures (eg, the lungs). As is evident in Figures 3.2 to 3.7, the transmural pressure calculated with the

pericardium intact and the intracavitary pressure after pericardiectomy tended to form a single curvilinear relationship (with respect to %strain) for all dogs.

Table 3.2 shows the percent increases in cavitary strain after the pericardium was removed, compared at various end-diastolic pressures (see Figure 3.8). The RV distended much less than the RA after pericardiectomy. The increase in RV strain and RA strain induced by pericardiectomy, for all dogs, is shown in Figure 3.9. Although the pericardium-on and pericardium-off pressure-strain curves continued to diverge somewhat at high pressures (Figures 3.2 to 3.7), most of the increase in strain with pericardiectomy was achieved at low pressures (ie, 5 mm Hg).

Table 3.3 shows the reduction in cavitary pressure (ΔEDP) required to maintain the same strain after the removal of the pericardium. (see Figure 3.10) The fall in cavitary pressure (ΔEDP) tabulated in Table 3.4 indicates that the transmural pressure of either chamber does not contribute substantively to its end-diastolic cavitary pressure. Furthermore, over the range of strains experienced physiologically with an intact pericardium (ie, pericardium-on cavitary pressure < 15 mm Hg), the transmural pressure-volume relation of the RV is almost flat and we are unable to distinguish the RA transmural pressure from zero.

Figure 3.11 shows the right ventricular cavitary pressure plotted against RV pericardial pressure measured with our balloon. This plot shows that the RV cavitary pressure at any volume is mostly due to pericardial constraint.

The same conclusion can be reached in Figure 3.12 which shows RA cavitary pressure plotted against RA pericardial pressure measured with our small atrial balloon.

Figure 3.13 and 3.14 represents the pooled data of all dogs and shows the RV and RA transmural pressure (before and after pericardiectomy) plotted against cavitary strain. The RA is much more distensible than the RV.

Results - Human Studies

The RA transmural and cavitary pressure measured in six patients is plotted vs CVP in Figure 3.15. The RA pericardial pressure rises in a 1:1 ratio with central venous pressure describing a line of identity. The slope (1.10) and intercept (-1.85) of the regression line (correlation coefficient = 0.95, $p<0.0005$) describing the relationship between central venous pressure and RA pericardial pressure indicates that the RA transmural pressure is very small and cannot be distinguished from zero. The calculated RA transmural pressure (CVP minus RA pericardial pressure) was 1.0 $\pm$ 1.5 over CVPs ranging from 3 to 16 mm Hg.

The data shown in figure 3.15 shows that there was no discernible relationship between RA transmural pressure and central venous pressure. This is in agreement with the animal data which shows extremely small transmural pressures found at physiological RA pressures (5 to 14 mm Hg).

The protocol for the human study allowed for the continuous

measurement of RV cavitary and pericardial pressure and therefore, the calculation of transmural pressure over the range of CVPs obtained during the volume load. Table 3.4 gives the linear regression coefficients which describe the RV cavitary, pericardial and transmural pressure vs CVP relationships for each patient shown in Figures 3.16 and 3.17. Table 3.5 gives pooled results of the calculated RV cavitary, pericardial and transmural pressure at CVPs of 5, 10 and 15 mm Hg. These values are based on the regression coefficients given in Table 3.4. At pericardium-intact RV cavitary pressures of 4.9 ± 0.7, 9.7 ± 0.9, and 14.5 ± 1.3 mm Hg the RV pericardial pressures were 3.9 ± 2.3, 7.7 ± 2.7, 11.3 ± 3.2, respectively.

Discussion

The transmural pressure-dimension relationships for both chambers are relatively flat; that is, transmural pressure increases only minimally in the range of strains seen when the pericardium is intact (ie, when cavitary pressure is less than 10 mm Hg). It is of interest that the RA intracavitary pressure-dimension curves were always very steep when the pericardium was intact and, in some of our dogs, volume loading and/or pulmonary artery constriction actually resulted in a decrease in RA dimension when RA cavitary pressure increased.

The transmural pressures measured and calculated in this experiment were found to be small when compared to pericardial pressure. The RA end-

diastolic cavitary pressure after pericardiectomy needed to be reduced to 1 mm Hg or less, in all dogs, to achieve the values of RA strain that were obtained when the pericardium was intact. This was extremely difficult since the preparation frequently became unstable. Because it was not possible to make the RA and RV as small after the pericardium had been removed as before, the calculated transmural pressure- (ie, intracavitary pressure minus local pericardial pressure) dimension data have been combined with directly measured pressure-dimension data (ie, those data recorded after the pericardium had been opened widely). The fact that there is no discontinuity between the two sets of data strongly support the validity of the balloon-transducer measurements of pericardial pressure.

Perhaps because of the scatter in the RA data, our study did not demonstrate that, with pericardium intact, RV compliance is greater than that of the RA (67); however, the normal, preferential filling of the RV when the tricuspid valve is open and the fact that the cavitary pressures are very similar demands that this must be so. A comparison of the RA and RV transmural pressure-strain curves shows that the compliance of the RV is remarkably less than that of the RA, as one would expect from the relative differences in chamber wall thickness. We submit that it is the presence of the pericardium which equalizes the compliance of the two chambers. That is, pericardial constraint effectively shifts the RA and, to a lesser extent, the RV transmural pressure-strain curves leftward so that they are approximately superimposable

when the pericardium is intact. Thus, it is the presence of the pericardium which enables the normal filling of the RV without considerable distension of each chamber. In the absence of the pericardium (or any other constraining structure) both chambers dilate greatly. At a moderate RV filling pressure (eg. 10 mm Hg), these results predict that the RA would dilate by a factor of 1.7 and the RV by 1.4, without a pericardium.

In one dog, we placed (in addition to RA appendage dimension sono-micrometer crystals) set of RA segment length crystals in the free wall just cephalad to the position of the pericardial balloon. It is interesting to note that segment length crystals in this animal (Dog #6) recorded strains approximately twice as large as its counterpart on the RA appendage. This difference in compliance might be due to the presence of trabeculae in the RA appendage which would increase its stiffness. Furthermore, the presence of trabeculae in the atrial appendage may help explain the wide variability in atrial stiffness between animals (see Figure 3.12 to 3.17). This phenomenon requires further investigation.

The use of three different types of regression techniques to describe the transmural pressure-dimension relationship in the dogs resulted in significant differences in the unstressed dimensions. In most cases the regression equations modeled the cavitary stiffness quite well (ie, pressure increased monotonically with dimension and the raw data points were symmetrically distributed around the regression curve). The cubic regression equation

seemed to be the most prone to become unstable (ie, to deviate from a monotonic function) and fit the transmural pressure data less convincingly (see figure 3.21); furthermore, it seemed to intersect the zero pressure axis prematurely causing an over-estimation of unstressed dimension (Table 3.6). The zero pressure intercept of the LV has been studied extensively (66,69) since the ellipsoid geometry of that chamber lends itself well to developing negative pressures at low end-systolic volumes. The RV and RA are thinner than the LV and their non-symmetrical geometries might not be capable of supporting any negative transmural pressure gradients without buckling. Nonetheless, if any negative transmural pressures could be developed in the RV or RA it seems reasonable that the cubic regression technique would correctly yield the unstressed dimension. The 3-parameter exponential regression equation consistently converged onto solutions describing the transmural pressure-dimension relationship with correlation coefficients greater than 0.83 and 0.92 for RA and RV, respectively. The 3-parameter exponential regression equation was used to estimate RA and RV transmural pressure for later analysis. The unstressed dimensions obtained by the use of three different regression techniques (equations 1,2 and 3) are given in Table 3.6 of the appendix. The parameters for the regression techniques (ie logarithmic, exponential and cubic) using the transmural pressure-dimension data for individual dogs are provided in the appendix. Comparison of the zero-pressure intercepts (unstressed dimension) derived by the three different

regression techniques with those obtained using the rules for unstressed dimension determination mentioned previously clearly shows that no single regression method consistently provided the value of unstressed dimension judged to be best in all dogs. Because the transmural pressure-dimension relationship has such a small slope when the chamber is small, small uncertainties or errors in pressure measurement may cause large changes in the zero pressure intercept. This uncertainty in the determination of the unstressed dimension using regression equations is quite evident when comparing the 1.0 and 0.1 mm Hg intercepts of the ln(pressure) vs dimension linear regression (52). Tables 3.6 illustrate how much the unstressed dimension can vary when only a 0.9 mm Hg difference in pressure is considered.

The potential space between visceral and parietal pericardium can contain varying amounts of fluid. The suggestion that the epicardial radial stress or pericardial pressure can be considered to be comprised of two components, liquid and surface pressure (11), might have been born from similar arguments made by Agostoni et. al. (14,18,70) and others (34,22,71) using various catheters and balloons to measure "pleural pressure". The measurement of a distribution of normal stresses between two deformable serous membranes separated by a thin layer of fluid has been extensively studied by Lai Fook et. al. and others using micropipette (24) and rib capsule techniques (25,26). They have shown that the conceptual separation of

pleural pressure into liquid and surface pressure is not necessary to understand the transmission of normal stress between two serous membranes separated by a thin layer of fluid (12). The same arguments can be effectively applied to the measurement of epicardial radial stress.

This study has shown that a small silastic liquid-containing balloon can be used to estimate the epicardial radial stress imposed by the pericardium upon the heart. The techniques used to measure epicardial radial stress (ie, "pericardial pressure) continue to be controversial. This is true in spite of the fact that there is almost unanimous acceptance of the proposition that the true value of "pericardial pressure" is equal to the isovolumic difference in end-diastolic pressures (ΔEDP), before and after the removal of the pericardium (11). This controversy persists (52-56) in spite of the facts that Smiseth et al (11) showed that the pressure measured by a liquid-containing balloon transducer was equal to ΔEDP, regardless of the volume of fluid in the pericardial space.

Conclusions

In conclusion we find that during diastole the pericardium influences the RA and RV in a major way. When the pericardium is intact, the transmural pressure of both chambers is quite small but the pericardial constraint can be measured accurately with a small Silastic liquid-containing balloon. Our animal data do not confirm the findings that the compliance of the RA is less than the

RV with the pericardium intact (67); however, they do indicate that the compliance of the two chambers are comparable due to the constraining effects of the pericardium.

Pooled data of all six animals indicate that, at pericardium-intact RA and RV P_{cav} of 5, 10 and 15 mm Hg, the RV P_{peric} was 4.3 ± 0.3, 8.6 ± 1.0 and 13.3 ± 1.5 mm Hg and RA P_{peric} was 4.8 ± 0.3, 9.6 ± 0.6 and 14.6 ± 0.6 respectively (mean ± SD). Furthermore, we determined that, in the dog, RV strain would increase by 14% and RA by 68%, to maintain P_{cav}= 10 mm Hg upon pericardiectomy.

The RA P_{trans} of the 6 patients was found to be 1.0 ± 1.5 mm Hg over central venous pressures ranging from 3.0 to 15.8 mm Hg. Also, at RV end-diastolic P_{cav} of 4.9 ± 0.7, 9.7 ± 0.9 and 14.5 ± 1.3 mm Hg, the RV P_{peric} were 3.9 ± 2.3, 7.7 ± 2.7, 11.3 ± 3.2 respectively.

In conclusion, diastolic pericardial constraint accounts for:

1) 95% of the RA cavitary pressure in the dog and 89% in humans

2) 85% of the RV cavitary pressure in the dog and 78% in humans.

Table 3.1 Patient Data

Patient	Sex	Age	Surgery
1	M	71	CABG + IM
2	M	50	ASD
3	M	19	WPW + PFO
4	M	22	WPW + PFO
5	M	67	CABG
6	M	76	CABG + IM
7	M	72	CABG + IM

Patient data for right atrial and ventricular transmural pressure human study.

CABG = coronary artery bypass graft

IM = internal mammary bypass graft

ASD = atrial septal defect repair

WPW = wolf parkinson white ablation of aberrant conductive pathway

PFO = repair of patent foramen ovale.

Table 3.2 Change in Percent Strain after Pericardiectomy

A. Right Atrium

Dog	P = 5 mm Hg	P = 10 mm Hg	P = 15 mm Hg
1	40	55	64
2	32	57	*
3	88	90	*
4	45	74	*
5	65	70	*
6	47	63	*
Mean ± SD	53 ± 20	68 ± 13	64 ± 0

B. Right Ventricle

Dog	P = 5 mm Hg	P = 10 mm Hg	P = 15 mm Hg
1	13.0	15.0	18.5
2	8.5	9.0	12.5
3	4.5	5.0	*
4	7.5	17.5	*
5	17.5	24.5	*
6	11.0	12.0	12.5
Mean ± SD	10.2 ± 4.4	13.9 ± 6.8	14.5 ± 3.5

Comparison of RA (A) and RV (B) increases in strain upon pericardiectomy at the same intracavitary pressure. The increase in strain was calculated at intracavitary pressures of 5, 10 and 15 mm Hg. *- indicated that after the pericardium had been removed, 15 mm Hg was not achieved in these animals; At the bottom of each column is the mean ± SD.

Table 3.3 Change in Cavitary Pressure after Pericardiectomy

A. Right Atrium

Dog	P = 5 mm Hg	P = 10 mm Hg	P = 15 mm Hg
1	4.5	9.5	14.5
2	5.0	10.0	15.0
3	4.5	9.5	14.5
4	5.0	10.0	15.0
5	4.5	8.5	13.5
6	5.0	10.0	15.0
Mean ± SD	4.8 ± 0.3	9.6 ± 0.6	14.6 ± 0.6

B. Right Ventricle

Dog	P = 5 mm Hg	P = 10 mm Hg	P = 15 mm Hg
1	4.5	9.0	14.0
2	4.5	7.5	12.0
3	4.0	7.5	11.0
4	5.0	8.5	14.0
5	4.5	9.5	14.5
6	4.5	9.9	14.5
Mean ± SD	4.3 ± 0.3	13.9 ± 6.8	13.3 ± 1.5

Comparison of RA (A) and RV (B) decreases in cavitary pressure upon pericardiectomy at the same percent strain (all pressure are in mm Hg). The decrease in cavitary pressure was calculated at pre-pericardiectomy intracavitary pressures of 5, 10 and 15 mm Hg. At the bottom of each column is the mean ± SD.

Table 3.4 Linear Regression Coefficients for Human RV Data

Slope

Patient	1	2	3	4	5	6	7
Transmural	0.356	0.145	0.132	0.349	0.118	0.277	0.191
Cavitary	0.780	0.998	0.951	0.913	0.995	1.037	1.038
Pericardial	0.423	0.853	0.822	0.564	0.876	0.761	0.847

Intercept

Patient	1	2	3	4	5	6	7
Transmural	-1.06	3.50	-0.91	0.76	1.49	-2.51	-1.01
Cavitary	0.54	0.55	0.99	-0.15	-0.99	-0.60	0.39
Pericardial	1.62	-2.94	-2.87	-0.91	-2.48	1.91	1.40

This table gives the slope (upper panel) and intercept (lower panel) of the regression lines shown in Figure 11 of cavitary pressure (A), pericardial pressure (B) and transmural pressure (C) vs CVP.

Table 3.5

Pressures at CVP = 5,10 and 15 mm Hg.

CVP	5	10	15
Transmural	1.2 ± 1.9	2.3 ± 1.9	3.4 ± 2.0
Cavitary	4.9 ± 0.7	9.7 ± 0.9	14.5 ± 1.3
Pericardial	3.9 ± 2.3	7.7 ± 2.7	11.4 ± 3.3

The mean transmural, pericardial and cavitary pressure calculated at CVPs of 5, 10 and 15 mm Hg using the regression equations of each patient described in table 4 is given above.

Table 3.6 Pressure Intercepts using Various Regression Techniques

A. Right Atrium

Dog	EXP	ln 0.1	ln 1.0	Cubic	Value used
1	6.20	3.2	6.9	6.95	6.20
2	5.72	2.6	5.6	6.40	5.72
3	5.70	4.6	6.3	5.30	3.90
4	6.35	5.5	8.1	6.20	6.35
5	5.26	4.5	9.0	7.15	6.50
6	*	4.8	6.8	4.90	7.15

Tables 3.6 through 3.9 contain the regression coefficients of the equations used for regression of the transmural pressure data for the RA and RV against cavitary dimension. The transmural pressure is calculated by subtracting intracavitary pressure from pericardial pressure with an intact pericardium and is equal to intracavitary pressure with the pericardium removed. Using these coefficients (Tables 3.7, 3.8 and 3.9) and the unstressed lengths (Table 3.6) the transmural pressure-dimension regression equations can be rewritten as function of percent cavitary strain.

B. Right Ventricle

Dog	EXP	ln 0.1	ln 1.0	Cubic	Value used
1	10.10	9.20	10.80	10.01	10.10
2	4.30	4.10	4.56	4.44	4.16
3	12.30	11.70	12.60	12.50	11.70
4	10.90	9.00	10.90	11.00	10.90
5	10.10	9.00	10.60	10.20	9.96
6	7.75	7.40	8.70	8.15	7.75

Comparison of the unstressed RV (B) segment length and unstressed RA (A) appendage dimension derived using a least-squares regression algorithm on a 3-parameter exponential, logarithmic and cubic equation to the transmural pressure vs dimension data of each dog:

Column 1 - The 0.0 mm Hg intercept of a 3-parameter exponential equation;

Column 2 - The 0.1 mm Hg intercept of the linear regression of ln(transmural pressure) vs dimension;

Column 3 - The 1.0 mm Hg intercept of the linear regression of ln(transmural pressure) vs dimension;

Column 4 - The 0.0 mm Hg intercept of a cubic regression

Column 5 - The unstressed dimension selected (see criteria in text)

Table 3.7 3-Parameter Exponential Equation

A. Right Atrium

Dog	Corr.Coeff.	A	B	C
1	0.983	4.55 e-3	7.12 e-1	-3.77 e-1
2	0.975	1.39 e+2	2.03 e-2	-1.57 e+2
3	0.925	1.34 e-2	7.53 e-1	-9.77 e-1
4	0.995	1.95 e+0	3.74 e-1	-2.11 e+0
5	0.957	2.64 e-2	4.36 e-1	-2.62 e-1
6	0.831	1.89 e-5	1.08 e+0	2.18 e+0

B. Right Ventricle

Dog	Corr.Coeff.	A	B	C
1	0.994	2.35 e-7	1.42 e+0	-4.07 e-1
2	0.981	7.68 e+6	2.83 e+0	-1.47 e+0
3	0.935	6.84 e-12	2.10 e+0	-1.19 e+0
4	0.951	4.25 e+2	9.43 e-3	-4.72 e+2
5	0.916	1.41 e-3	7.20 e-1	-2.01 e-0
6	0.920	4.78 e-18	4.80 e+0	6.89 e-2

Contains the parameters obtained by fitting the 3-parameter exponential regression equation to the RA (A) and RV (B) transmural pressure-dimension data.

Table 3.8 Logarithmic Equation

A. Right Atrium

Dog	Corr. Coeff.	Slope	Intercept
1	0.961	0.265	-1.842
2	0.933	0.327	-1.845
3	0.798	0.315	-1.969
4	0.864	0.383	-3.095
5	0.812	0.222	-2.000
6	0.873	0.327	-1.452

B. Right Ventricle

Dog	Corr. Coeff.	Slope	Intercept
1	0.971	0.619	- 6.703
2	0.963	2.152	- 9.809
3	0.812	1.173	-14.766
4	0.709	0.508	- 5.575
5	0.831	0.631	- 6.692
6	0.834	1.186	- 9.693

Contain the parameters obtained by fitting the logarithmic regression equation to the RA (A) and RV (B) transmural pressure-dimension data.

Table 3.9 Cubic Equation

A. Right Atrium

Dog	Corr. Coeff.	A	B	C	D
1	0.991	0.285	-6.913 e+0	5.702 e+1	-1.582 e+2
2	0.995	-0.825	1.799 e+1	-1.248 e+2	2.776 e+2
3	0.948	0.213	-3.568 e+0	2.020 e+1	-3.862 e+1
4	0.995	0.020	-1.270 e-1	-4.060 e-1	2.537 e+0
5	0.965	0.076	1.976 e+1	1.976 e+1	-6.163 e+1
6	0.846	0.113	2.654 e+0	2.052 e+1	-5.038 e+2

B. Right Ventricle

Dog	Corr. Coeff.	A	B	C	D
1	0.993	1.539	-4.912 e+1	5.232 e+2	-1.859 e+3
2	0.985	-4.633	8.567 e+1	-4.811 e+2	8.527 e+2
3	0.888	0.000	6.109 e+0	-1.477 e+2	8.913 e+2
4	0.961	-0.657	2.265 e+1	-2.541 e+2	9.287 e+2
5	0.949	-0.758	2.671 e+1	-3.079 e+2	1.166 e+3
6	0.884	0.000	1.508 e+1	-2.417 e+2	9.687 e+2

Contain the parameters obtained by fitting the cubic regression equation to the RA (A) and RV (B) transmural pressure-dimension data.

Figures

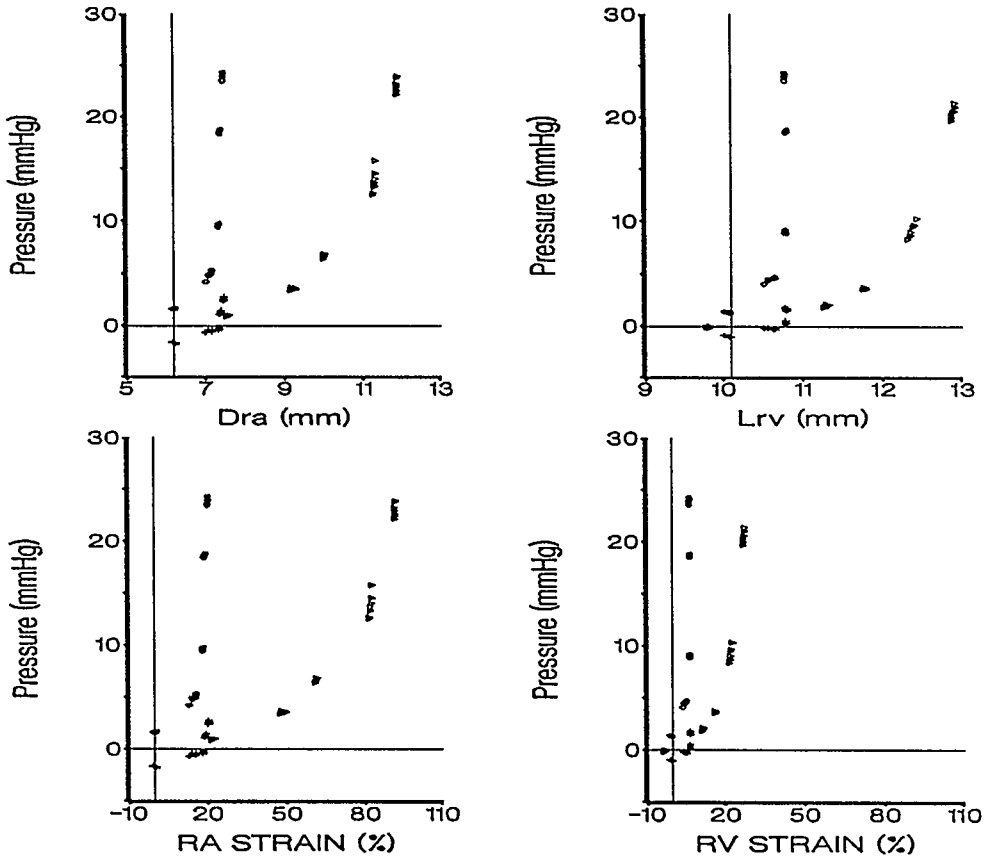

Figure 3.1

Upper Panels - RV and RA pressure vs dimension data for dog one is shown with open circles representing cavitary pressure with an intact pericardium, crosses represent transmural pressure with an intact pericardium and open triangles represent intracavitary pressure after pericardiectomy. The vertical line in each plot represents the value selected as the unstressed dimension.

Lower Panels - RV and RA pressure vs percent strain for dog one is shown with symbols being the same as the upper panel. A single vertical line in each plot represents 0% strain (Note that the strain scales are the same for the RA and RV)

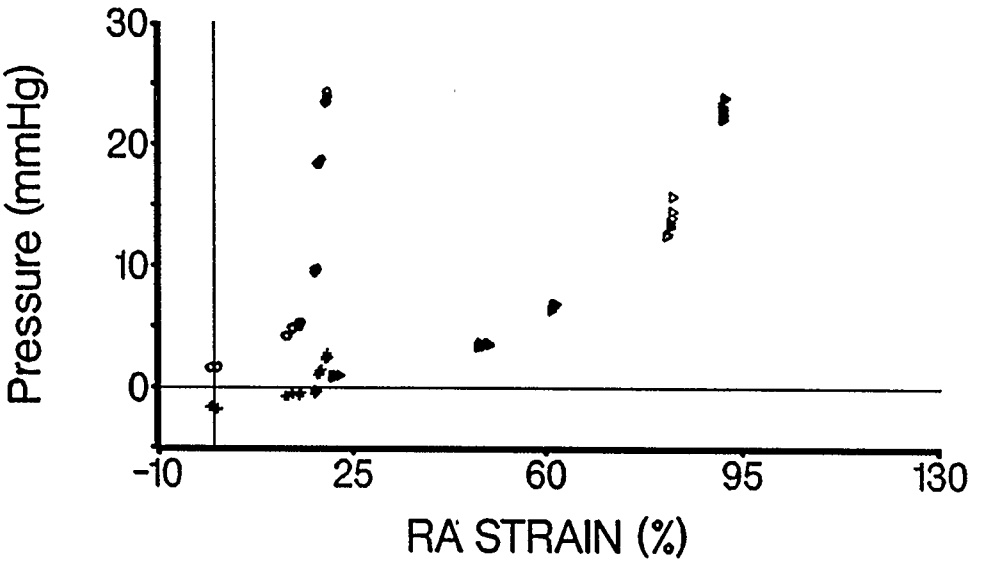

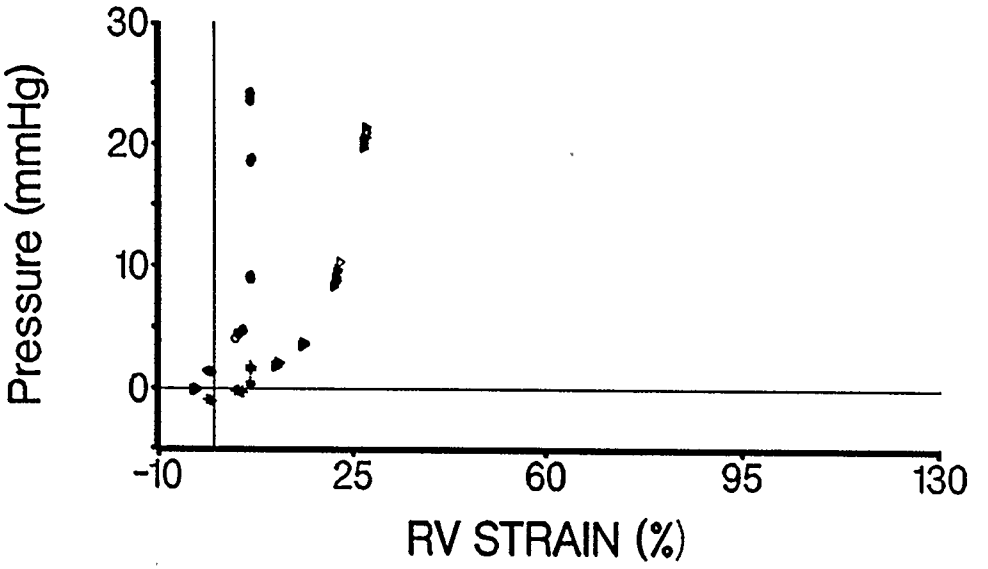

Figure 3.2 DOG 1.

RV and RA pressure vs percent strain for dog 1. RA pressure vs RA strain and RV pressure vs RV strain is plotted. Open circles represent cavitary pressure with an intact pericardium, crosses represent transmural pressure with an intact pericardium and open triangles represent intracavitary pressure after pericardiectomy.

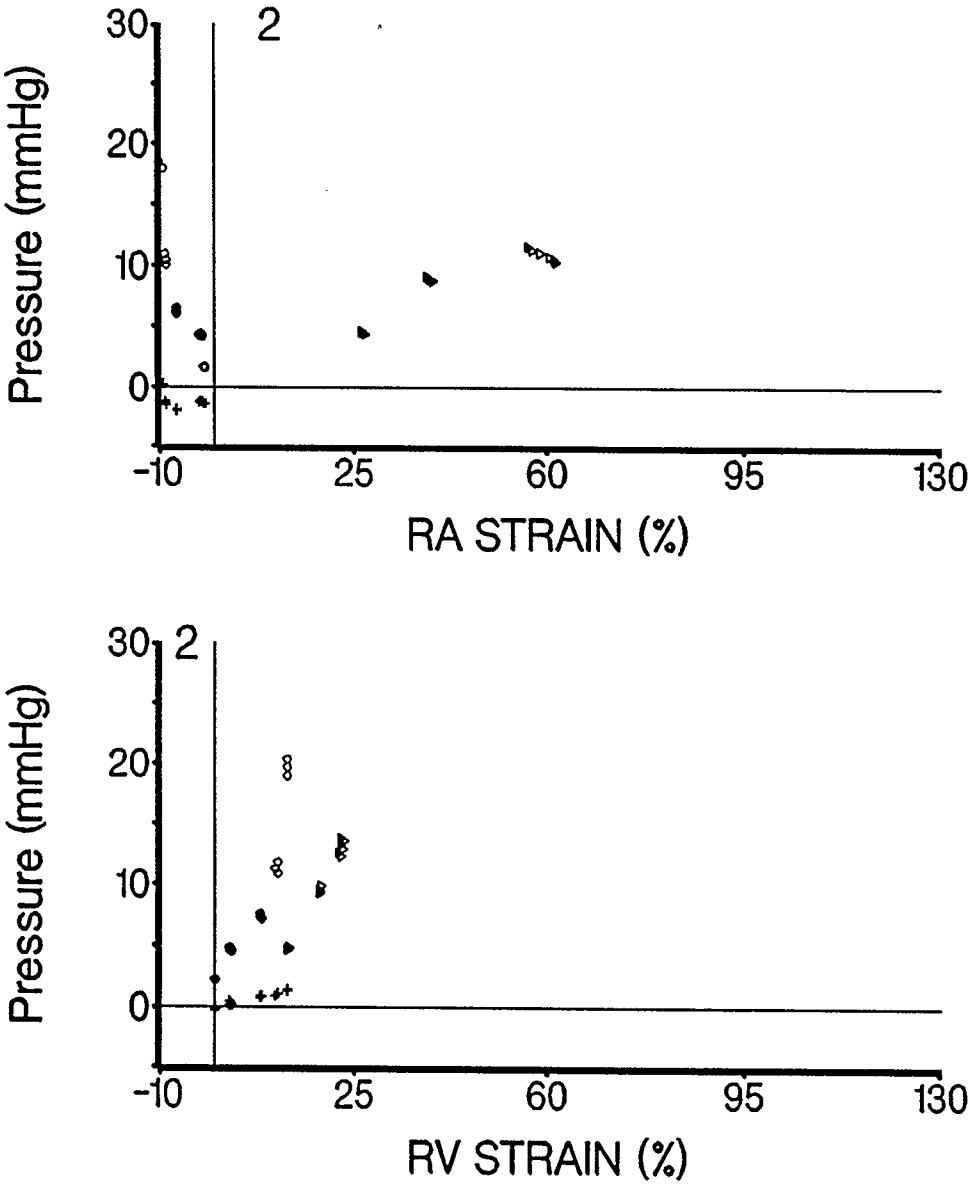

Figure 3.3 DOG 2

RV and RA pressure vs percent strain for dog 2. RA pressure vs RA strain and RV pressure vs RV strain is plotted. Open circles represent cavitary pressure with an intact pericardium, crosses represent transmural pressure with an intact pericardium and open triangles represent intracavitary pressure after pericardiectomy.

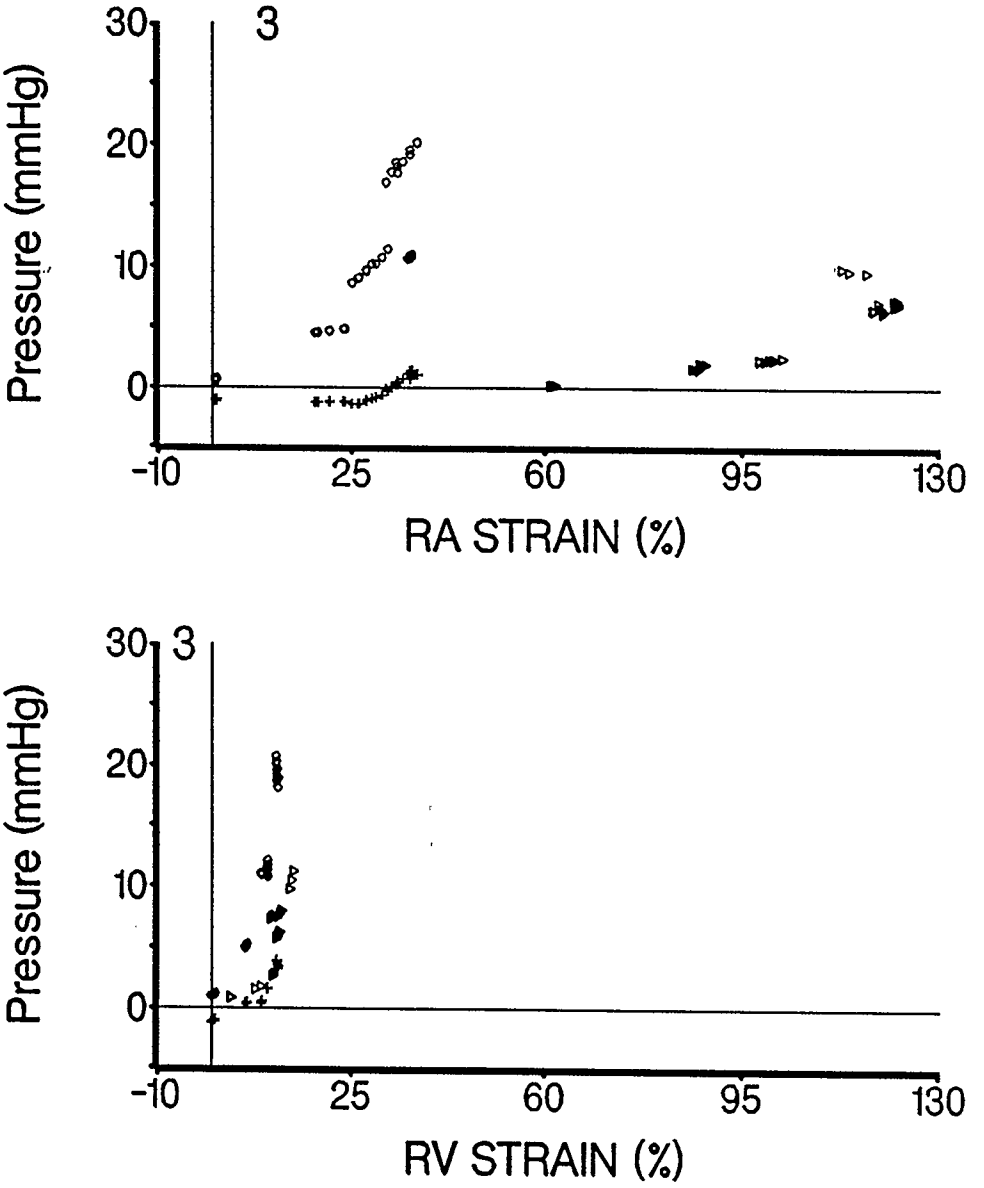

Figure 3.4 DOG 3.

RV and RA pressure vs percent strain for dog 3. RA pressure vs RA strain and RV pressure vs RV strain is plotted. Open circles represent cavitary pressure with an intact pericardium, crosses represent transmural pressure with an intact pericardium and open triangles represent intracavitary pressure after pericardiectomy.

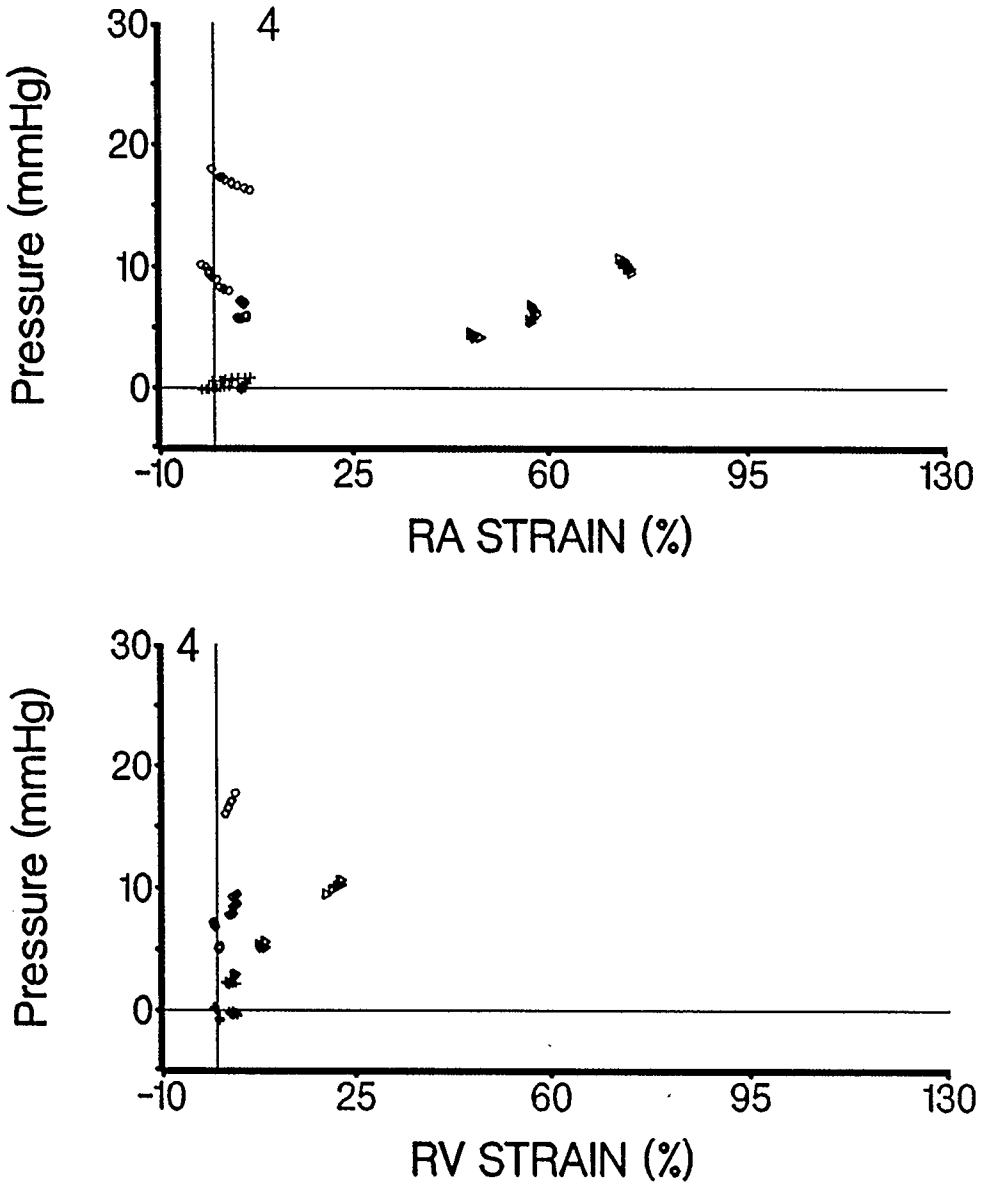

Figure 3.5 DOG 4.

RV and RA pressure vs percent strain for dog 4. RA pressure vs RA strain and RV pressure vs RV strain is plotted. Open circles represent cavitary pressure with an intact pericardium, crosses represent transmural pressure with an intact pericardium and open triangles represent intracavitary pressure after pericardiectomy.

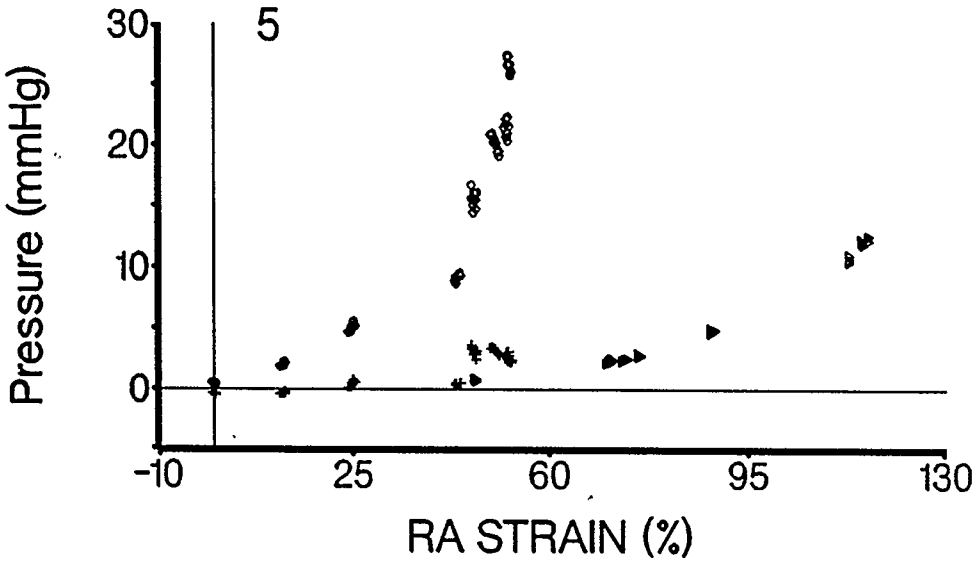

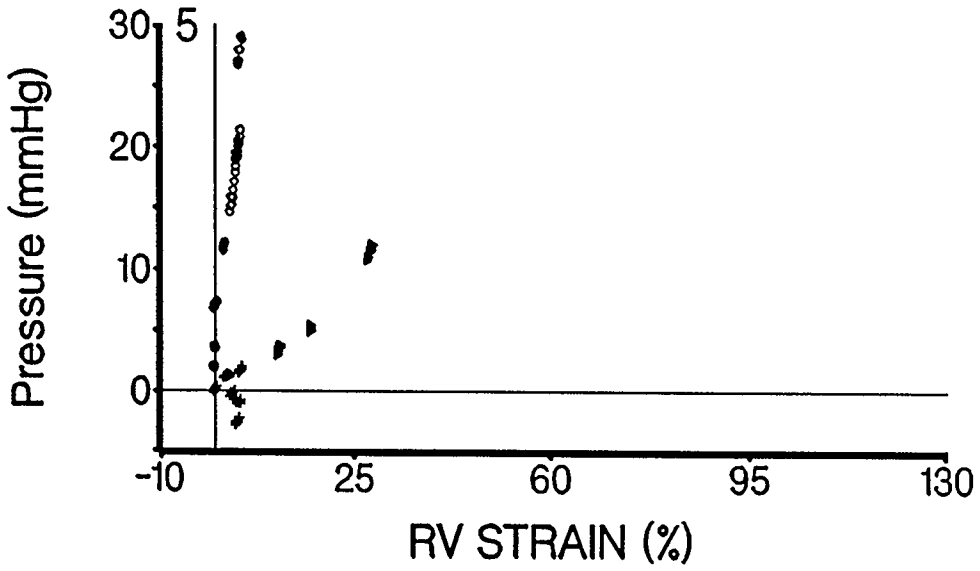

Figure 3.6 DOG 5.

RV and RA pressure vs percent strain for dog 5. RA pressure vs RA strain and RV pressure vs RV strain is plotted. Open circles represent cavitary pressure with an intact pericardium, crosses represent transmural pressure with an intact pericardium and open triangles represent intracavitary pressure after pericardiectomy.

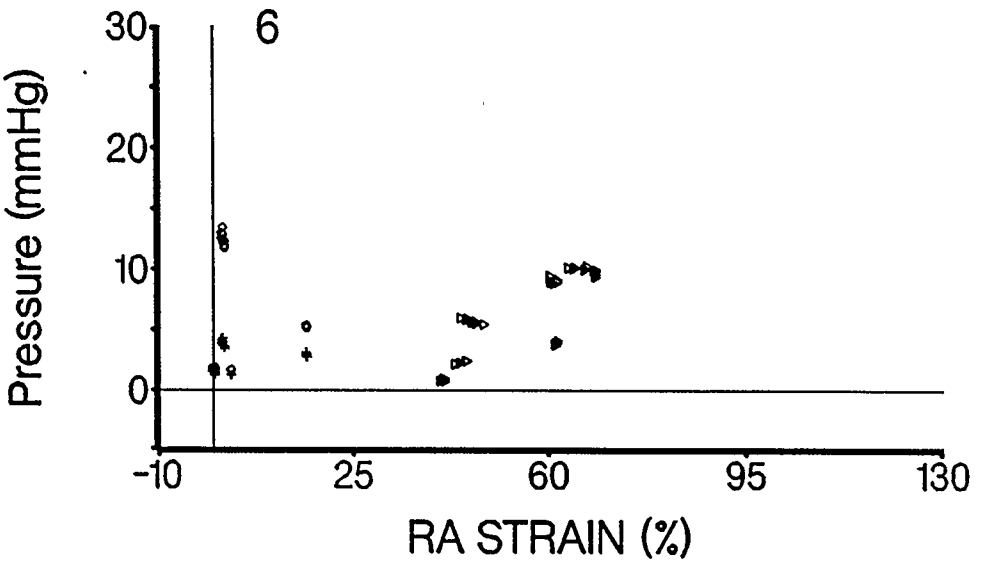

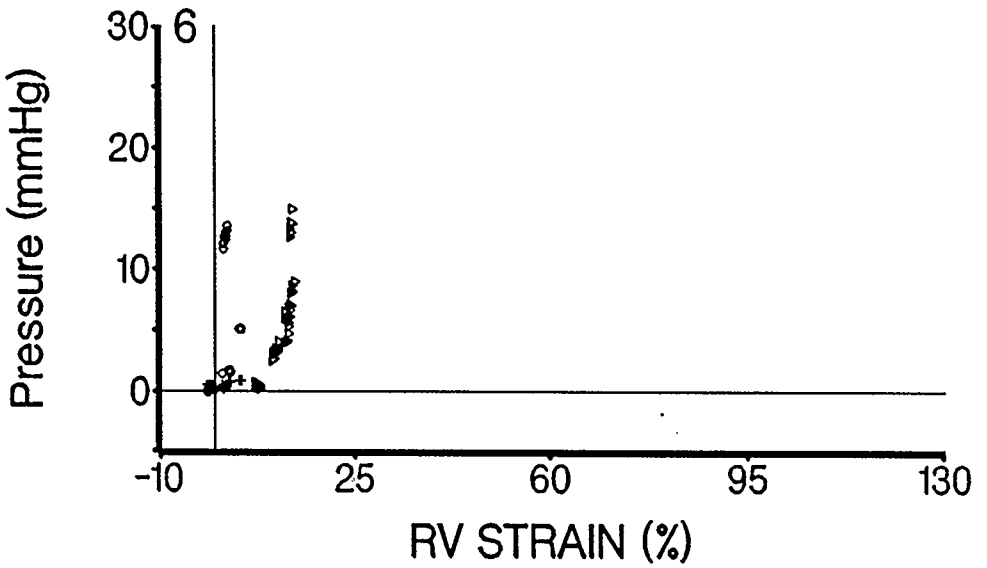

Figure 3.7 DOG 6.

RV and RA pressure vs percent strain for dog 6. RA pressure vs RA strain and RV pressure vs RV strain is plotted. Open circles represent cavitary pressure with an intact pericardium, crosses represent transmural pressure with an intact pericardium and open triangles represent intracavitary pressure after pericardiectomy.

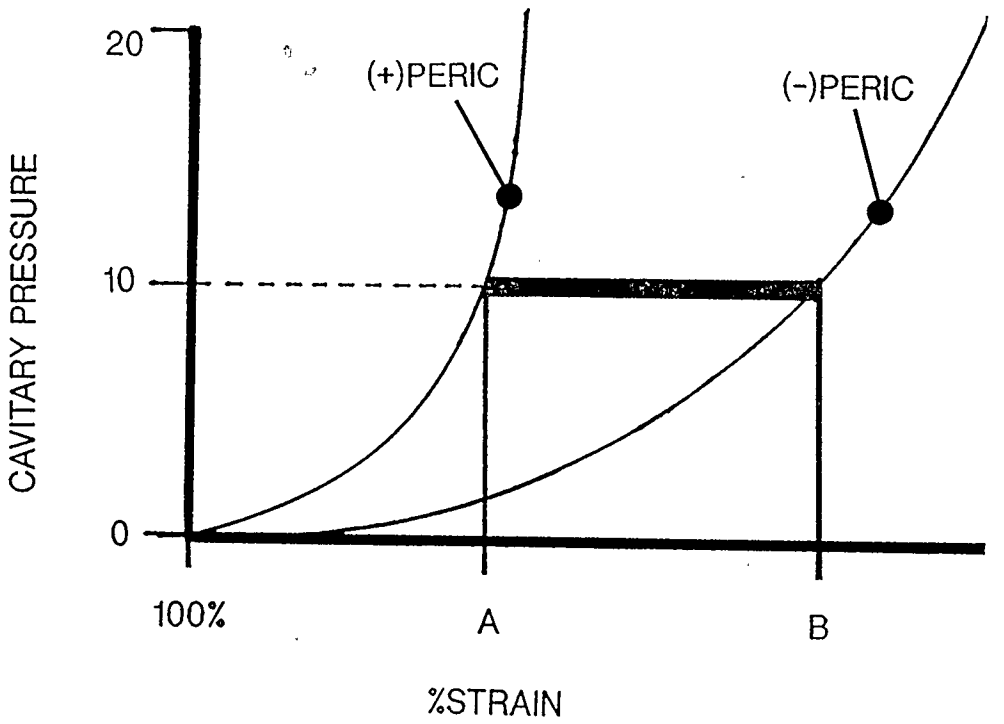

Figure 3.8

A schematic representation of the estimation of cavitary strain increase following pericardiectomy. The increase in strain is calculated as the difference in strain before and after pericardiectomy at the same pressure (ie strain at A minus strain at B).

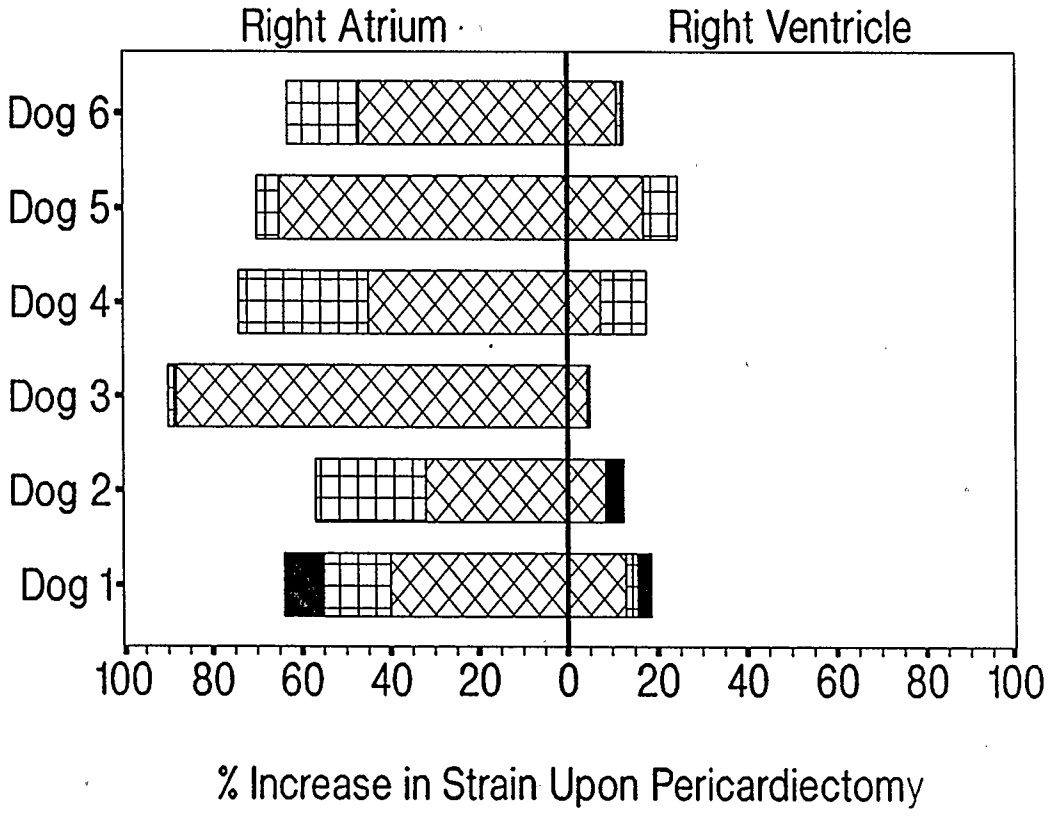

Figure 3.9

Increase in strain calculated at intracavitary pressures of 5 (diagonal hatch fill), 10 (cross hatch fill), and 15 (solid fill) mm Hg. for individual dogs. Zero strain is located at the centre of the abscissa with RV strain plotted to the right and RA strain plotted to the left. It can seen that the RA distended more than the RV in all dogs. Most distension occurred before pressure exceeded 5 mmHg.

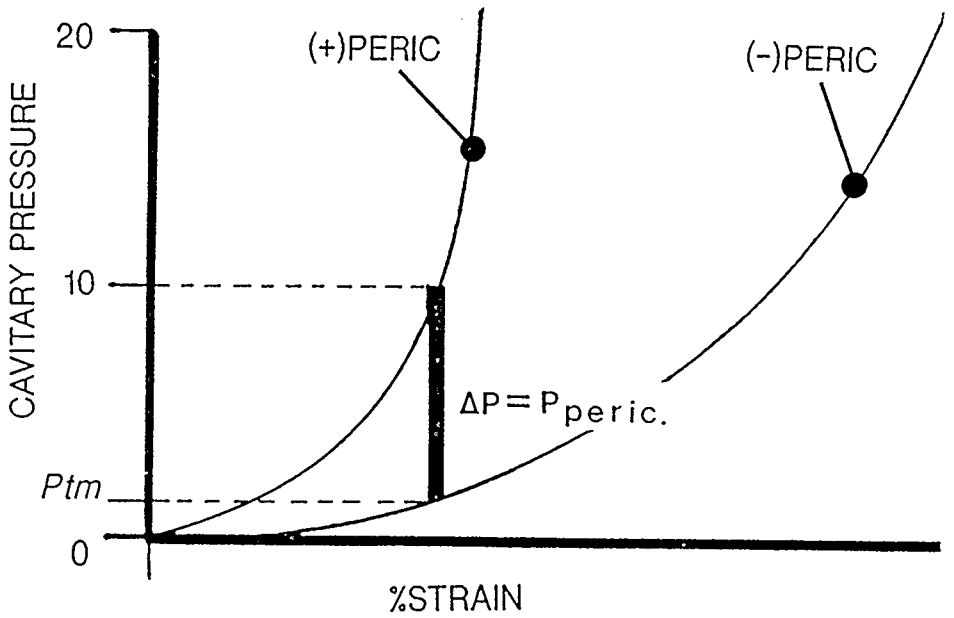

Figure 3.10

A schematic representation of the calculation of the decrease in intracavitary pressure upon pericardiectomy measured at the same strain. The decrease in pressure should equal the pericardial constraint that was present before pericardiectomy (ΔEDP). The decrease in intracavitary pressure was estimated at intracavitary pressures of 5, 10, and 15 mm Hg. P_{tm} = Transmural pressure.

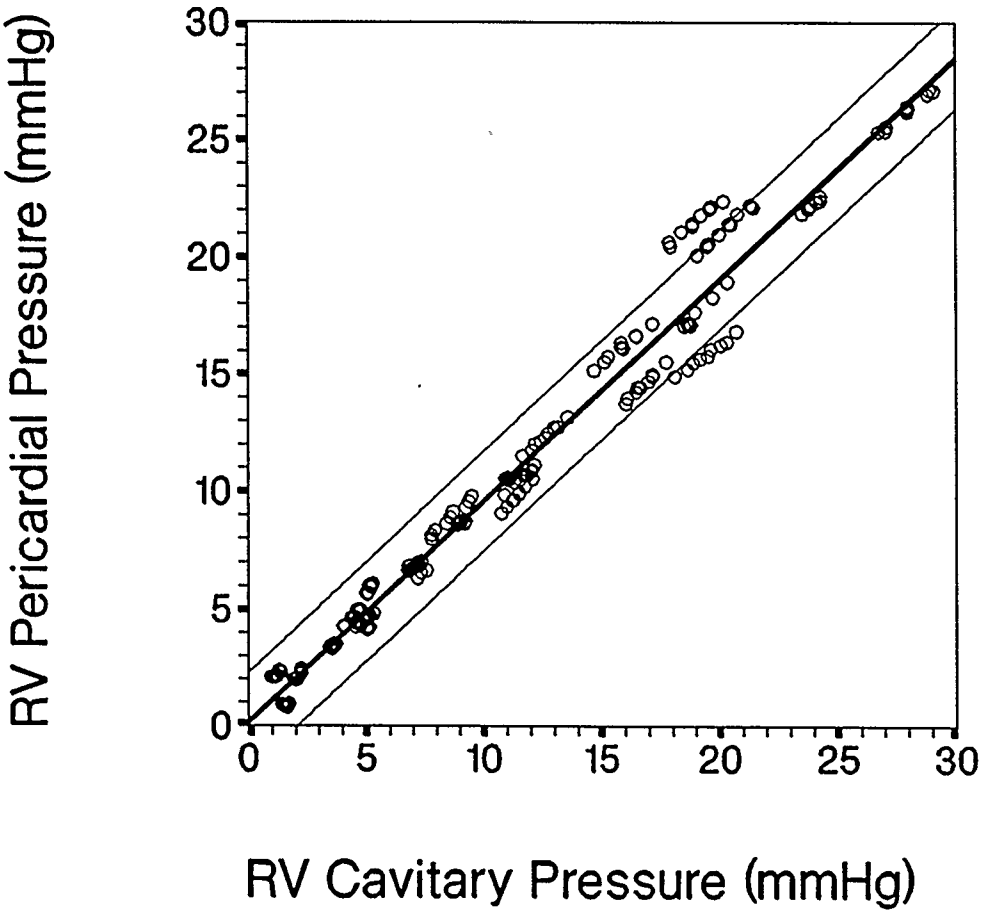

Figure 3.11

RV cavitary pressure vs RV pericardial pressure measured with a balloon (intact pericardium). All pressures are in mm Hg. the solid line represents a linear regression of the pooled data from all dogs (slope = 0.94, intercept = 0.17, correlation coefficient = 0.98), with 95% confidence limits.

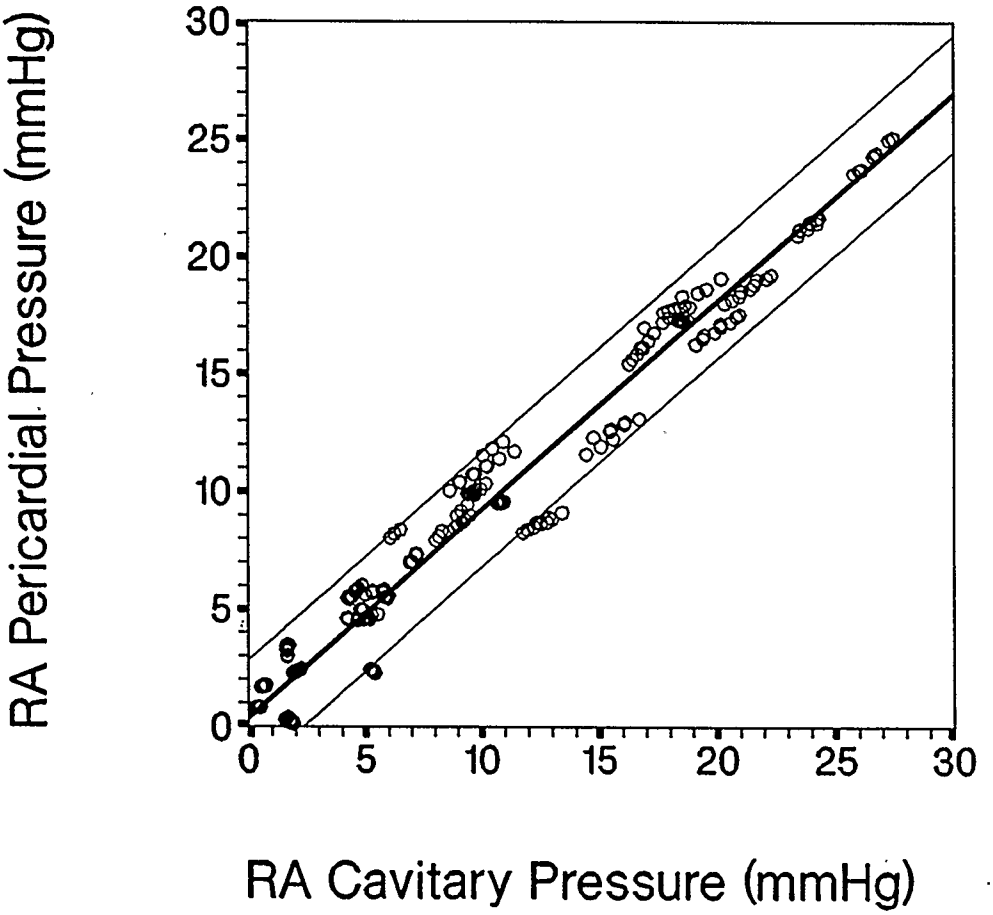

Figure 3.12

RA intracavitary pressure vs RA pericardial pressure measured with a balloon (intact pericardium). All pressures are in mm Hg. the solid line represents a linear regression of the pooled data from all dogs (slope = 0.89, intercept = 0.37, correlation coefficient = 0.97), with 95% confidence limits.

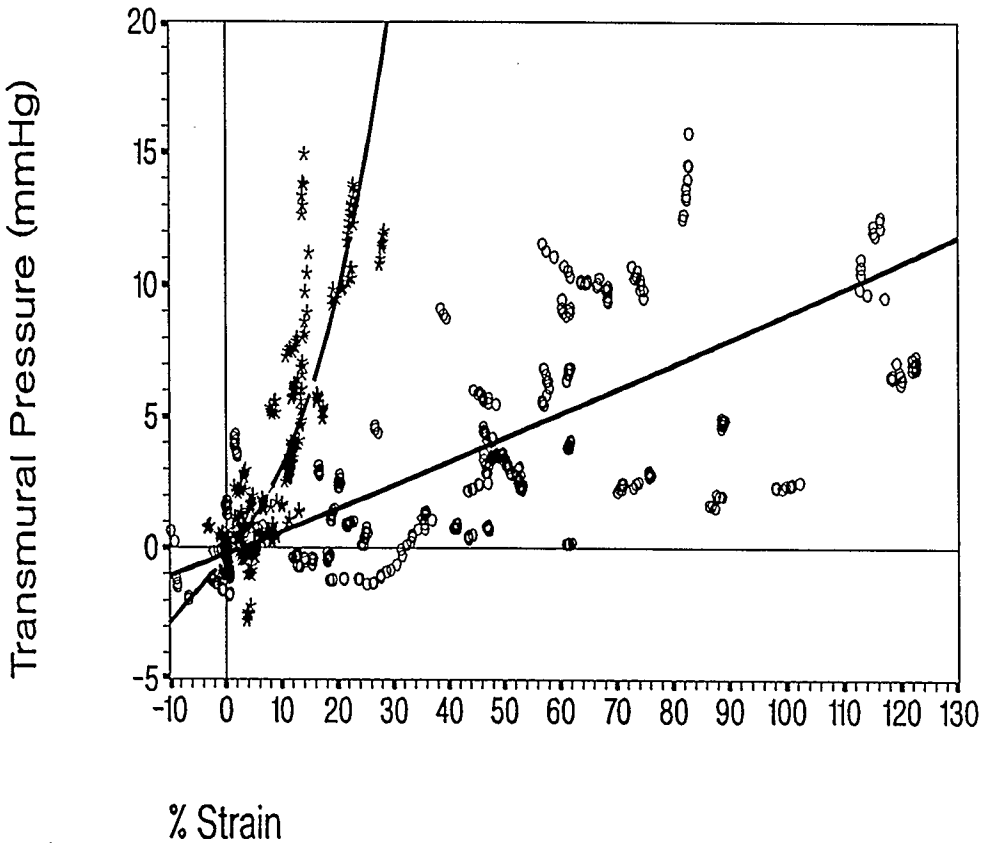

Figure 3.13

Plot of pooled data for all dogs of RV (stars) and RA (open circles) transmural pressure vs percent strain (full scale). The solid lines represents the 3-parameter exponential (equation 1) least-square regression of the RA transmural pressure vs percent strain (pooled data of all dogs). The dashed lines represents the 3-parameter exponential least-squares regression of the RV transmural pressure vs percent strain (pooled data of all dogs).

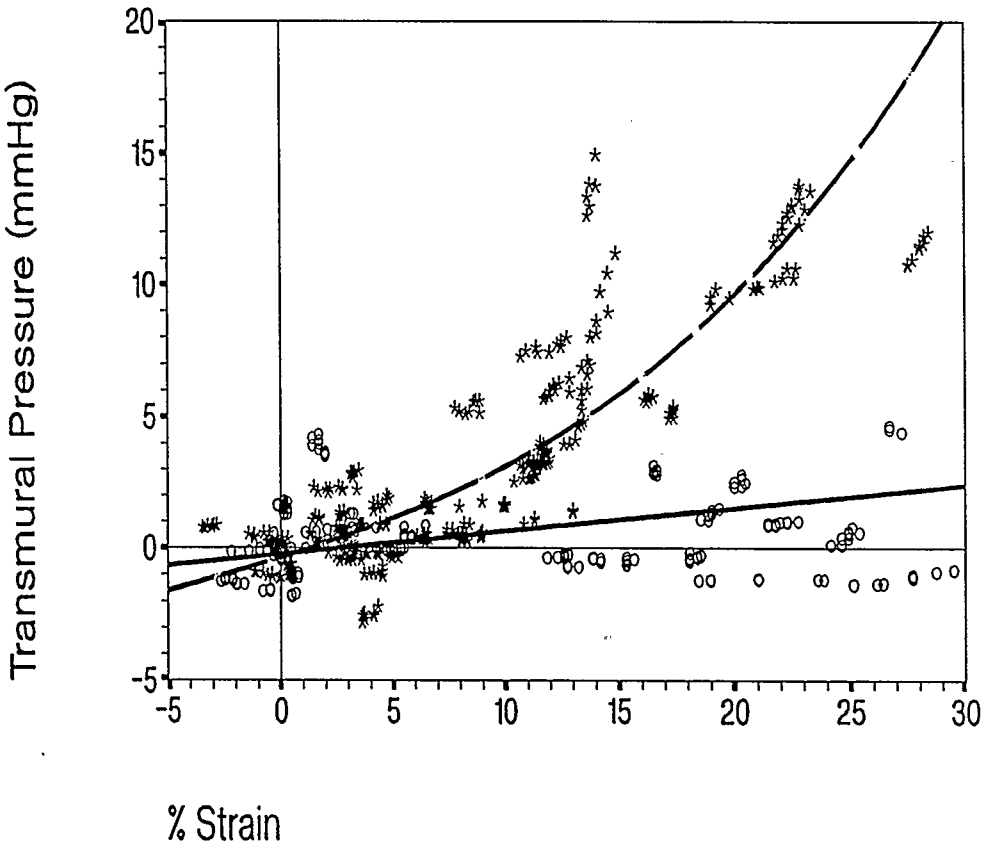

Figure 3.14

Plot of pooled data for all dogs of RV (stars) and RA (open circles) transmural pressure vs percent strain (expanded scale). The solid lines represents the 3-parameter exponential (equation 1) least-square regression of the RA transmural pressure vs percent strain (pooled data of all dogs). The dashed lines represents the 3-parameter exponential least-squares regression of the RV transmural pressure vs percent strain (pooled data of all dogs).

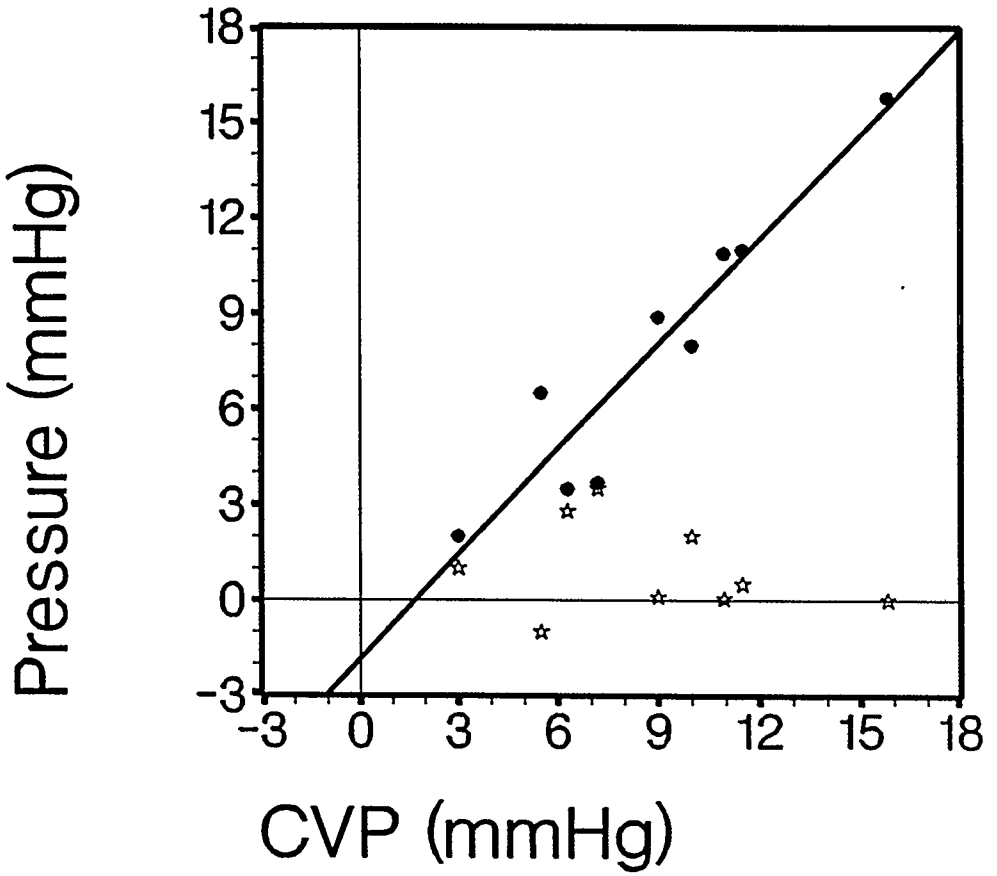

Figure 3.15

Plot of pooled data for six patients of RA transmural pressure (stars) and RA pericardial pressure (closed circles) vs CVP. The solid line is the linear regression of RA pericardial pressure with CVP. (Slope = 1.10, intercept = -1.85 , correlation coefficient = 0.95). The mean RA transmural pressure was 1.0 ± 1.5 mm Hg.

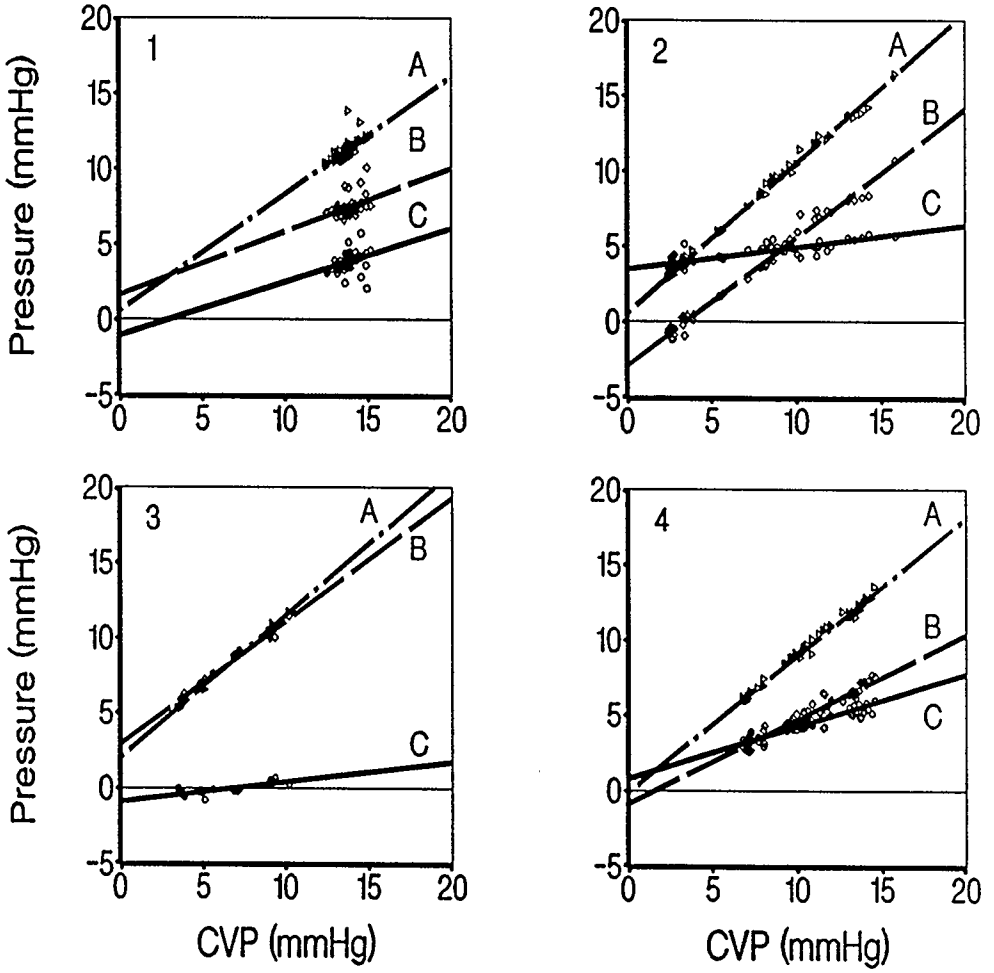

Figure 3.16 Patients 1 to 4

Shows the raw data and linear regression for patients 1 to 4 with RV end-diastolic pressure (A, raw data - open triangles), RV pericardial pressure (B, raw data - open diamonds) and RV transmural pressure (C, raw data - open circles) plotted against CVP.

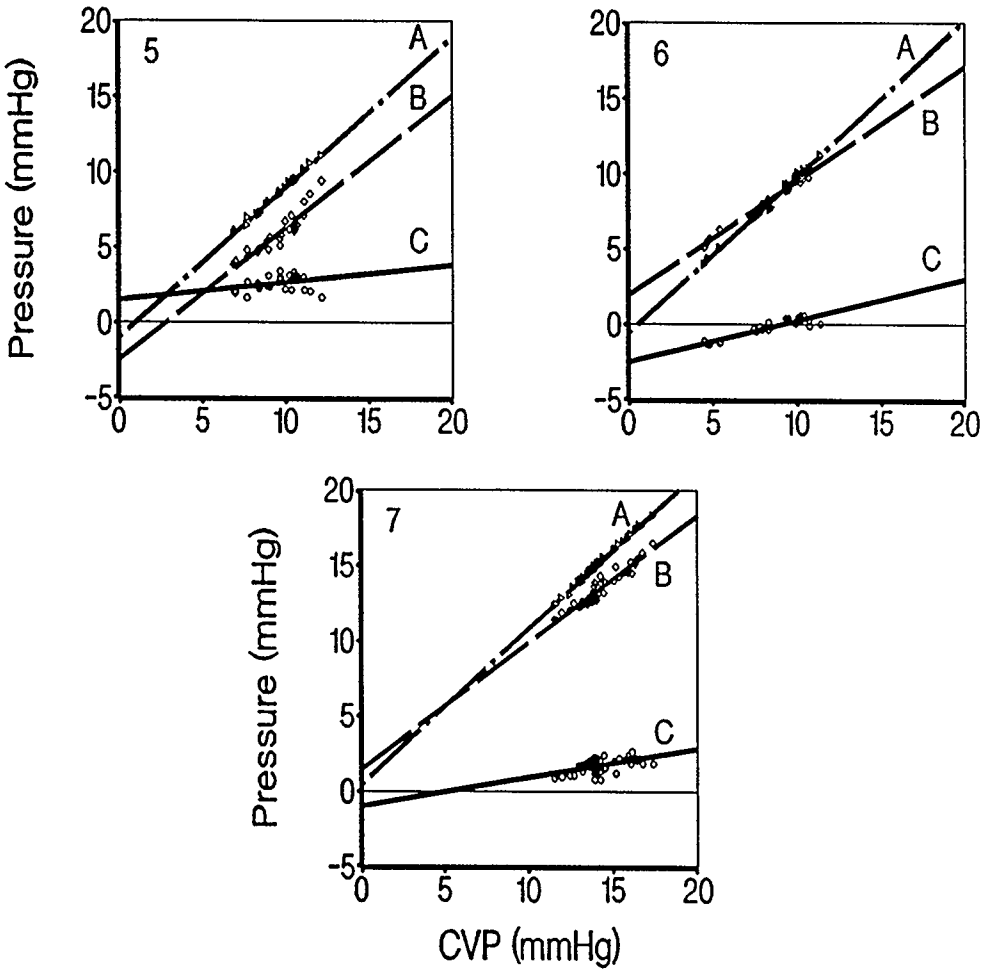

Figure 3.17 Patients 5 to 7

Shows the raw data and linear regression for patients 5 to 7 with RV end-diastolic pressure (A, raw data - open triangles), RV pericardial pressure (B, raw data - open diamonds) and RV transmural pressure (C, raw data - open circles) plotted against CVP.

Figure 3.18 Time Domain Plot Showing Atrial Transmural A-Wave

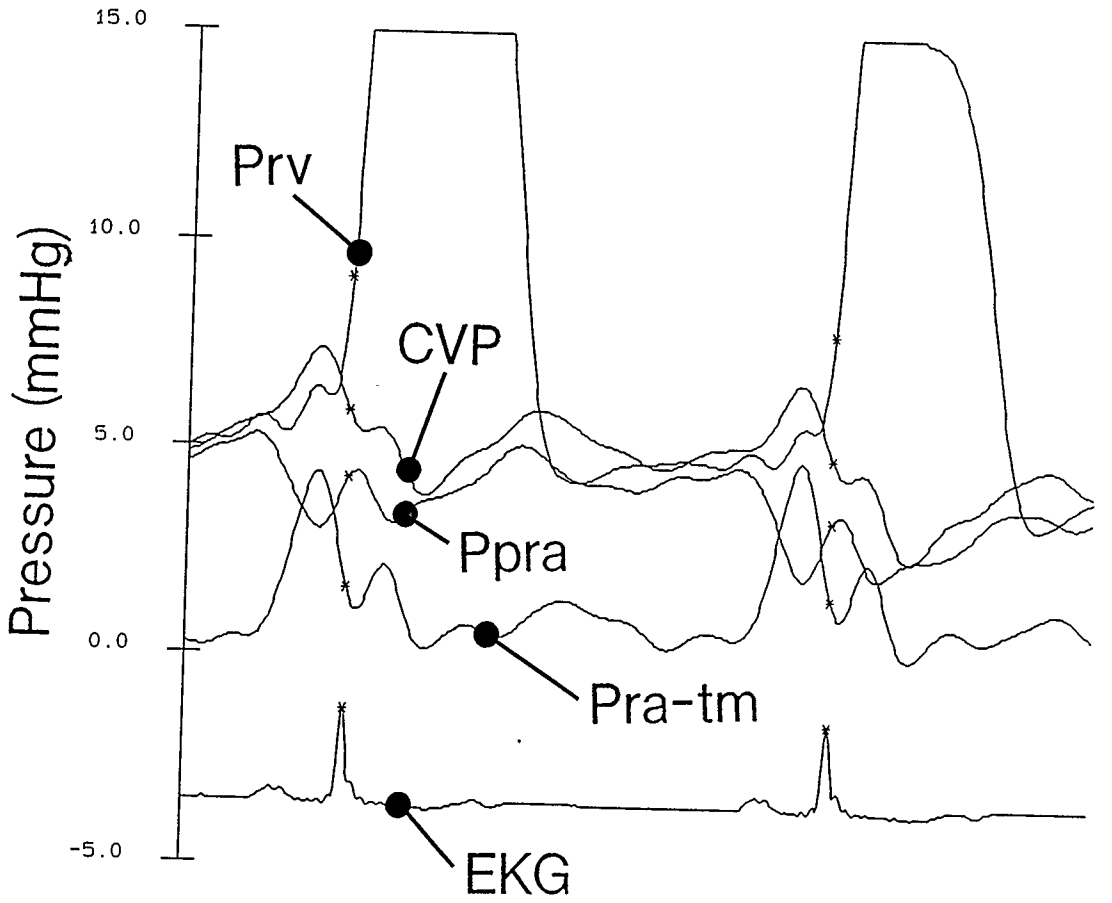

Time domain plot of RV cavitary pressure (P_{rv}), central venous pressure (CVP), RA pericardial pressure (P_{pra}), calculated RA transmural pressure ($P_{ra\text{-}tm}$) and the EKG for temporal reference. The decrease in RA pericardial pressure occurs as the CVP pressure tracing is increasing (A-wave) causing a substantial atrial transmural pressure (4 mm Hg).

Figure 3.19 Cubic and Exponential Regression Curves for the RV

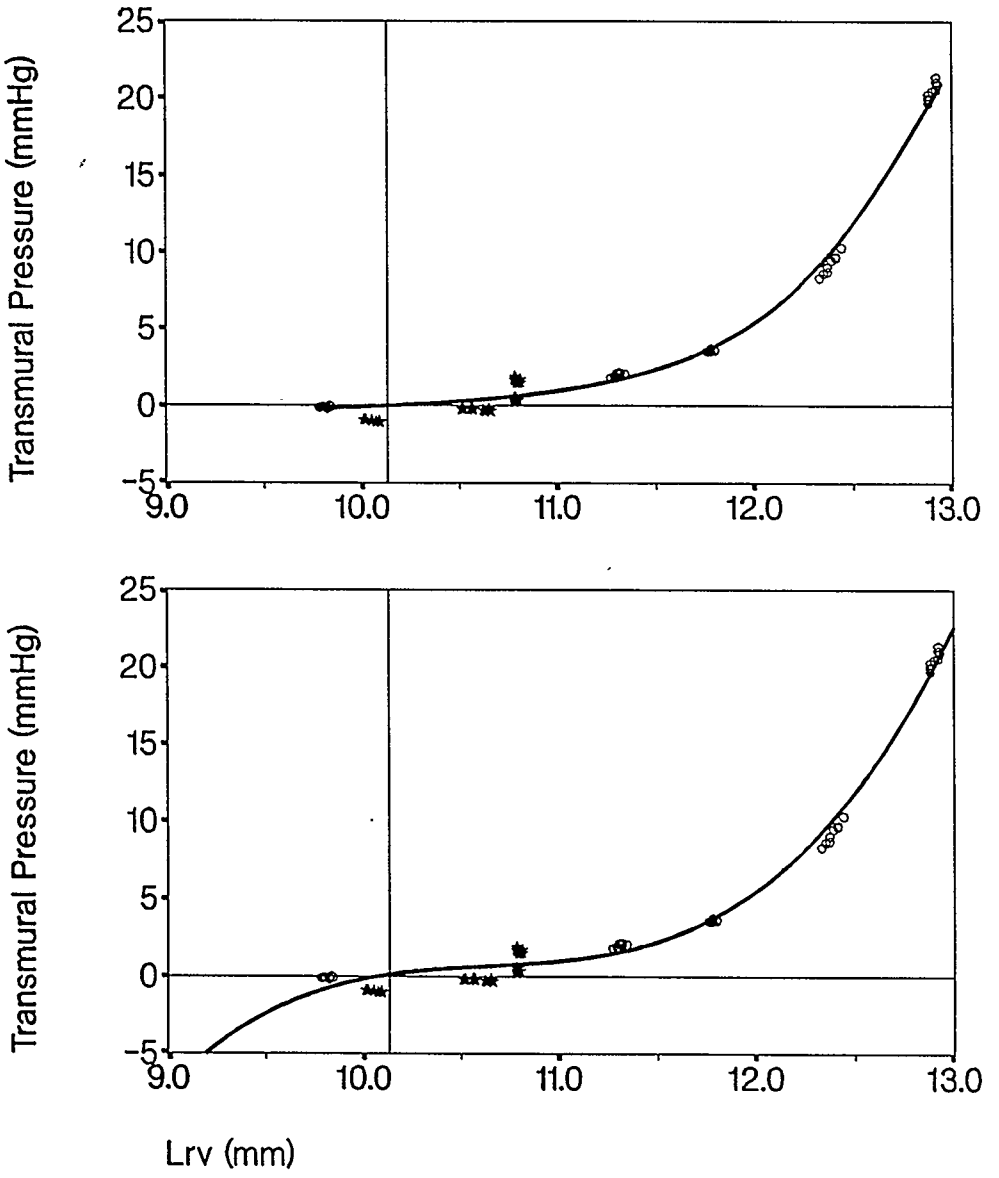

Plots of RV transmural pressure vs RV segment length showing the regression curves for the three parameter exponential equation (upper panel) and the cubic equation (lower panel) for Dog 1. Notice that the shape of the cubic regression behaves similar to the transmural pressure-dimension relationship of a thick walled chamber (ie. the left ventricle). A vertical reference line (10.13 mm) is drawn to indicate the unstressed length used for the analysis of this dog.

Figure 3.20 Cubic and Exponential Regression Curves for the Right Atrium

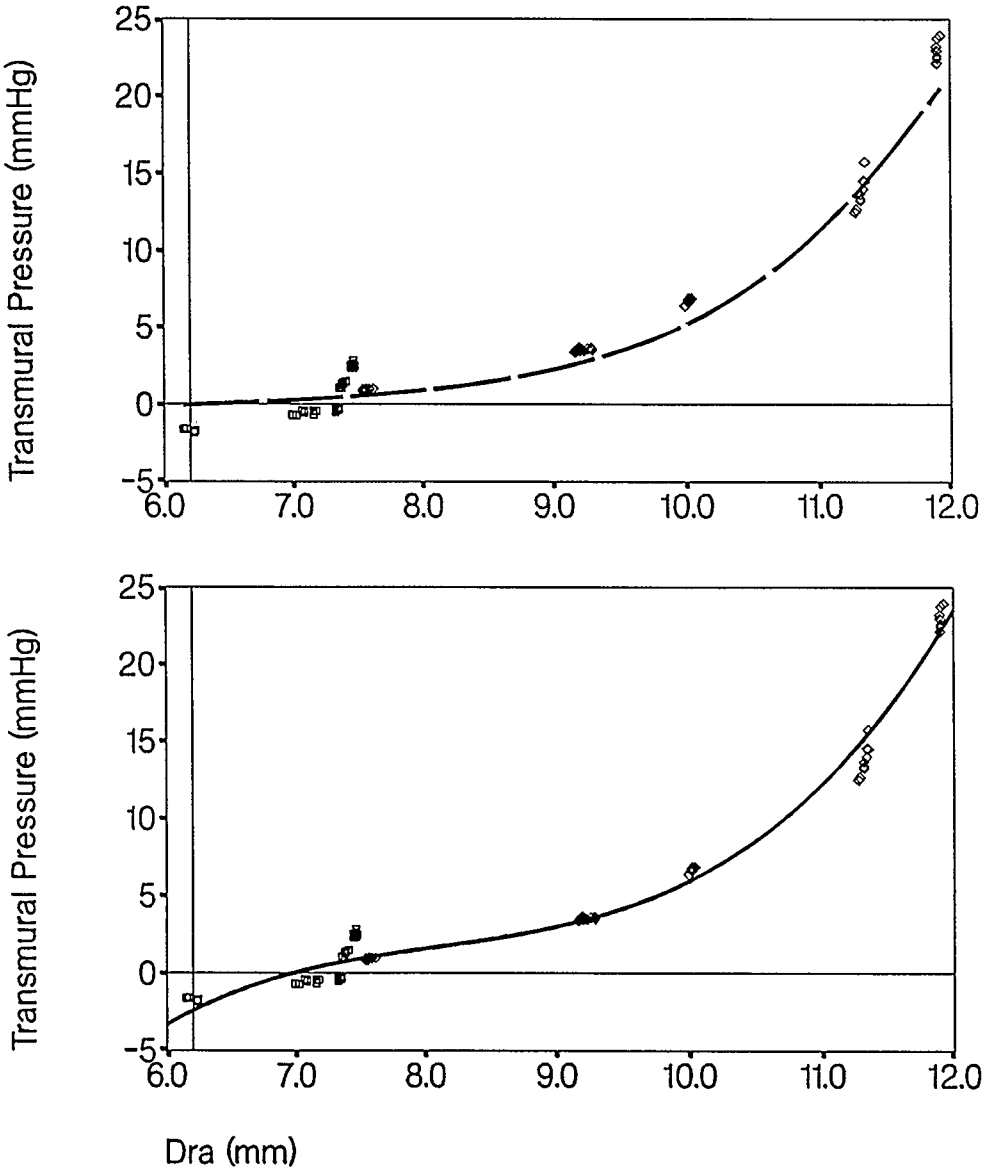

Plots of right atrial transmural pressure vs dimension of Dog 1 using a 3- parameter exponential (upper panel) and a cubic (lowe panel) regression technique. Notice the cubic gives a greater unstressed length. The unstressed length chosen to calculate strain in this document is shown as a vertical reference line at 6.2 mm.

Figure 3.21 Examples of Regression Equations Which Vastly Differ

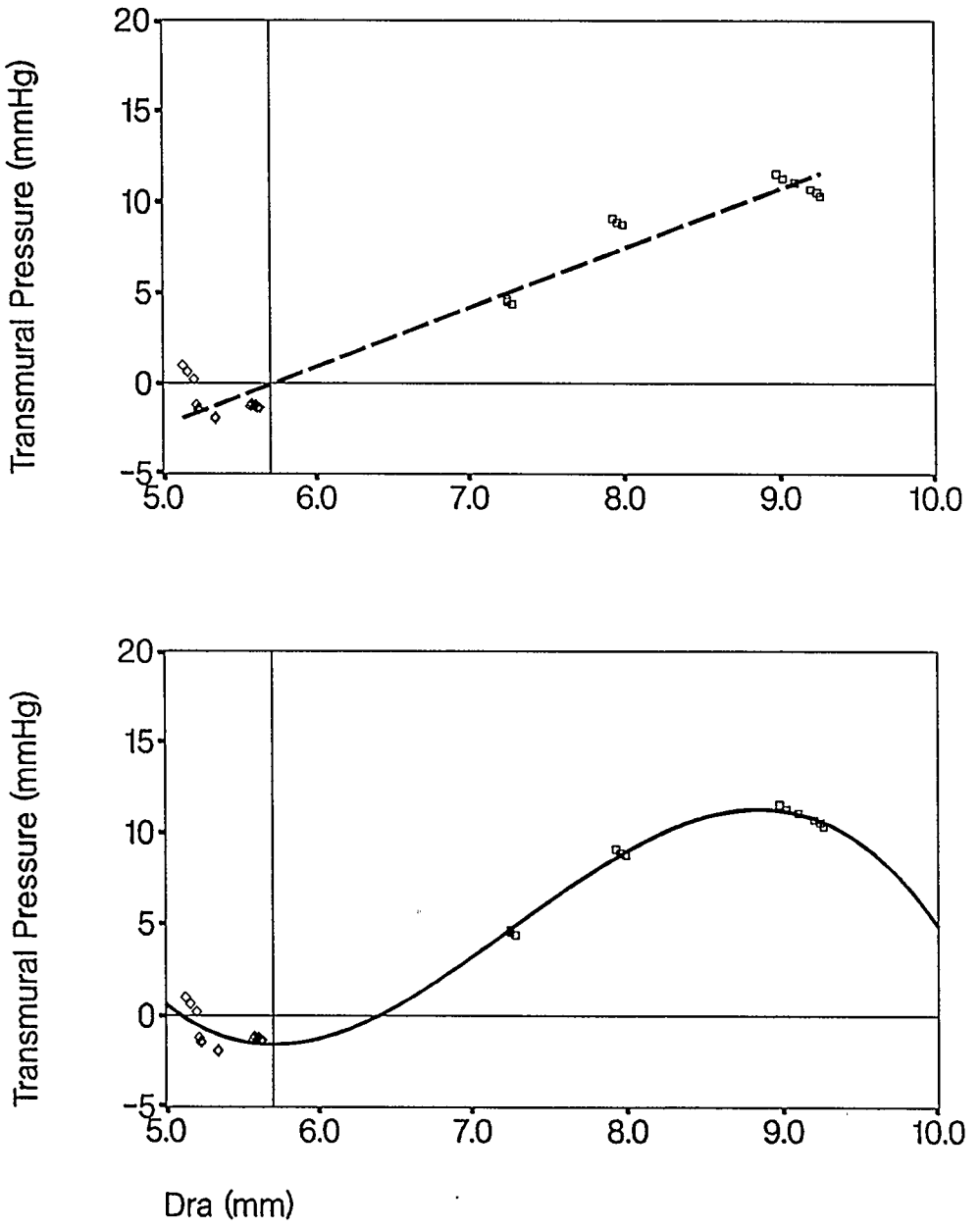

Plots showing right atrial transmural pressure vs dimension of Dog 2 with a 3 parameter exponential (upper panel) and cubic (lower panel) regression curve. Notice the cubic equation fits the data very tight but implies an unrealistic transmural pressure-dimension behaviour.

Figure 3.22 Logarithmic Regression Curves for the RA and RV

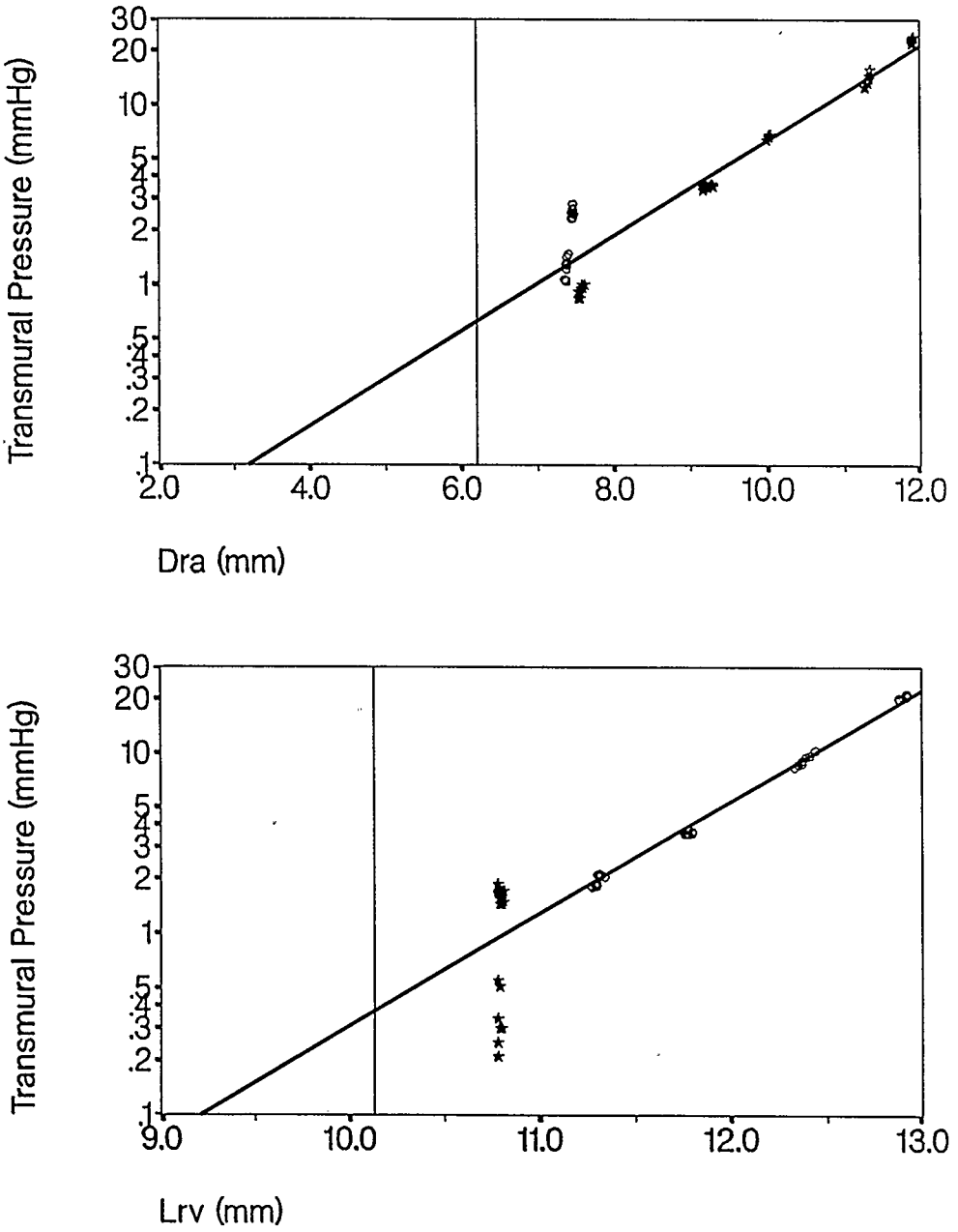

Plots of the logarithm RA (upper panel) and RV (lower panel) transmural pressure vs dimension for Dog 1. The data sets for this type of regression analysis have been truncated since the logarithm of negative transmural pressures are not defined.

Chapter 4

HIGH FIDELITY MEASUREMENT OF RIGHT ATRIAL AND VENTRICULAR PERICARDIAL PRESSURE OVER THE WHOLE CARDIAC CYCLE IN DOGS.

Introduction

The pericardium influences the intracavitary pressure of all chambers of the heart, in particular diastolic filling. The myocardium in all chambers is relaxed before the A-wave of atrial contraction and the pressure gradient and flow across the atrio-ventricular valve is small at this time in the cardiac cycle. The relatively static state of the heart at this time in the cardiac cycle lends itself well to measurement of epicardial radial stress. It has been generally assumed that, except for hydrostatic differences, the pericardial pressure (epicardial radial stress) is uniform throughout the heart during this period. This has been investigated by Smiseth et al (72) and Tyberg et al (73) who advocate the concept that right atrial pressure can be used to estimate left ventricular pericardial pressure at end diastole. Chapter 3 confirms the minor role the myocardium plays in the development of right atrial and right ventricular end-diastolic cavitary pressure therefore it seems reasonable that the pericardial pressure over these regions are equal in magnitude at end-

diastole under normal physiological conditions. Recent studies however, (33) have shown that, during acute changes in afterload, the epicardial radial stress at end-diastole can be nonuniform.

The measurement of pericardial pressure over the whole cycle has not been accomplished until recently due to limitations in transducer technology. The regional deformation of the pericardium has been measured during the cardiac cycle by Goto et al (55) with findings which imply that, without tamponade, the pericardium causes regional variation in epicardial radial stress during systole. The anisotropic nature of the pericardium prevents us from directly estimating the pericardial pressure form the strain measurements of Goto (55). With this in mind we have taken advantage of recent advances in pericardial balloon technology which permit the high fidelity measurement of pericardial pressure throughout the whole cardiac cycle.

Rationale

The purpose of this study was to illustrate the cycle specific regional differences in pericardial pressure by using high fidelity pericardial balloons to measure epicardial radial stress throughout the whole cardiac cycle. This new method will help evaluate the findings of Goto (55) that the regional cycle specific deformations of the pericardium are due to regional cycle specific variations in epicardial radial stress.

Methods

After receiving 10 - 20 mg morphine sulfate (i.m.), five mongrel dogs (20-25 Kg.) of both sexes were anaesthetized with 12.5 mg/Kg sodium thiopental. Anaesthesia was maintained with 30 μg/Kg/min fentanyl while ventilation with a 2:1 nitrous oxide:oxygen mixture was delivered by a constant-volume ventilator. All dogs received positive end-expiratory pressure of 2 cm H_2O and a tidal volume of 15 ml/kg. The animals were maintained at 37°C using a circulating-water warming blanket and a constant temperature heating system. The ECG was continuously monitored throughout the experiment.

With the dog in the supine position, a midline sternotomy was performed and 100 to 200 ml of heparinized Ringer's lactate solution were infused to maintain normal aortic pressure. The left lateral surface of the pericardium was opened using a longitudinal incision, with the ventricles delivered through this incision for purposes of instrumentation. RV free-wall segment length (L_{rv}) and RA appendage diameter (D_{ra}) were measured by sonomicrometry as previously described by Smiseth et al (33). The RV segment length crystal were placed in the inflow tract approximately parallel to the atrioventricular groove in a manner similar to Raines et al (74). Two flat liquid-containing balloon transducers were attached loosely to the epicardium with single stay sutures; one was positioned over the RV free wall adjacent to the crystals, and the other was positioned cephalad to the sonomicrometer

crystals on the RA appendage. The heart was repositioned into the pericardium and the pericardial margins reapproximated using interrupted 3-0 silk sutures spaced 1 cm apart, taking care to avoid compromising pericardial volume. RV and RA cavitary pressures were measured using 8F micromanometer-tipped catheters with reference lumens inserted through the internal jugular and femoral veins, respectively. Aortic pressure was measured with an 8-F fluid-filled catheter introduced through the femoral artery. Inferior vena cava and pulmonary arterial pneumatic vascular constrictors were also positioned on all dogs. The RV balloon (3.0 cm x 3.0 cm) was fabricated from Silastic sheets and attached to a 70-cm 8F cardiac catheter. The RA balloon dimensions were 1.2 cm x 1.4 cm with a 20-cm length of Silastic medical grade tubing connected directly to a pressure transducer. A calibration curve for both balloons and transducers was described before and after each experiment using techniques described in chapter 1. No differences between pre- and post-experiment calibration curves were found in any experiment. Each balloon had a 3F micromanometer-tipped catheter positioned internally to provide a high fidelity measurement of balloon pressure. Intra-balloon catheter-tip pressure transducers do not sense the artifacts and oscillations generated from catheter motion and also are free of the frequency-dependent transmission characteristics of fluid-filled tubes. The dynamic response of this high fidelity balloon pressure measuring system is linear with a flat frequency response to 200 Hz (68, Chapter 1).

Conditioned signals were acquired using a personal computer digitizing analog signals (pressure, dimension and ECG) that were scaled using gain and offset amplifiers and then filtered with a 7th order Cauer elliptic lowpass active anti-aliasing filter before being sampled at 200 Hz using a 12-bit analog-to-digital converter. The digitized data were subsequently analyzed on a different personal computer, using analytical software developed in our laboratory and statistical and graphics software.

Protocol

After preparatory surgery, all animals were stabilized for 1/2 hour before any data were recorded. Mean RA pressure was caused to vary from 0 to 25 mm Hg by adjusting intravascular volume (Ringer's lactate solution was infused or blood removed through a large-bore catheter in an external jugular vein) or by manipulating the inferior vena cava or pulmonary artery vascular pneumatic occluders.

Hemodynamic and sonomicrometer measurements were obtained continuously for 1 minute at each volume load state (ie. after each incremental increase of mean RA cavitary pressure), each recording interval beginning with a 20-second control period. The ventilation was interrupted at the end-expiratory position for several cardiac cycles during each recording interval.

Data Analysis

Only data collected at end expiration were analyzed. Each high fidelity micromanometer-tipped catheter signals was corrected to equal its corresponding pressure recorded via the fluid-filled catheter at end diastole. This correction was performed using software that automatically adjusted the mean pressure of the micromanometer-tipped catheter to equal the mean of its fluid-filled counterpart. This method was completely automatic and therefore eliminated operator input; nonetheless, all pressure tracing corrections were inspected visually to ensure validity, although no adjustments were made.

All data were collected over 60-second intervals. The post-experiment analysis involved the extraction of three consecutive cardiac cycles at end expiration from the sampled data file (5 milliseconds sampling interval). The end-diastolic portion of the cardiac cycle was delineated between the bottom of the y-descent to just before the A-wave (Pre A-wave). The systolic portion was delineated between the bottom of the x-descent and the peak of the V-wave (see Figure 4.1).

Results

A typical time domain plot of the pressure and dimension signals is given in Figure 4.2. It can be seen that there is a significant divergence in the pericardial pressures during systole. The increase in RA pericardial pressure while the RV pericardial pressure decreases in systole suggests that the

structure of the pericardium prevents the fall in RV pericardial pressure from being communicated to the RA.

Figures 4.3 through 4.7 show the RA pericardial pressure plotted against the RV pericardial pressure for each dog. The plots are broken into diastole (from the bottom of the y-descent to Pre A-wave) and systole (from the bottom of the x-descent to the peak of the v-wave) at mean right atrial pressures ranging from 2 to 20 mmhg. The results of all five dogs are consistent in that RA and RV pericardial pressure rose approximately in a 1:1 fashion during the diastole describing a line of identity. During systole however, the RV pericardial pressure decreases while the RA pericardial pressure remains the same.

Dog 1 (figure 4.3) and dog 2 (fig 4.4) show RV pericardial pressure falling before RA pericardial pressure while Dog 3, 4 and 5 (Figures 4.5 through 4.7) show the RV pericardial pressure falling after the RA pericardial pressure causing the systolic relationship to cross the diastolic relationship. This can be seen in Figure 4.8 and 4.9 showing the time domain plots of RA and RV pericardial and cavitary pressure for dog 1 (Figure 4.8) and 3 (Figure 4.9). Dog 1 and 3 are representative of the two cases where RV pericardial pressure falls before (dog 3) or after (Dog 1) RA pericardial pressure. This difference in the timing of the fall in RV pericardial pressure between dog1 and dog3 might be due to the positioning of the RV segment length sono-micrometer crystals. The right ventricle develops from two embryologically

distinct components the sinus (inflow tract) and conus (outflow tract). The bulbus cordis is a separate chamber which grows distal to both ventricles in the mammalian embryo. This structure becomes incorporated into the ventricles as development proceeds. Keith (76) showed that the bulbus disappeared completely in the left ventricle but remains in the right ventricle. The retention of the circumvascular muscles of the primitive bulbus cordis by the right ventricle is responsible for the existence of the two distinct functional regions (76). The anatomically distinct infundibulum has been shown to undergo significant delays in contraction with a resultant early systolic bulging of the outflow tract (74,75). It has been shown that the ventricular systole is characterized by a sequential contraction beginning at the inflow tract and extending into conal region (74,75). The placement of RV segment length crystals over the outflow tract might be responsible for the observed delayed fall in RV pericardial pressure relative to RA pericardial pressure. Nonetheless the systolic regional difference in pericardial pressure (P_{pra} - P_{prv}) increases with right atrial pressure and is not affected by the timing of the fall RV pericardial pressure (see Figure 4.10 and 4.11). Figures 4.10 (dog 1) and 4.11 (dog 3) show maximum systolic and diastolic difference between RA and RV pericardial pressure at various RA end diastolic cavitary pressures. The magnitude of the systolic regional difference between RA and RV pericardial pressure does not seem to be affected by the timing of RV contraction.

The absolute change in pericardial pressure over the delineated

portions of the cardiac cycle (figure 4.1) are shown in figure 4.12. The increase in diastolic RA and RV pericardial pressure was measured from the bottom of the y-descent to pre a-wave. The absolute changes in RA and RV pericardial pressure over the delineated diastolic period increased linearly with RA end diastolic pressure (correlation coefficient = 0.92 and 0.93 for RV and RA respectively). The change in systolic RA and RV pericardial pressure was measured from the bottom of the x-descent to the peak of the v-wave. Figure 4.12 confirms the nonuniformity of pericardial pressure during systole with negative changes in RV pericardial pressure and positive changes in RA pericardial pressure (correlation coefficient = 0.42 and 0.80 for RV and RA respectively). The magnitude of the positive increases in RA pericardial pressure does during systole are not as great as its diastolic counterpart. In some cases the RA pericardial pressure initially falls before rising at the end of systole (figure 4.8 and 4.9). The fall in RV pericardial pressure during systole did not correlate well with RA end diastolic pressure. This might be due to the timing aspect of the RV contraction. The delineation of the systolic portion of the cardiac cycle was performed using the RA cavitary pressure tracings. In those animals where the RV pericardial pressure decreased after the fall in RA pericardial pressure during systole, the RV pericardial pressure measured might not have reached its lowest value at the time the RA cavitary pressure was at the bottom of the x-descent.

Conclusions

The use of high fidelity pericardial balloons permitted the accurate measurement of RA and RV pericardial pressure over the whole cardiac cycle without catheter motion induced artifacts. This technology provides a method of measuring transmural pressure with high fidelity with an intact pericardium.

During diastole, the pericardial pressure over the right atrium seems to track its right ventricular counterpart from the bottom of the y-descent to the beginning of the a-wave, describing a line of identity between the two pressures. However, in systole, between the bottom of the x-descent and the peak of the v-wave, these two epicardial radial stresses seem to be completely decoupled with P_{prv} falling while P_{pra} remains constant or increases. This systolic decoupling indicates a considerable independence between the right atrium and right ventricle. That is, the systolic emptying of the right ventricle lowers the right ventricular pericardial pressure but right atrial pericardial pressure continues to increase. This suggests that the relation of the pericardium to the right atrium must allow effective constraint even though the right ventricular pericardium is momentarily slack.

In conclusion right atrial and right ventricular pericardial pressure are closely coupled during diastole and during right ventricular systole they become decoupled in that right atrial pericardial pressure rises even though right ventricular pericardial pressure decreases.

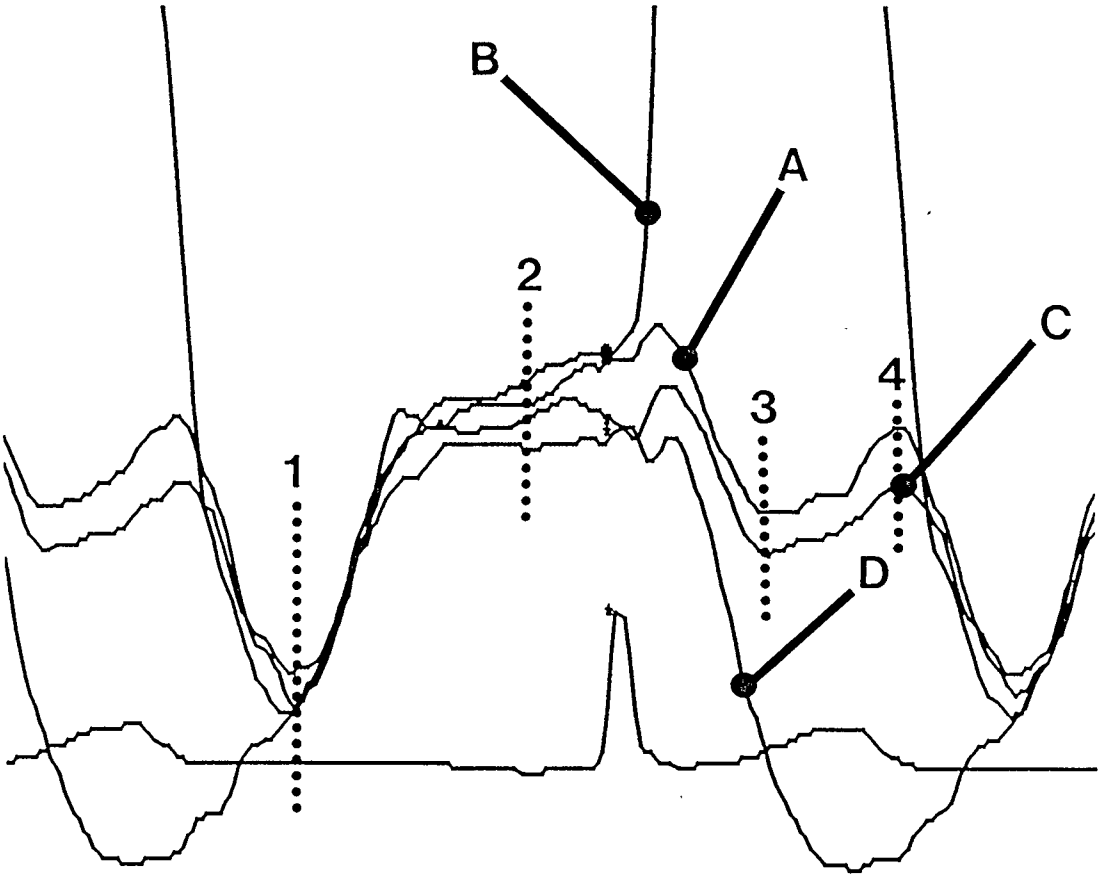

Figure 4.1 Time domain plot showing diastolic and systolic delineators

Time Domain plot of RA cavitary pressure (A), RV cavitary pressure (B), RA pericardial pressure (C) and RV pericardial pressure (D). An EKG is included for timing reference. For the purposes of this paper the cardiac cycle has been broken into two segments:

1.) Diastole - extending from the bottom of the y-descent to just preceding the a-wave. (segment 1 - 2)

2.) Systole - extending from the bottom of the x-descent to the peak of the v-wave. (segment 3 - 4)

Figure 4.2

Time domain plot of RA cavitary pressure (P_{ra}), RV cavitary pressure (P_{rv}), RA pericardial pressure (P_{pra}), RV pericardial pressure (P_{prv}), RV free wall segment length (L_{rv}) and RA appendage dimension (D_{ra}). An EKG tracing is given below for timing reference. Notice the divergence of P_{prv} from P_{pra} during systole.

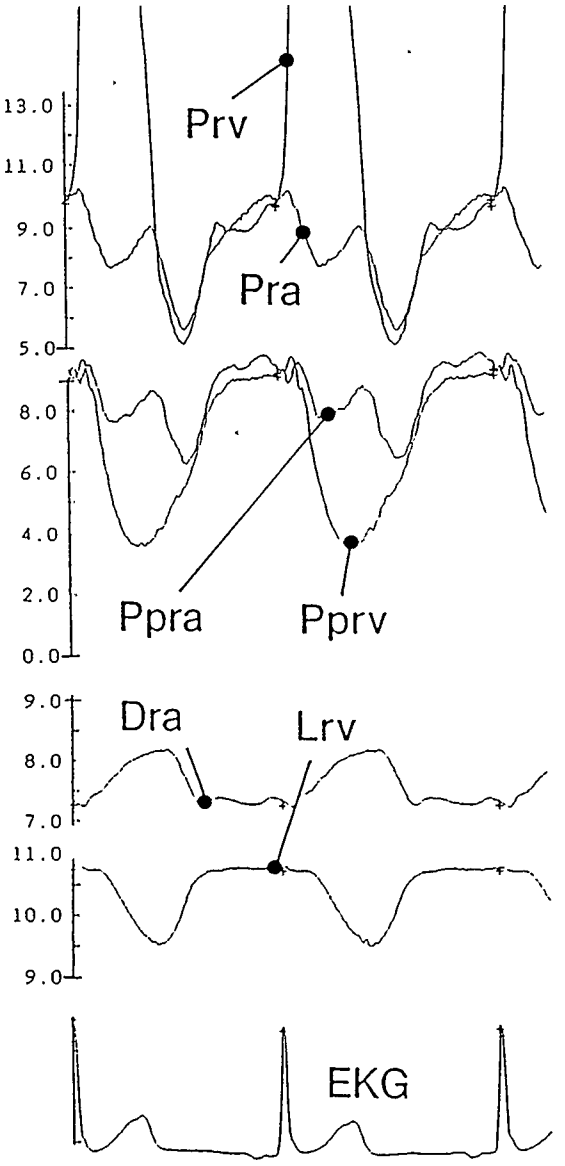

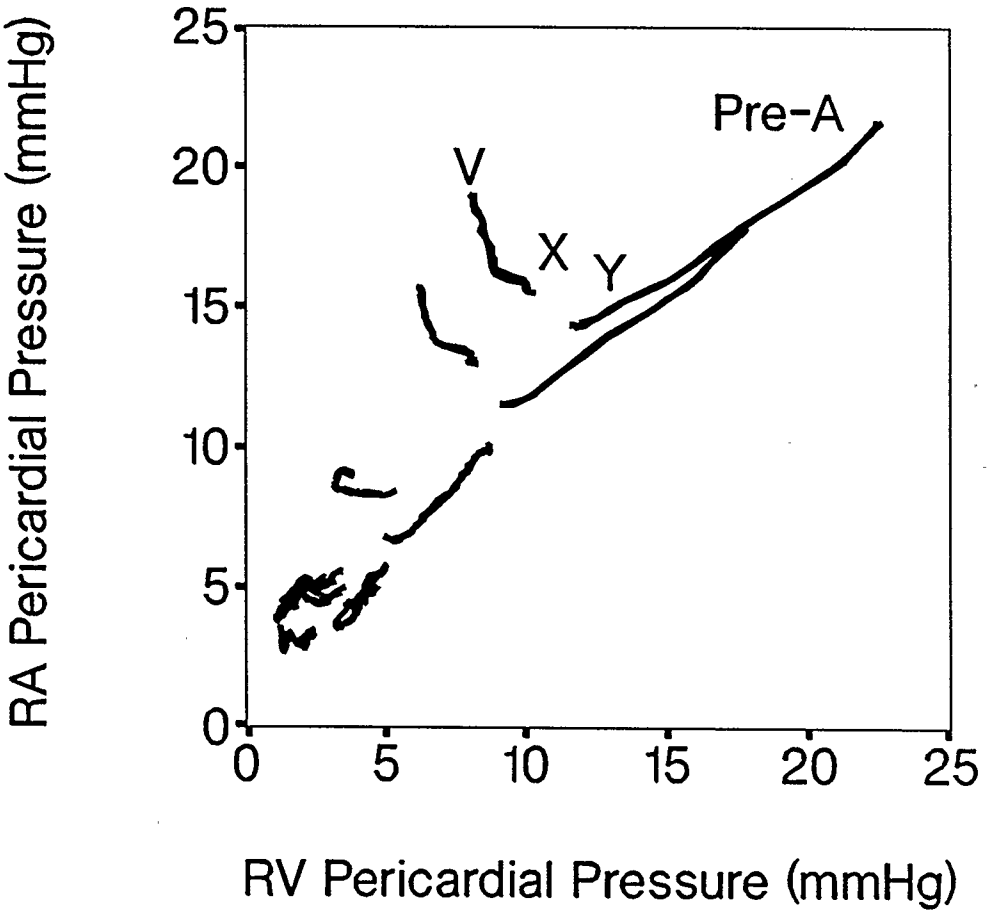

Figure 4.3 - DOG 1

RA pericardial pressure vs RV pericardial pressure. The diastolic segment begins at the bottom of the y-descent and ends just before the a-wave. The systolic segment begins at the bottom of the x-descent and ends at the peak of the v--wave. Diastolic segments fall along the line of identity while a decoupling of these pressures is seen during systole. The diastolic and systolic segments are plotted at various right atrial pressures.

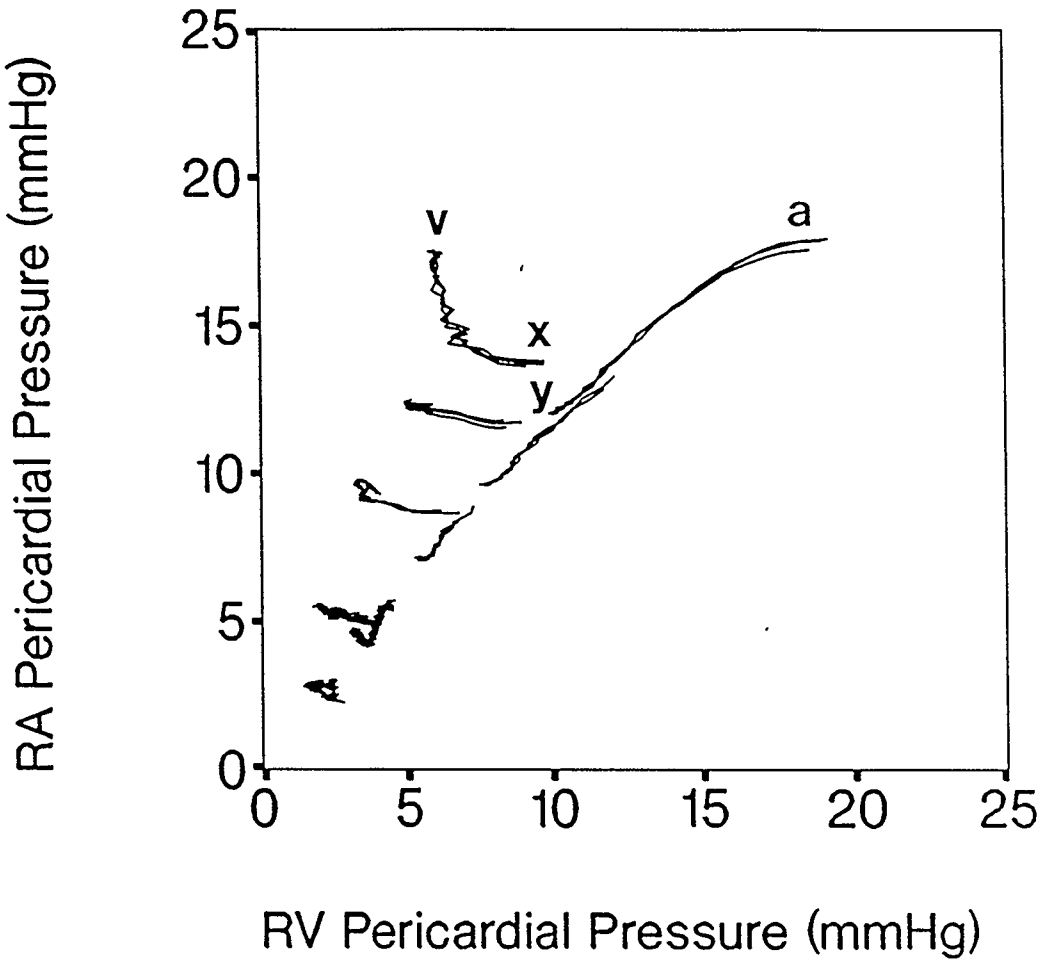

Figure 4.4 - DOG 2

RA pericardial pressure vs RV pericardial pressure. The diastolic segment begins at the bottom of the y-descent and ends just before the a-wave. The systolic segment begins at the bottom of the x-descent and ends at the peak of the v--wave. Diastolic segments fall along the line of identity while a decoupling of these pressures is seen during systole. The diastolic and systolic segments are plotted at various right atrial pressures.

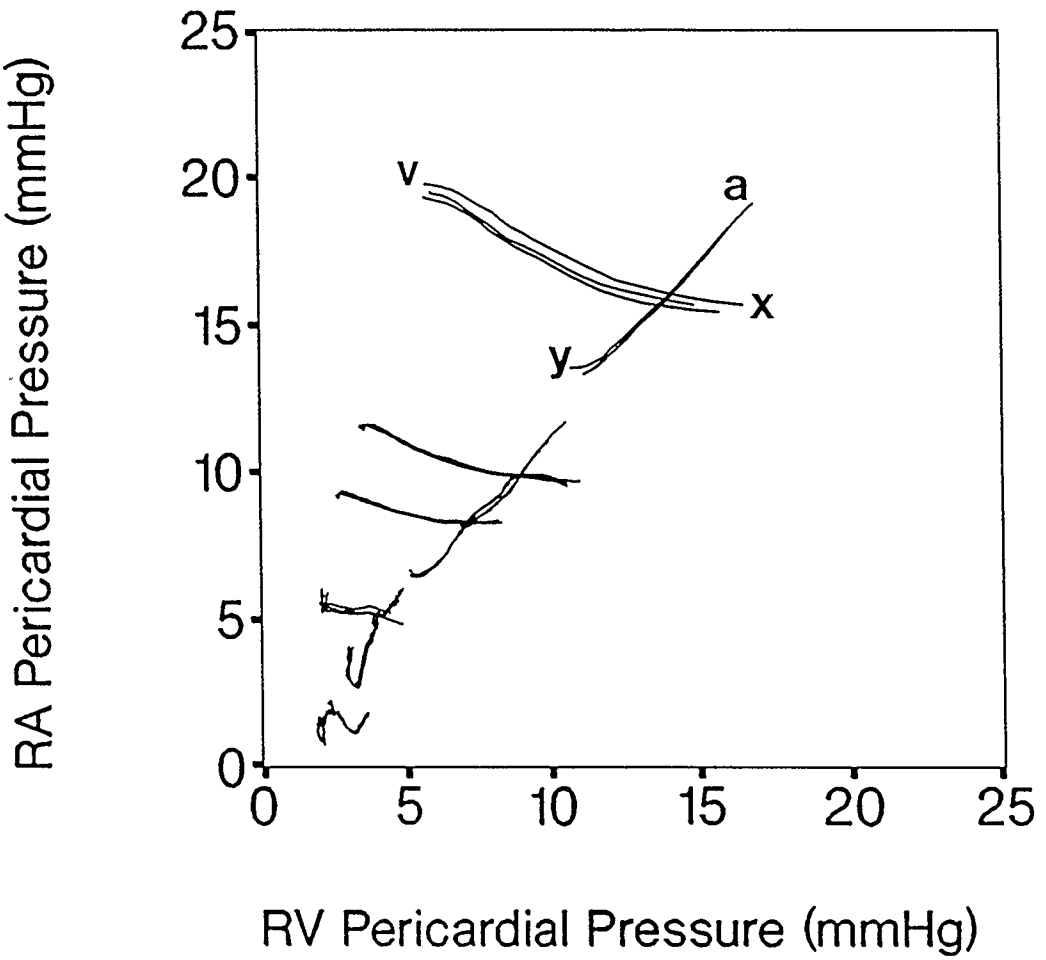

Figure 4.5 - DOG 3

RA pericardial pressure vs RV pericardial pressure. The diastolic segment begins at the bottom of the y-descent and ends just before the a-wave. The systolic segment begins at the bottom of the x-descent and ends at the peak of the v--wave. Diastolic segments fall along the line of identity while a decoupling of these pressures is seen during systole. The diastolic and systolic segments are plotted at various right atrial pressures.

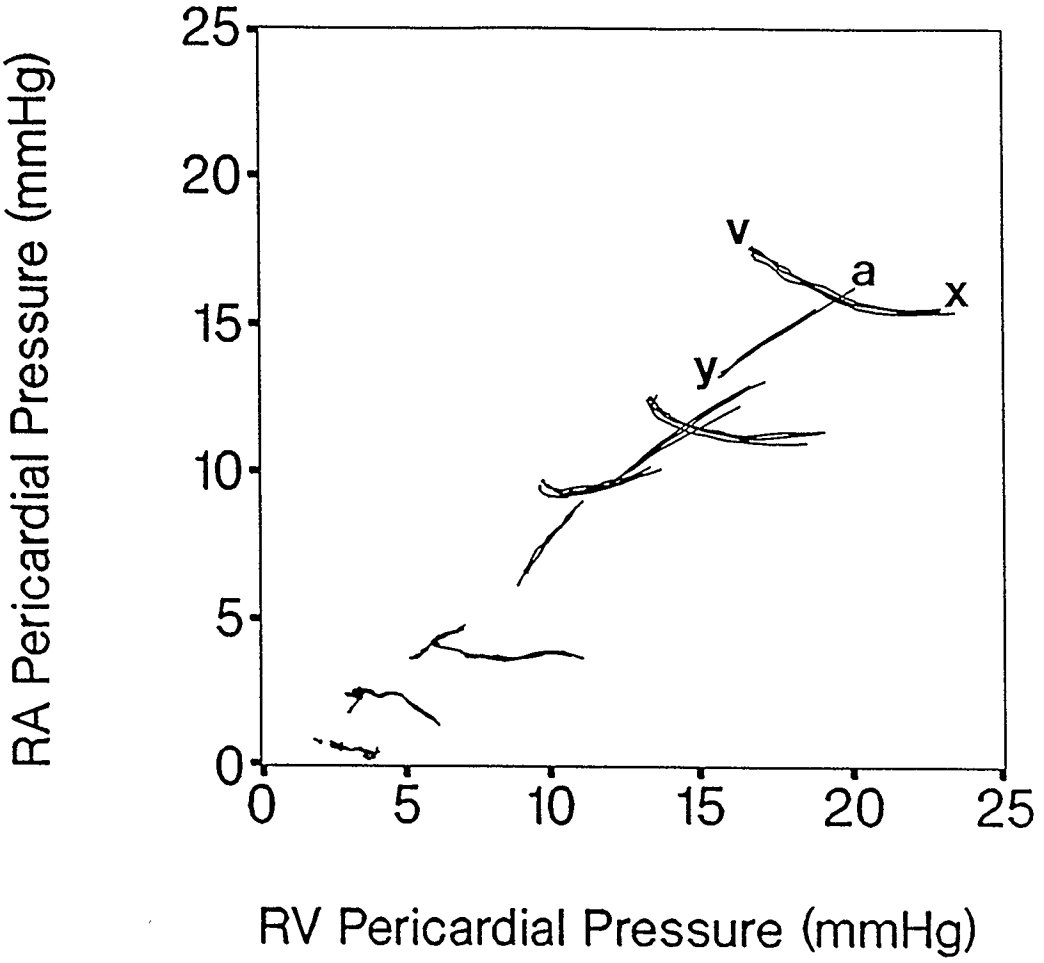

Figure 4.6 - DOG 4

RA pericardial pressure vs RV pericardial pressure. The diastolic segment begins at the bottom of the y-descent and ends just before the a-wave. The systolic segment begins at the bottom of the x-descent and ends at the peak of the v--wave. Diastolic segments fall along the line of identity while a decoupling of these pressures is seen during systole. The diastolic and systolic segments are plotted at various right atrial pressures.

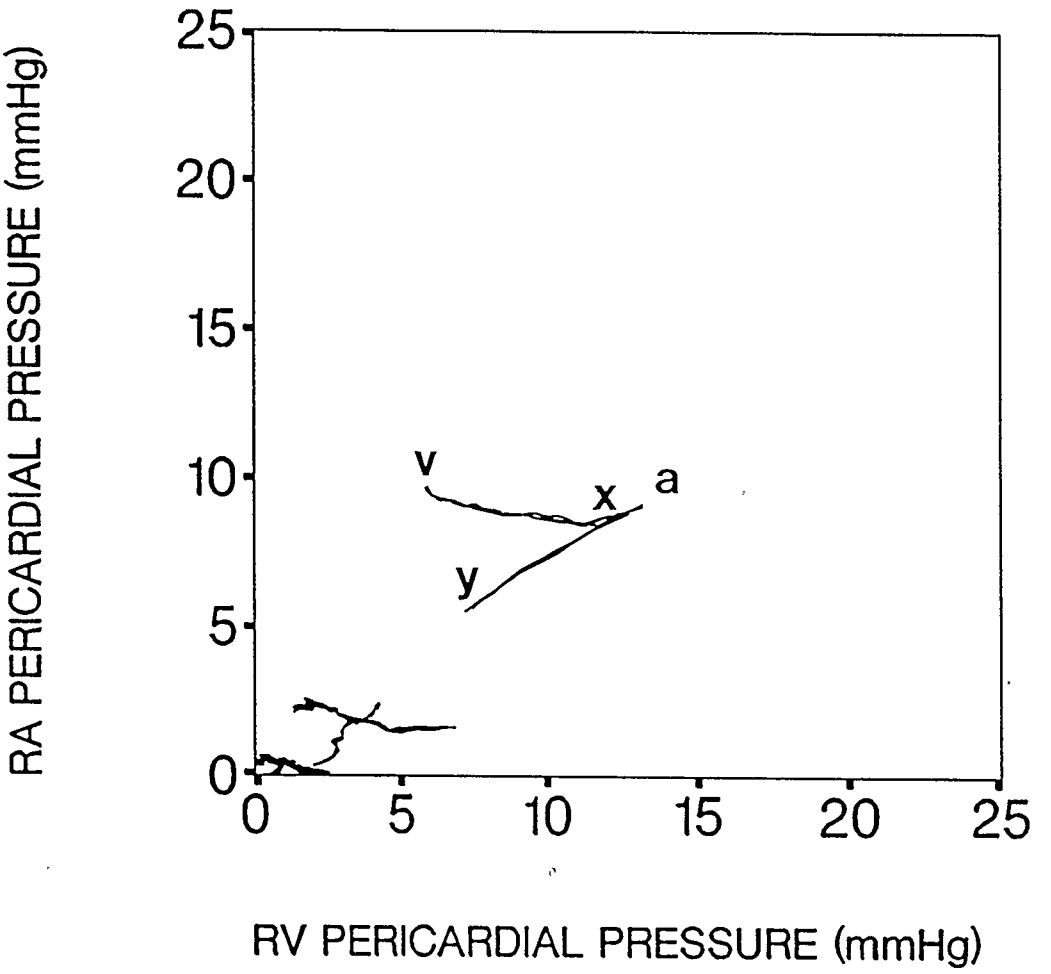

Figure 4.7 - DOG 5

RA pericardial pressure vs RV pericardial pressure . The diastolic segment begins at the bottom of the y-descent and ends just before the a-wave. The systolic segment begins at the bottom of the x-descent and ends at the peak of the v--wave. Diastolic segments fall along the line of identity while a decoupling of these pressures is seen during systole. The diastolic and systolic segments are plotted at various right atrial pressures.

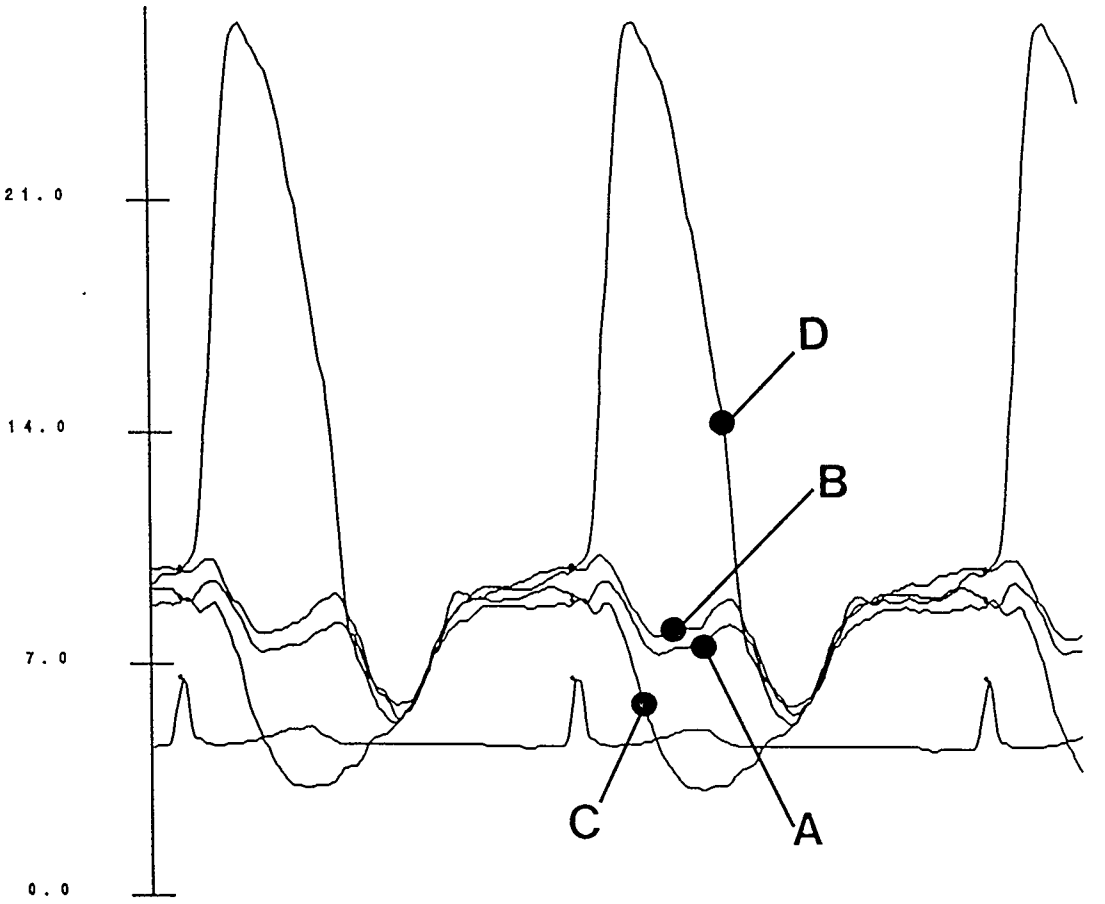

Figure 4.8 Dog 1 - Time Domain Plot

Time domain plot of RA pericardial pressure (A), RA intracavitary pressure (B), RV pericardial pressure (C) and RV intracavitary pressure (D). Mean right atrial pressure = 8 mmhg (Pressure scale is in mmhg). Notice how RV pericardial pressure falls **before** RA pericardial pressure in early systole (see Figure 4.3 - Dog 1). RV pericardial pressure falls while RA pericardial pressure increases in late systole. This systolic decoupling suggests there is considerable independence between the RA and RV.

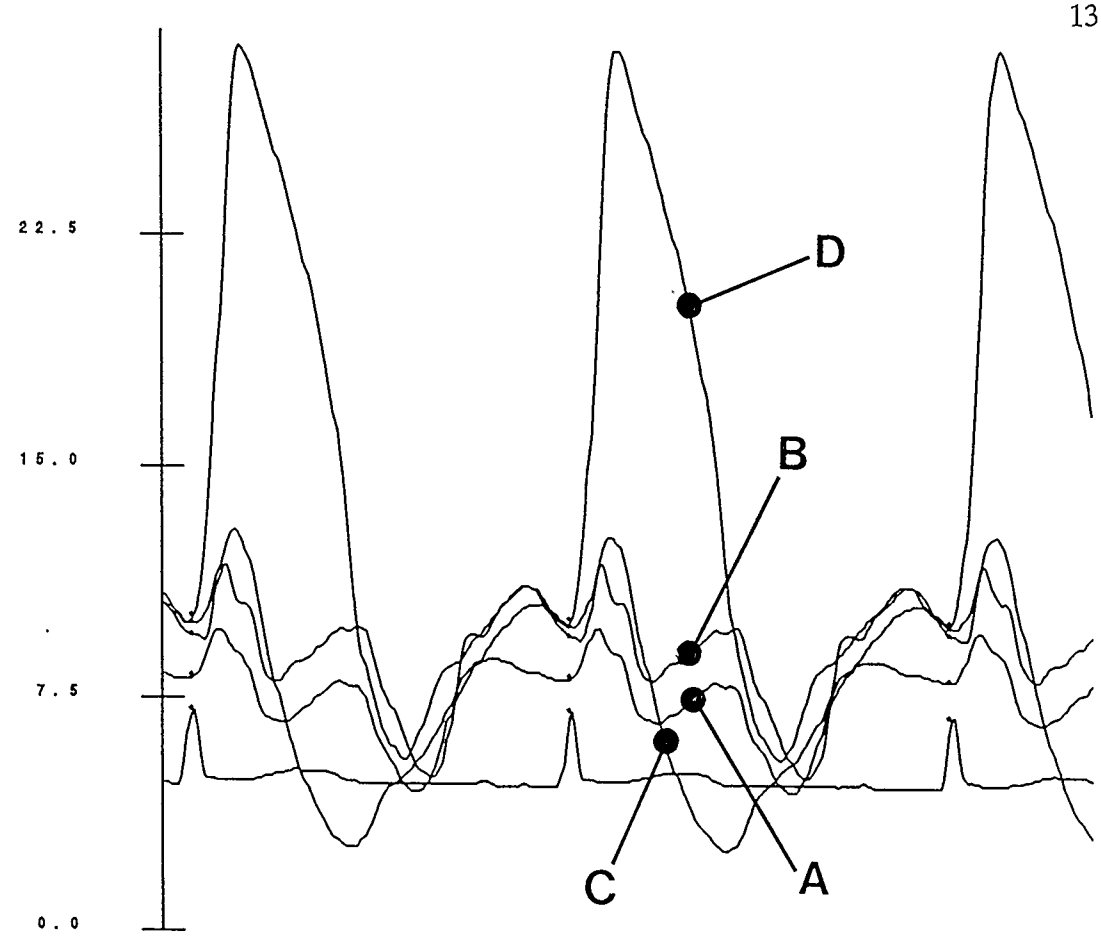

Figure 4.9 Dog 3 - Time Domain Plot

Time domain plot of RA pericardial pressure (A), RA intracavitary pressure (B), RV pericardial pressure (C) and RV intracavitary pressure (D). Mean right atrial pressure = 12 mmhg (Pressure scale is in mm Hg). Notice how RV pericardial pressure falls **after** RA pericardial pressure in early systole (See Figure 4.5 - Dog 3). This might be due to delayed contraction of the RV outflow tract (See text). RV pericardial pressure falls while RA pericardial pressure increases in late systole. This systolic decoupling suggests there is considerable independence between the RA and RV.

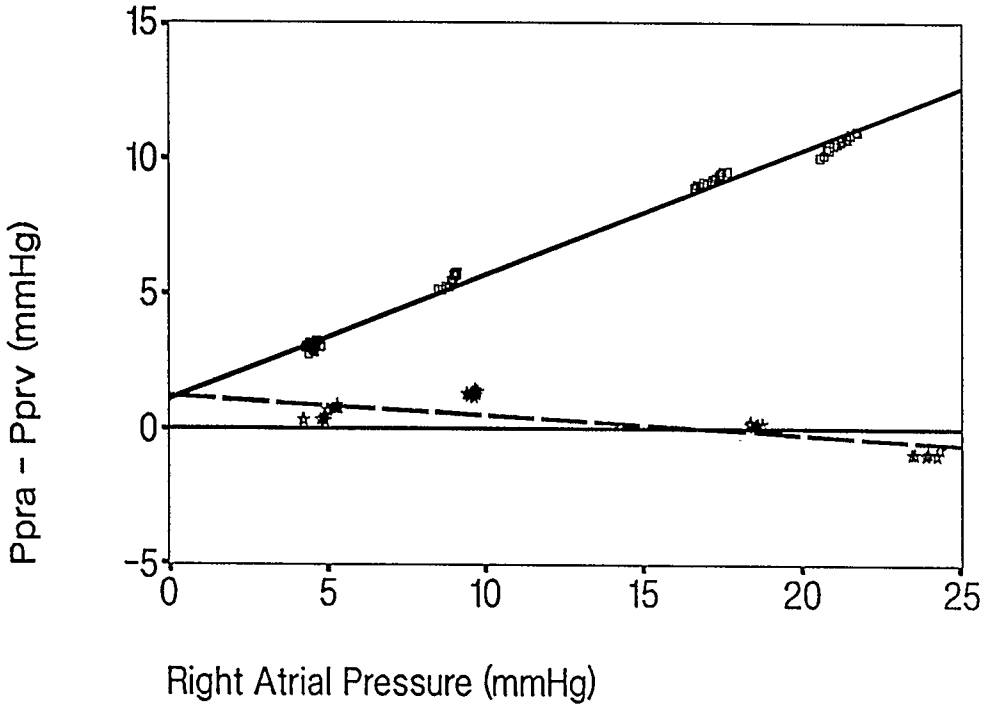

Figure 4.10 - Dog 1 Maximum Regional Difference vs Pra

Plot of the maximum difference between RA and RV pericardial pressure during systole (solid line - squares) and diastole (dashed line - stars) vs RA end-diastolic pressure for Dog 1. Notice the regional difference in pericardial pressure during systole increase with right atrial end-diastolic pressure. This increase in regional pressure differences with loading does not seem to be affected by the timing of the fall in RV pericardial pressure relative to RA pericardial pressure (see Figure 4.8 - Dog 3). The difference in pericardial pressure during diastole is small and does not seem to be sensitive to increases in right atrial pressure.

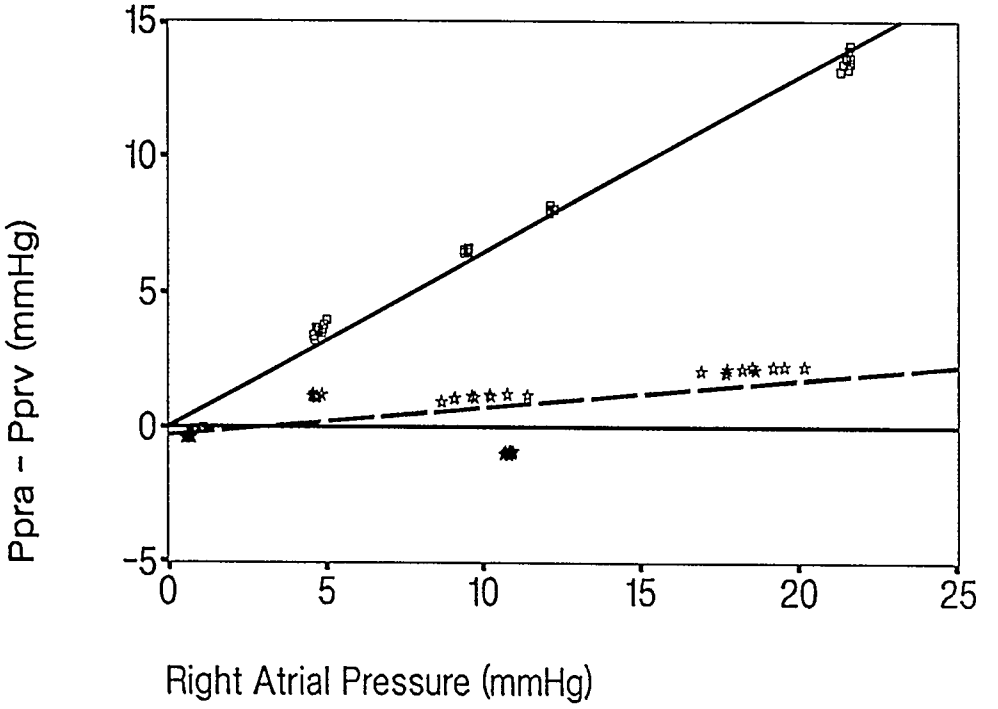

Figure 4.11 - Dog 3 Maximum Regional Difference vs Pra

Plot of the maximum difference between RA and RV pericardial pressure during systole (solid line - squares) and diastole (dashed line - stars) vs RA end-diastolic pressure for Dog 3. Notice the regional difference in pericardial pressure during systole increase with right atrial end-diastolic pressure. This increase in regional pressure differences with loading does not seem to be affected by the timing of the fall in RV pericardial pressure relative to RA pericardial pressure (see Figure 4.9 - Dog 1). The difference in pericardial pressure during diastole is small

and does not seem to be sensitive to increases in right atrial pressure.

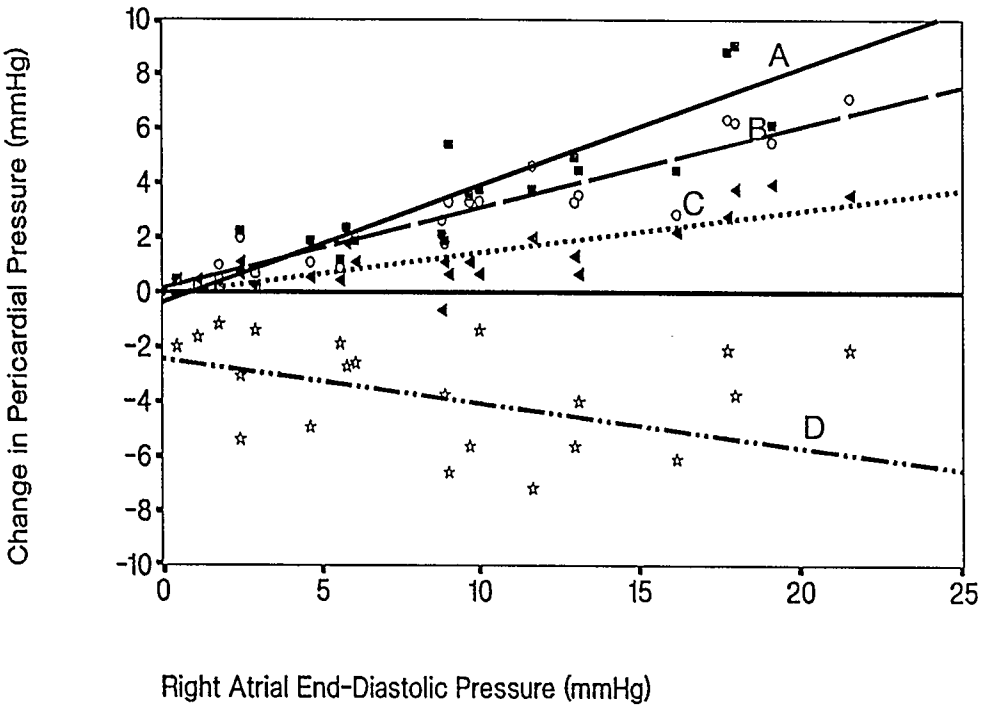

Figure 4.12 Change in Pericardial Pressure vs RA Cavitary Pressure

Line A. - Absolute change in RV pericardial pressure during diastole (Correlation Coefficient = 0.92)

Line B. - Absolute change in RA pericardial pressure during diastole (Correlation Coefficient = 0.93)

Line C. - Absolute change in RA pericardial pressure during systole (Correlation Coefficient = 0.80)

Line D. - Absolute change in RV pericardial pressure during systole (Correlation Coefficient = 0.42)

Plot of the absolute change in RA and RV pericardial pressure during systole and diastole vs right atrial pressure (pooled data all dogs). During diastole, both RA and RV pericardial pressure increase in almost equal amounts from the bottom of the y-descent to just before the a-wave. During systole, the RA pericardial pressure increases but RV pericardial pressure decreases. The magnitude of RV pericardial pressure decrease during systole does not correlate well with right atrial end-diastolic pressure.

Chapter 5

POSITIVE WORK IS TRANSMITTED ON SEGMENTS OF THE RIGHT VENTRICLE VIA THE OVERLYING PERICARDIUM IN DOGS

Introduction

The basis of many techniques used to assess myocardial contractile performance is a quantification of the muscle's ability to generate mechanical work in its normal environment. For the chambers of the heart this requires that the stroke volume or work be assessed as a function of end-diastolic volume or transmural pressure. The accurate determination of ventricular dimensions or volumes using sonomicrometry or 2D-echocardiography has been widely employed for the purposes of quantifying left ventricular (LV) hydrodynamic work. Assessment of right ventricular (RV) dimension and volume has been more difficult because the greater complexity of the RV geometry and contraction pattern (77). Investigation of RV mechanics has focused primarily on describing the heterogeneity of RV free wall contraction (74). Morris et al (77) showed that accurate assessments of beat-to-beat RV volume and stroke work can be obtained by analysis of dynamic RV free wall

chord dimension or segment length.

Nagano et al (67) and Arakawa (78) measured left atrial (LA) compliance using biplane cineangiography to determine volume and the Brockenbrough technique to measure pressure. They found the diastolic LV cavitary compliance to be 2-3 times larger than the LA compliance. Chapter 3 has shown that the end-diastolic transmural compliance of the right atrium (RA) in dogs and humans to be significantly greater than its RV counterpart. This difference in cavitary and transmural pressure-volume relationships has never been examined over the whole cardiac cycle.

The full understanding of the dynamic behaviour of the heart requires that its contractile performance should be observed in its natural milieu. This has been difficult since the assessment of pericardial constraint, without tamponade, over the whole cardiac cycle has been difficult due the poor dynamic response of available pericardial radial stress transducers. Recently developed high-fidelity pericardial balloon technology allows the researcher to measure the pericardial pressure over the free wall of any cardiac chamber over whole cardiac cycle with fidelity sufficient for the determination of most hemodynamic parameters. The investigator can now determine the dynamic transmural pressure-dimension relationship of any chamber with an intact pericardium. Chapter 3 has shown that a conventional liquid-filled pericardial balloon may be used to the determine extremely small diastolic transmural pressures of the right atrium and ventricle with remarkable accuracy and

minimal physiological disturbance. The-high fidelity balloon is essentially identical to the conventional pericardial balloon with the exception of the insertion of a 3F micromanometer catheter into the catheter lumen of the balloon.

Rationale

The high fidelity pericardial balloon technology has permitted the accurate determination of transmural pressure of any chamber of the heart over the whole cardiac cycle. With this in mind we designed an experiment which would examine the dynamic behaviour of the right atrial and ventricular pericardium and myocardium with an intact pericardium. In particular, we are interested in the contribution the pericardium makes in the systolic behaviour of these chambers. Chapter 3 shows the significant contribution the pericardium makes to the end-diastolic transmural pressure-dimension relationship of the right atrium and ventricle. The purpose of this study is to quantify the work being done on the fluid of the right atrium and ventricle by pericardium and myocardium over the whole cardiac cycle.

Methods

After receiving 10 - 20 mg morphine sulfate (i.m.), seven mongrel dogs (20-25 Kg.) of both sexes were anaesthetized with 12.5 mg/Kg sodium thiopental. Anaesthesia was maintained with 30 μg/Kg/min fentanyl while ventilation with

a 2:1 nitrous oxide:oxygen mixture was delivered by a constant-volume ventilator. All dogs received a tidal volume of 15 ml/kg and a positive end-expiratory pressure of 2 cm H_2O was applied. The animals were maintained at 37°C using a circulating-water warming blanket and a constant-temperature heating system. The ECG was continuously monitored throughout the experiment.

With the dog in the supine position, a midline sternotomy was performed and 100 to 200 ml of heparinized Ringer's lactate solution were infused to maintain normal aortic pressure. The left lateral surface of the pericardium was opened using a longitudinal incision, with the ventricles delivered through this incision for purposes of instrumentation. RV free-wall segment length (L_{rv}) and RA appendage diameter (D_{ra}) were measured by sonomicrometry as previously described by Smiseth et al (33). The RV segment-length crystals were placed in the inflow tract approximately parallel to the atrioventricular groove in a manner similar to the placement by Raines et al (74). Two flat liquid-containing balloon transducers were attached loosely to the epicardium with single stay sutures; one was positioned over the RV free wall adjacent to the crystals, and the other was positioned cephalad to the sonomicrometer crystals on the RA appendage. The heart was repositioned into the pericardium and the pericardial margins reapproximated using interrupted 3-0 silk sutures spaced 1 cm apart, taking care to avoid compromising pericardial volume. RV and RA cavitary pressures were

measured using 8F micromanometer-tipped catheters with reference lumens inserted through the internal jugular and femoral veins, respectively. Aortic pressure was measured with an 8-F fluid-filled catheter introduced through the femoral artery. Inferior vena cava and pulmonary arterial pneumatic vascular constrictors were also positioned on all dogs. The RV balloon (3.0 cm x 3.0 cm) was fabricated from Silastic sheets and attached to a 70-cm 8F cardiac catheter. The RA balloon dimensions were 1.2 cm x 1.4 cm with a 20-cm length of Silastic medical grade tubing connected directly to a pressure transducer. A calibration curve for both balloons and transducers was described before and after each experiment using techniques described in Chapter 1. No differences between pre- and post-experiment calibration curves were found in any experiment. Each balloon had a 3F micromanometer-tipped catheter positioned internally to provide a high-fidelity measurement of balloon pressure. Intra-balloon catheter-tip pressure transducers do not sense the artifacts and oscillations generated from catheter motion and also are free of the frequency-dependent transmission characteristics of fluid-filled tubes. The dynamic response of this high fidelity balloon pressure measuring system is linear with a flat frequency response to 200 Hz (68, Chapter 1).

Conditioned signals were acquired using a personal computer which digitized analog signals (pressure, dimension and ECG) that were scaled using gain and offset amplifiers and then filtered with a 7th order Cauer elliptic lowpass active anti-aliasing filter before being sampled at 200 Hz using a 12-bit analog-

to-digital converter. The digitized data were subsequently analyzed on a different personal computer, using analytical software developed in our laboratory and statistical and graphics software.

Protocol

After preparatory surgery, all animals were stabilized for 1/2 hour before any data were recorded. Mean RA pressure was caused to vary from 0 to 25 mm Hg by adjusting intravascular volume (Ringer's lactate solution was infused or blood removed through a large-bore catheter in an external jugular vein) or by manipulating the inferior vena cava or pulmonary artery vascular pneumatic occluders.

Hemodynamic and sonomicrometer measurements were obtained continuously for 1 minute at each volume load state (ie, after each incremental increase of mean RA cavitary pressure), each recording interval beginning with a 20-second control period. The ventilation was interrupted at the end-expiratory position for several cardiac cycles during each recording interval.

Data Analysis

Only data collected at end expiration were analyzed. All high-fidelity micromanometer-tipped catheter signals were corrected to equal their corresponding pressure recorded via the fluid-filled catheter at end diastole. This correction was performed using software that automatically adjusted the

mean pressure of the micromanometer-tipped catheter to equal the mean of its fluid-filled counterpart. This method was completely automatic and therefore eliminated operator input; nonetheless, all pressure tracing corrections were inspected visually to ensure validity, although no adjustments were made. All data were collected over 60-second intervals. The post-experiment analysis involved the extraction of three consecutive cardiac cycles at end expiration from the sampled data file (5 milliseconds sampling interval).

Pressure-dimension loop work was calculated by applying Green's theorem to determine loop area. The numerical algorithm is as follows:

$$Loop\ Area = \frac{1}{2}\sum_{i=0}^{n} (X_i - Y_{i+1}) - (X_{i+1} + Y_i)$$

$$X_i = Dimension\ of\ the\ i_{th}\ sample$$
$$Y_i = Pressure\ \ of\ the\ i_{th}\ sample$$

Results

The results from the six animals are quite consistent in that they all had positive (counter clockwise) right ventricular cavitary, pericardial and transmural pressure-dimension loops. The calculated values of RV cavitary work (W_{cav}), pericardial work (W_{peric}), transmural work (W_{trans}) and mean RA pressure (P_{ra}) are given in Table 5.1 for each dog (Dog 7 is not included

because it had an infarcted RV). The ratio of pericardial work to cavitary work (W_p/W_c) is given in the right most column of Table 5.1 as a percent, indicating the portion of the work being done on the blood by the pericardium over the RV free wall. The pericardial work was positive (see Table 5.1) in all dogs.

Table 5.2 gives the mean (± standard deviation) pericardial work to cavitary work ratio (W_{peric}/W_{cav}) for all dogs at mean RA pressures of 5, 7.5, 10 and 15 mmHg. The pericardium over the RV free wall seems to contribute approximately 20% of the cavitary work at physiological pressures and dimensions. The mean W_{peric}/W_{cav} ratio was calculated by interpolating the data in Table 5.1. Figure 5.1 gives the RV pressure-dimension loop for Dog 5 showing cavitary pressure-dimension (upper left panel), pericardial pressure-dimension (upper right panel) and transmural pressure-dimension relationships with a mean RA pressure of 10 mm Hg. Each pressure-dimension plot in Figure 5.1 consists of 3 consecutive superimposed cardiac cycles all going counter-clockwise (ie, performing positive work). The transmural loop was calculated by subtracting the time-domain pericardial pressure tracing from the cavitary pressure tracing. With reference to Figure 5.1, the total work imparted onto the blood by the endocardial surface of the free wall of the right ventricle (W_{cav} = 20.7 mm Hg-mm) is given by the loop-area of the RV cavitary pressure vs RV segment-length relationship. However, the actual contribution of work by the RV free wall myocardium (W_{trans} = 14.0 mm Hg-mm) is given by the RV transmural pressure vs segment-length relationship. The remainder

of positive work (W_{peric} = 6.7 mm Hg-mm), approximately 1/4 of the total W_{cav}, was delivered by the pericardium. The author suggests that this pericardial work is derived from the contraction of the LV in early systole. The iso-volumic contraction of the left ventricle causes it to assume a spherical shape. The wall stresses might be minimized if it assumes this shape rather than that of a truncated ellipsoid (a geometry which is commonly used to model its end-diastolic dimensions). The shortening of the major axis of the left ventricle during iso-volumic contraction has been documented widely (79). The conservation of mass requires that the septum to free wall and anterior-posterior dimensions of the left ventricle increase during the isovolumic period. The pericardium is a relatively noncompliant entity which should not accommodate these coronal increases in LV dimension . Figure 5.2 gives the time-domain plot of pressures and dimensions used to derive the loops displayed in Figure 5.1. Notice the increased RV pericardial pressure (P_{prv}) in early systole. This increase in RV pericardial pressure in early systole should be matched by an equivalent increase in LV pericardial pressure (to be confirmed by further investigations). The resultant early systolic increase in pericardial pressure imposed on the RV free wall might assist it in its task of pumping blood through the pulmonary circulation.

It is interesting to note the behaviour of the infarcted RV pressure-dimension loops for Dog 7 in Figure 5.3, showing the cavitary pressure-dimension (upper left panel), pericardial pressure-dimension (upper right panel) and

transmural pressure-dimension (lower right) relationships at a mean RA pressure of 12 mm Hg. Each plot consists of 3 consecutive superimposed cardiac cycles with the pericardial and cavitary pressure loops going clockwise (ie, performing negative work). The transmural loop is positive (W_{trans} = +1.2 (mm Hg-mm)) but the net work being done on the fluid (W_{cav} = -1.3 (mm Hg-mm)) is negative due to infarction. The partially functioning myocardium prevents the cavity fluid from performing the full amount of negative work on the pericardium (W_{peric} = -1.3 (mm Hg-mm)). If the myocardium was completely nonfunctional then the transmural loop area would be small and negative and the pericardial and cavitary pressure-dimension loops would be almost equal and also negative. Figure 5.4 shows the time-domain plots of pressure and dimension of the infarcted RV pressure-dimension loops shown in Figure 5.3. Notice the paradoxical increase in RV segment-length (L_{rv}) during systole.

Figure 5.5 gives a typical RA pressure-dimension loop showing cavitary pressure-dimension (upper left panel), pericardial pressure-dimension (upper right panel) and transmural pressure-dimension relationships with a mean RA cavitary pressure of 5 mm Hg. The transmural loop is calculated by subtracting the time-domain pericardial pressure tracing from the cavitary pressure tracing. The atrial pressure-dimension loop is counter-clockwise (positive work) for the a-loop (atrial contraction) and clockwise for the v-loop (ventricular contraction).

An expanded plot of the RA transmural pressure-dimension relationship in Figure 5.5 is given in Figure 5.6. Upon RA contraction, (a-wave) the RA pressure increases but the volume decreases, creating the positive-area a-loop. As the RV contracts, the RA volume, and then, the RA pressure increases, until RA filling and pressure reach a maximum near end systole at the peak of the v-wave. The atrio-ventricular valve then opens after the RV relaxes and the RA volume and pressure decrease rapidly. For the following ventricular slow filling period, beginning at the bottom of the y-descent and extending to the beginning of the a-wave, both the RA and RV fill passively during this period. The passive filling of the RA is called the v-loop. The cavitary loops measured in dogs are similar to those found in humans by Nagano et al (67). However the RA transmural pressure-dimension loop (see Figure 5.5 and 5.6) shows the extremely small transmural pressures developed during the v-loop. These small transmural prressures are significant when one considers the magnitude and range of cavitary pressures and dimension measured during this interval. It was not possible to examine the pooled data of RA work since several dogs had no measurable a-wave.

Conclusions

Advances in pericardial balloon technology permit the measurement of pericardial pressure over the whole cardiac cycle. We determined that pericardium contributes to the right ventricular free wall cavitary work significantly over mean right atrial pressures ranging from 5 to 15 mm Hg. The mechanism responsible for this requires further investigation involving instrumenting the left and right free walls of the heart with the high-fidelity pericardial balloons.

In conclusion, we have found the pericardium contributes approximately 20% of the total work being imparted to the blood by the RV free-wall under normal physiological conditions.

Table 5.1 Work Performed by Pericardium and Myocardium

Dog	P_{ra}	W_{cav}	W_{peric}	W_{trans}	W_p/W_c
1	5	7.6	2.0	5.6	26.3%
1	8	8.6	2.7	5.8	31.4%
1	12	10.4	3.0	7.4	28.8%
2	8	21.3	6.6	14.7	31.0%
2	12	19.6	8.4	11.2	23.3%
3	4	20.3	0.9	19.4	4.4%
3	7	18.6	1.8	16.7	9.7%
3	21	41.8	9.2	36.2	22.1%
4	3	20.4	1.1	19.3	5.6%
4	5	38.0	3.0	35.0	7.9%
4	10	39.4	6.0	33.4	15.2%
5	5	26.5	6.2	20.3	23.4%
5	10	20.7	6.7	14.0	32.4%
5	15	18.9	5.1	13.8	27.0%
6	11	19.7	8.4	11.3	42.6%
6	17	25.0	9.1	15.9	36.4%

The calculated cavitary work (W_{cav}), pericardial work (W_{peric}), transmural work (W_{trans}) and mean RA pressure (P_{ra}) are given for each dog. The ratio of pericardial work to cavitary work (W_p/W_c) is given in the right most column as a percent of the total work being done on the blood by that segment of RV free wall.

Table 5.2 Ratio of Pericardial to Cavitary Work at Various Mean Right Atrial Pressures (Pooled data of all Dogs)

Mean P_{ra}	(W_{peric} / W_{cav}) X 100%
5.0	15.9 ± 10.7
7.5	20.1 ± 10.9
10.0	22.3 ± 10.0
15.0	23.1 ± 12.4

The mean (± standard deviation) pericardial work to cavitary work ratio (W_{peric}/W_{cav}) for all dogs is given at mean RA pressures (P_{ra}) of 5, 7.5, 10 and 15 mm hg. The pericardium over the RV free wall seems to contribute approximately 20% of the cavitary work. The mean is calculated by interpolating data in Table 5.1.

Figure 5.1

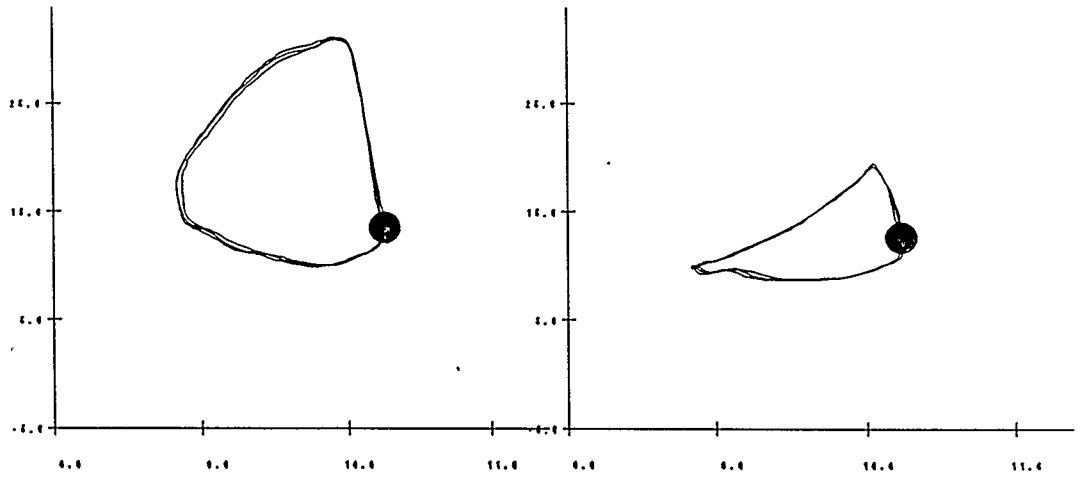

RV pressure-dimension loop for Dog 5 showing cavitary pressure-dimension (upper left panel), pericardial pressure-dimension (upper right panel) and transmural pressure-dimension (lower right panel) relationships with a mean RA pressure of 10 mm Hg. The

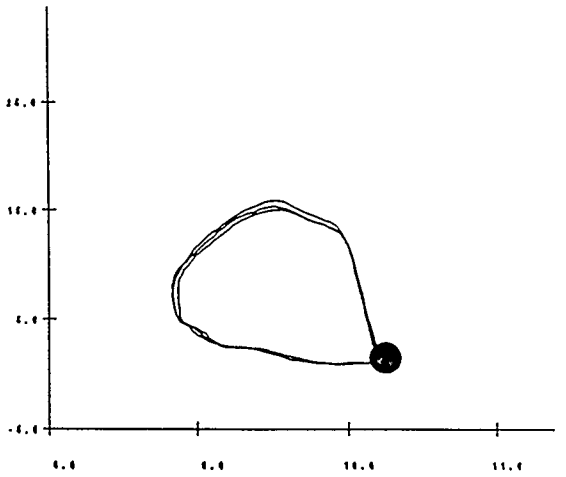

time-domain plot of the pressures for these loops are given in Figure 5.2. Each plot consists of 3 consecutive superimposed cardiac cycles all going counter-clockwise (ie, performing positive work). The transmural loop is calculated by subtracting the time-domain pericardial pressure tracing from the cavitary pressure tracing. In all dogs the pericardial work was positive (see Table 5.1). The dot ● in each plot is the end-diastolic delineator.

Figure 5.2 Time Domain Plot of Pressures and Dimension in Figure 5.1

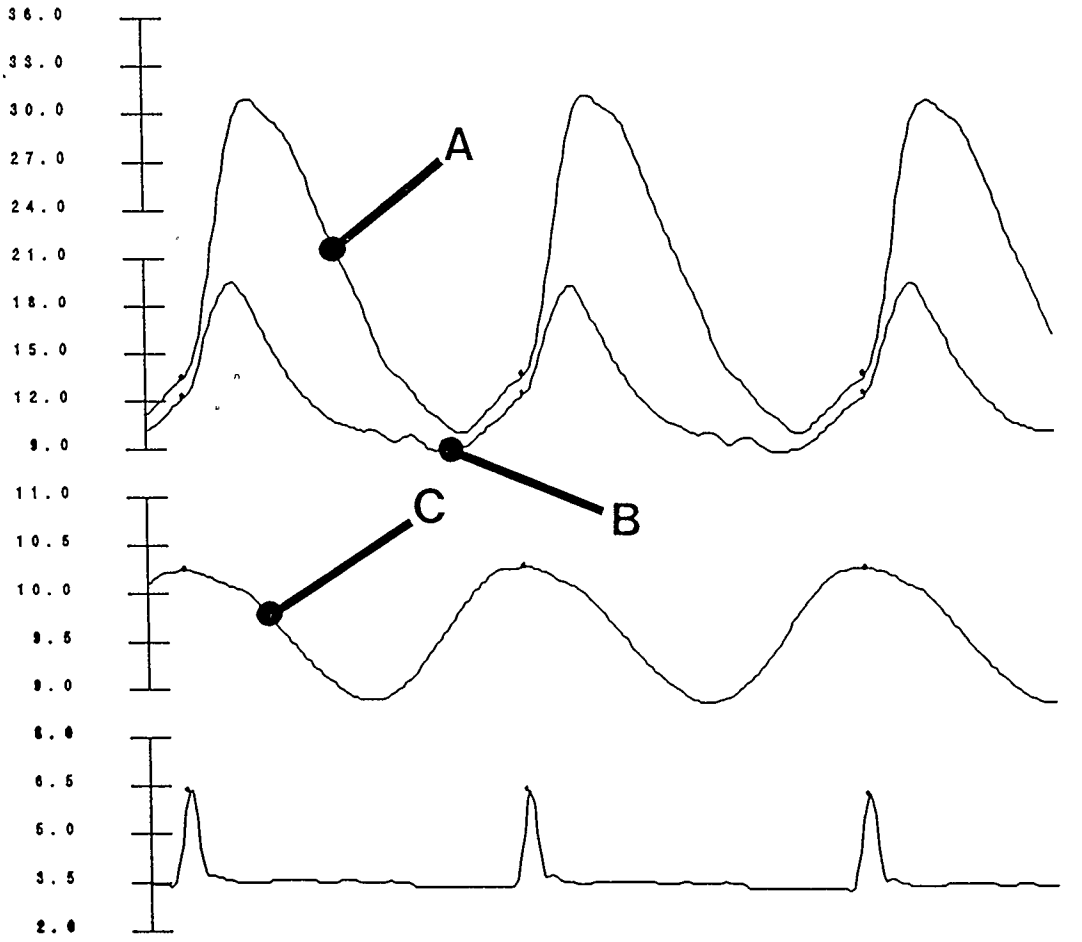

Time-domain plot of pressures displayed in figure 5.1. RV pressure (A), RV pericardial pressure (B), RV free-wall segment length (C) and EKG are shown. The reader may not expect a positive pericardial pressure-dimension loop (see Figure 5.1) since the RV pericardium slackens during systole. However, the fall in RV pericardial pressure is not rapid relative to RV segment length shortening and the loop is positive (Pressure units = mm Hg, Segment length units = mm).

Figure 5.3 Pressure-Dimension Loops for an Infarcted Right Ventricle

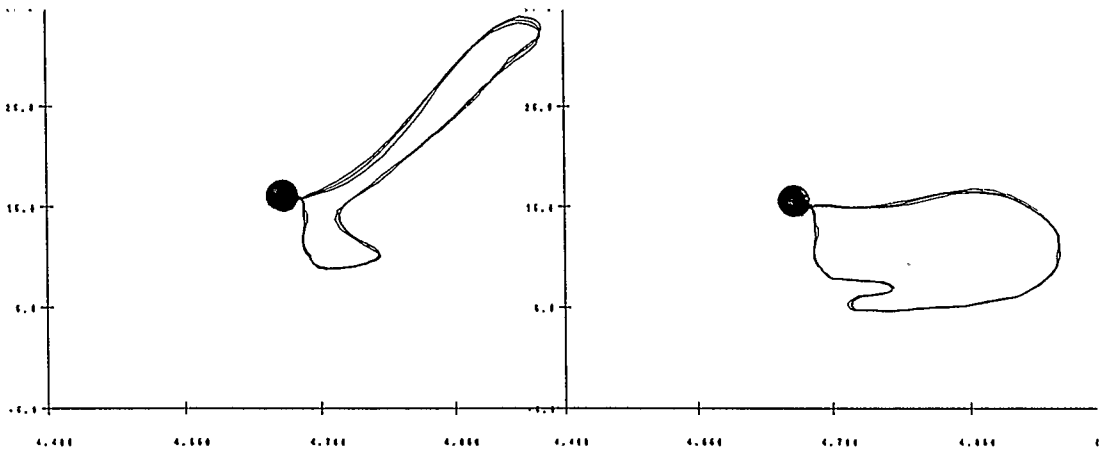

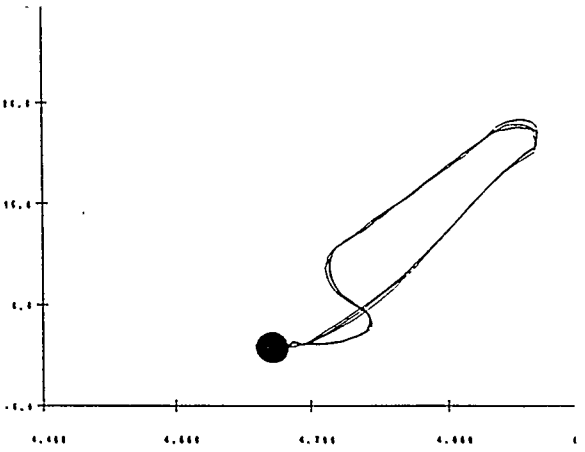

RV pressure-dimension loops for Dog 7 (not included in the pericardial work database due to infarction) showing cavitary pressure-dimension (upper left panel), pericardial pressure-dimension (upper right panel) and transmural pressure-dimension relationships with a mean RA pressure of 12 mm Hg. Each plot consists of 3 consecutive superimposed cardiac cycles with the pericardial and cavitary pressure loop going clockwise (ie, performing negative work). The transmural loop is calculated by subtracting the time-domain pericardial pressure tracing from the cavitary pressure tracing. The transmural loop is positive (W_{trans} = +1.2 (mm Hg-mm)) but the net work being done on the fluid (W_{cav} = -1.3 (mm Hg-mm)) is negative due to infarction. The partially functioning myocardium prevents the cavity fluid from performing the full amount of negative work on the pericardium (W_{peric} = -2.5 (mm Hg-mm)). If the myocardium was completely nonfunctional then the transmural loop area would be small and negative. The dot ● marks end diastole. Notice that the smallest dimension is found at end diastole, this is due to the paradoxical segment-length movement of the infarcted RV

Figure 5.4 Time-Domain Plot of Pressures and Dimensions for Figure 5.3

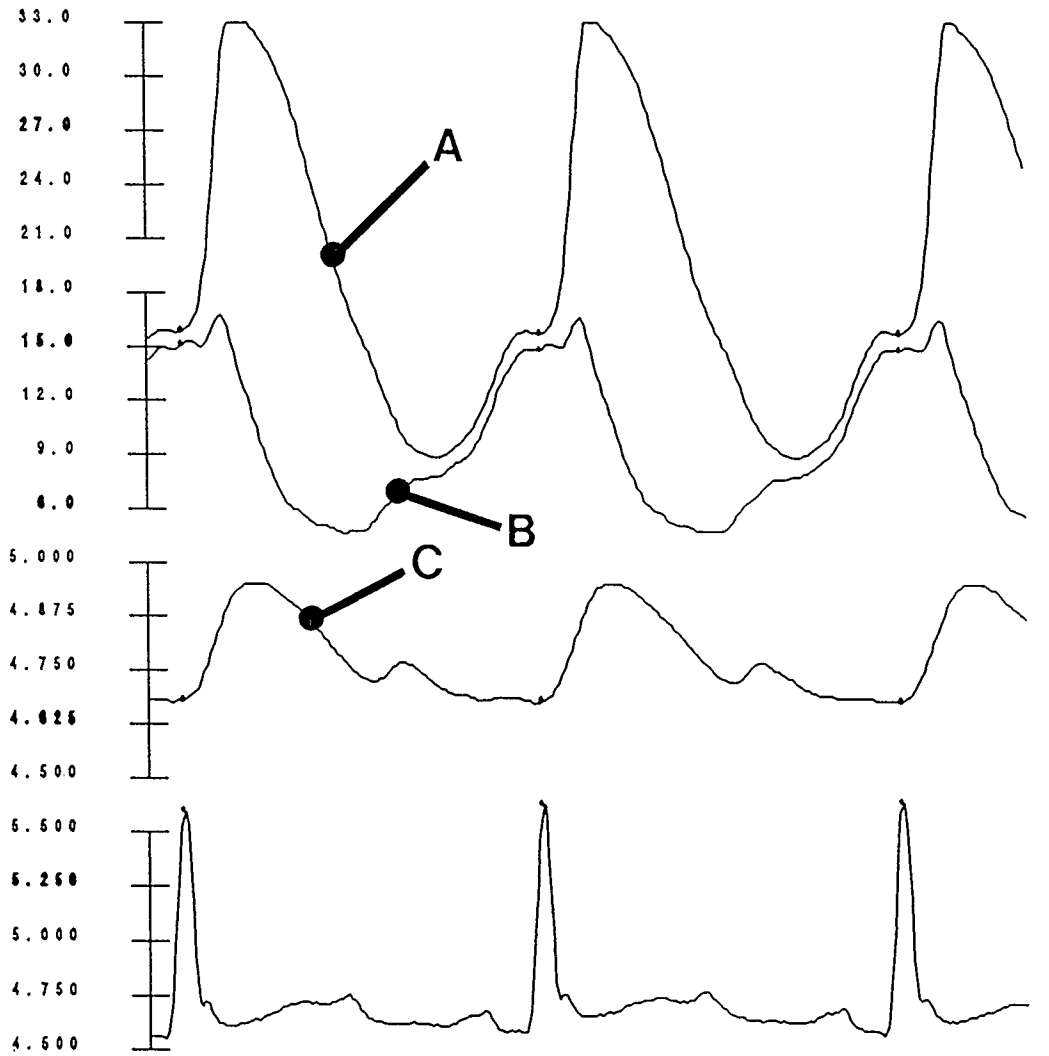

Time-domain plot of pressures displayed in figure 5.3. RV pressure (A), RV pericardial pressure (B), RV free-wall segment length (C) and EKG are shown. The reader may notice the paradoxical movement of the RV segment (ie, length increases during systole).

Figure 5.5 Right Atrial Pressure-Dimension Relationships

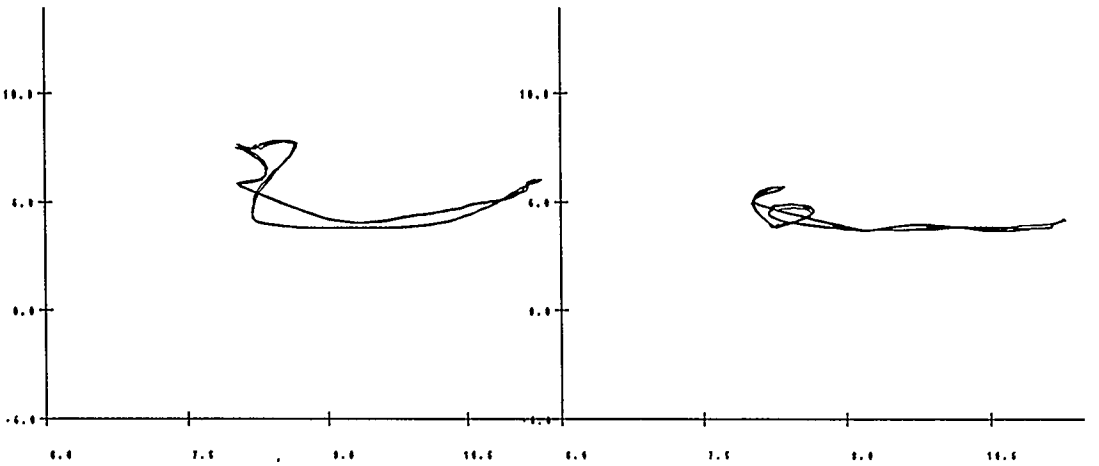

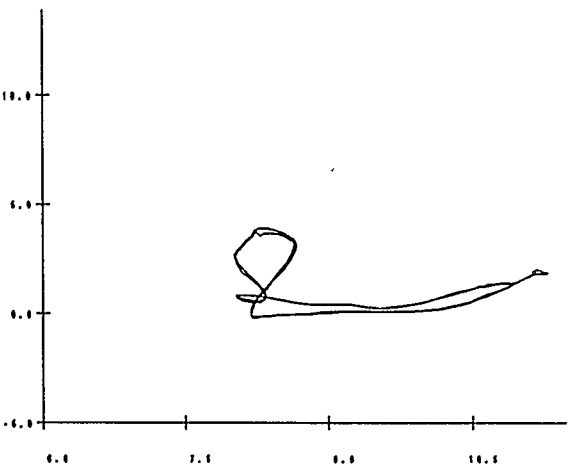

RA atrial pressure-dimension loop for Dog 5 showing cavitary pressure-dimension (upper left panel), pericardial pressure-dimension (upper right panel) and transmural pressure-dimension relationships with a mean RA pressure of 5 mm Hg. The transmural loop is calculated by subtracting the time-domain pericardial pressure tracing from the cavitary pressure tracing. The atrial pressure-dimension loop is counter-clockwise (positive work) for the a-loop (atrial contraction) and clockwise for the v-loop (ventricular contraction). An explanation of the atrial transmural pressure-dimension loop is given in Fig 5.6.

Figure 5.6 Atrial Transmural Pressure-Dimension Loop

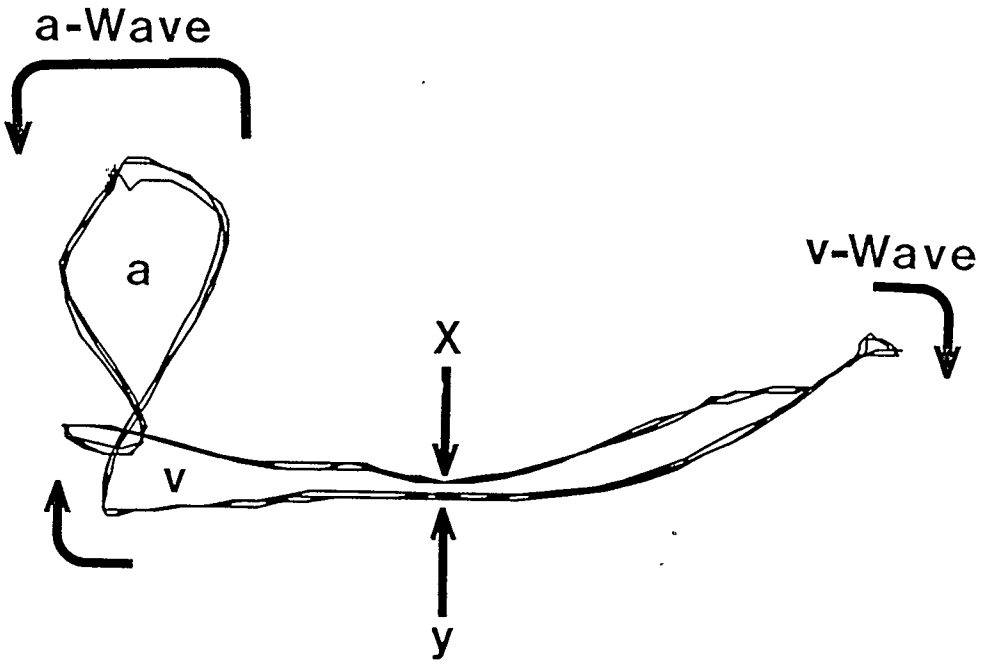

RA pressure-dimension relationship (expanded from Figure 5.5) at a RA atrial pressure of 5 mmHg (3 consecutive cycles are shown. As the RA contracts (**a-wave**) the atrial pressure increases but the volume decreases, creating the **a-loop.** As the RV contracts the atrial volume, and then, the RA pressure increases, until RA filling and pressure reach a maximum near end-systole at the peak of the **v-wave**. The atrio-ventricular valve then opens after the RV relaxes and the atrial volume and pressure decrease rapidly. For the following ventricular slow filling period, beginning at the bottom of the y-descent and extending to the beginning of the a-wave, both the right atrium and ventricle fill passively during this period. The passive filling of the atrium is called the **v-loop**.

Chapter 6

AN INTRA-OPERATIVE STUDY OF THE RELATIONSHIP BETWEEN LEFT AND RIGHT PERICARDIAL PRESSURES

Introduction

There is general agreement that LV preload is best estimated by left ventricular end-diastolic volume and that LV end-diastolic transmural pressure can be used to determine that volume. Since the measurement of ventricular volume is not readily available clinically, therapeutic decisions are usually based on cavitary pressure data. In the past, the pericardial pressure surrounding the heart was assumed to be small and constant resulting in the incorrect use of LV end-diastolic cavitary pressure as a measure of preload. Mangano and colleagues (80-83), found no significant change in right and left ventricular stroke work indexes related to right atrial and pulmonary artery wedge pressure after pericardiectomy. This result suggests that the effect of the pericardium is not easily measurable at the time of pericardiectomy during cardiac surgery and, therefore, is of little practical and clinical significance. Mangano's results do not account for the fact that the chest was reapproximated and the patients were being ventilated the time of

pericardiectomy; two factors which would provide extracardiac constraint. Mean pericardial pressure over the LV free wall has been measured with balloon transducers (73,80) in humans and the magnitude of this stress has been found to be similar to mean RV end-diastolic pressure. From these observations and the assumption that the pericardial pressure over both ventricles are similar (33), it follows that RV end-diastolic transmural pressure must be significantly less than RV intracavitary pressure. This has been confirmed in Chapter 3, and the assumption that LV pericardial pressure is similar to RV pericardial pressure has been studied by Boltwood et al (80). This excellent study correlated LV transmural pressure (calculated as pulmonary wedge pressure - 1/3 RA cavitary pressure - 2/3 LV pericardial pressure) with stoke work index. Boltwood's study also reported the similarity between mean RA, RV and LV pericardial pressure in 20 patients (all three pericardial pressures were not measured simultaneously in any patient). Tyberg et al (73) found a near identity relationship between mean RA intracavitary pressure and mean LV pericardial pressure in nine patients undergoing cardiac surgery. Multiple filling interventions in each patient permitted the generation of individual curves showing the linear relationship between mean RA pressure and mean LV pericardial pressure.

The individual patient data of RV vs LV pericardial pressure in Boltwood's study was not reported over a range of CVPs and all time varying pressure data was averaged over the whole cardiac cycle. The results of

Chapter 4 indicate that regional variations in pericardial pressure can exist depending on the part of the cardiac cycle being examined. Therefore, cycle averaged data may not reflect true end-diastolic behaviour. The RV and LV preload can only be measured at end-diastole and therefore cycle averaged data may not indicate the true relationship between RV and LV pericardial pressure. To better understand the similarity of RV and LV pericardial pressure in the human this study required a range of CVPs be created by challenging each patient with crystalloid and/or albumin. The RV and LV pericardial pressure was then measured at end-diastole (pre A-wave) instead of being averaged over the whole cardiac cycle.

Methods

Six patients (age 19-76 years) scheduled for elective cardiac surgery gave informed written consent to participate in this study. The protocol had previously been reviewed and approved by a joint University-Hospital ethics committee. Patient data are given in Table 6.1. No patient had valvular disease or right ventricular hypertrophy. General anaesthesia was induced with an intravenous combination of 2-7 mg. of midazolam, 500 mcg of sulfenta, and vecuronium bromide (0.08 to 0.10 mg/Kg). Anaesthesia was maintained with: (1) sulfenta (8 mcg/Kg iv), or (2) fentanyl (25 mcg/Kg iv) and isoflurane, or (3) enflurane. A median sternotomy exposed the pericardial sac. One-centimetre horizontal pericardial incisions were made over the RV free wall and

3 cm above the apex of the LV. Through these apertures, a previously described 3 cm. X 3 cm., flat, liquid-containing Silastic™ balloons (see Chapter 2) were inserted and positioned to lie over the RV and LV free walls. A 7.5F Swan Ganz catheter (Model 93A-931H-7.5F Thermodilution Paceport(tm) Catheter with Thromboshield(tm), American Edwards Laboratories, Anasco, Puerto Rico) was also inserted. The pericardial balloons were calibrated before sterilization. Following gas sterilization, the previously determined volume of saline was injected into the balloons after they had been flushed to remove all air. A calibration curve for each balloon was also described after each experiment, using the same methods described in the Chapter 3. Post-operatively, all balloons were found to calibrate linearly within 1 mm Hg applied pressure in the balloon calibrator chamber. The volume of saline in the balloon was measured after the experiment and compared to the amount injected pre-operatively to detect inadvertent volume changes.

Stay sutures were placed at the edges of the pericardotomy and secured to the balloon catheters to prevent excessive motion. The Swan-Ganz catheter was used to measure central venous pressure, RV pressure (measured from the RV pacing port), pulmonary arterial and pulmonary capillary wedge pressure. All pressures were measured using disposable semiconductor strain-gauge pressure transducers (Trantec(tm) Disposable Pressure Transducer, American Hospital Supply, Irvine, California) connected to a patient monitoring system (Model 78534C, Hewlett-Packard, Palo Alto,

California). All transducers were calibrated using internal calibration signals and then checked post-operatively using a mercury manometer, before being disconnected from the patient monitoring system. Post-operatively all transducers were found to calibrate linearly to 100 mm Hg. Conditioned signals were acquired on a computer (Model 2551 80286/80287 12-MHz personal computer, Compaq Computer Corporation, Houston, Texas) using a 12-bit analog-to-digital converter (Model 2801, Data Translation, Marlboro, Massachusetts). The analog signals were scaled using gain and offset amplifiers and then filtered with a 7th order Cauer elliptic lowpass active anti-aliasing filter (cutoff frequency = 100 Hz, 78dB attenuation at floor = 165 Hz, Model 675, Frequency Devices, Haverhill Massachusetts) before being sampled at 200 Hz. The digitized data were subsequently analyzed on a computer (Model ST-1144A Packard Bell 386X 80386/80387 Personal Computer, Chatsworth, California) , using analytical software developed in our laboratory (CVSOFT, Odessa Computer Systems Limited, Calgary, Alberta) and statistical and graphics software (SPSS Incorporated, Chicago, Illinois) running on a multi-tasking computer (Model VAX 11/750 Digital Equipment Corporation, VMS version 4.6, operating system).

Before each set of measurements was made the pressure transducers were zeroed at the mid-plane of the left ventricle. Volume loading was achieved by an intravenous infusion of 1-2 litres of Ringer's lactate or normal saline. In two cases, 100 ml of 25% albumin was given in addition to the

crystalloid solutions. Depending on the patient's status during the operative procedure the mean central venous pressure was increased 5 - 10 mm Hg from baseline during volume loading. The RV and LV pericardial pressure was measured continuously throughout the volume load.

Data Analysis

The pericardial balloons were connected to their respective transducer via a 100-cm length of extension tubing. All data were collected over 60-second intervals. The zero reference level ports of all transducers were all mounted on a rack to ensure that they remained at the same hydrostatic level. The error in each pressure measurement was found to be within ±1 mm Hg when the automatic balancing and gain adjustment features of the patient monitoring system were calibrated against a mercury manometer. Therefore, the error in the calculated transmural pressures could have been no more than ± 2 mm Hg. These errors should have been random and should not have affected the mean values of the pooled data. The post-experiment analysis involved the extraction of last three late-diastolic data points (5 milliseconds sampling interval) immediately preceding atrial contraction. To compensate for the delay introduced by the extension tubing, a correction of 50 milliseconds was use to temporally align the pericardial pressures to those obtained from the Swan-Ganz catheter (the time shift from the various Swan-Ganz ports was negligible for the purposes of this study). Any significant

motion-induced oscillations in the pressure tracings were filtered using a 101-term, finite impulse response, linear phase digital lowpass, time-corrected filter (breakpoint = 20 Hz, attenuation of 80 db in 5 Hz, Remez exchange algorithm, Signal Technology Incorporated, Santa Barbara, California).

Results

All data in this study was analyzed in diastole just preceding the A-wave. The individual plots (Figures 6.1 to 6.6) of RV pericardial pressure vs LV pericardial pressure show very strong linear relationships. The pooled data of all six patients are shown in Figure 6.7 (slope = 0.968, intercept = -0.436, correlation coefficient = 0.996). This strong linear fit of the pooled data of all patients is a strong argument that the pericardial pressure over the left and right ventricle of the human heart is equal over a range of CVPs from 2 to 18 mm Hg. Figure 6.8 shows the plot using the pooled data of all patients of RV cavitary pressure vs LV pericardial pressure. (slope = 0.767, intercept = 2.622 and correlation coefficient = 0.987). This plot shows that RV end-diastolic cavitary pressure can be used to approximate (±2 mm Hg) LV pericardial pressure. Furthermore, the correlation coefficient (0.987) of the linear regression of the pooled data indicates that changes in RV end-diastolic pressure can be use to predict changes in LV pericardial pressure.

Conclusions

The pooled data of all patients demonstrates RV pericardial pressure is equal to LV pericardial pressure in the presence of a normal human pericardium over central venous pressures ranging from 2 to 18 mm Hg. The RV end-diastolic (pre A-wave) cavitary pressure is a good predictor of LV pericardial pressure and that changes in RV end-diastolic pressure should reflect similar changes in LV pericardial pressure.

Table 6.1 Patient Data

Patient	Sex	Age	Surgery
1	M	71	CABG + IM
2	M	50	ASD
3	M	19	WPW + PFO
4	M	67	CABG
5	M	76	CABG + IM
6	M	72	CABG + IM

Patient data for right and left pericardial pressure human study.

CABG = coronary artery bypass graft

IM = internal mammary bypass graft

ASD = atrial septal defect repair

WPW = wolf parkinson white ablation of aberrant conductive pathway

PFO = repair of patent foramen ovale.

Table 6.2 Regression Coefficients of Pprv vs Pplv

Patient	Slope	Intercept	Corr. Coeff.
1	0.249	5.820	0.517
2	1.034	-0.877	0.986
3	0.904	0.669	0.995
4	0.831	-1.383	0.966
5	0.891	-0.073	0.996
6	0.850	1.404	0.954

The coefficients for the linear regression of P_{plv} vs P_{prv} for the six patients displayed in figures 6.1 to 6.6.

Figure 6.1 Pprv vs Pplv for Patient #1

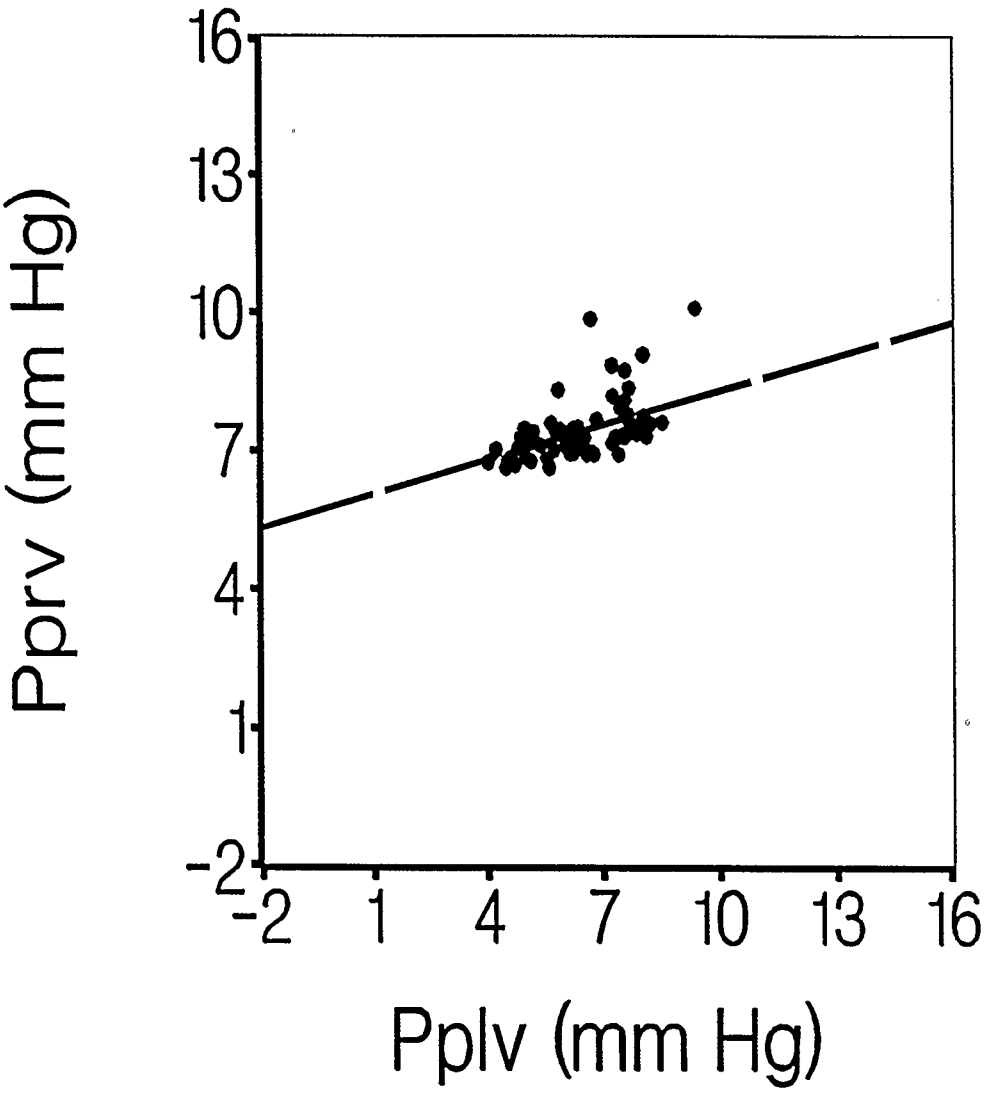

LV pericardial pressure is plotted against RV pericardial pressure over a range of central venous pressures for patient 1 (see table 1 for patient data). (slope = 0.249,intercept = 5.820, correlation coefficient = 0.517).

Figure 6.2 Pprv vs Pplv for Patient #2

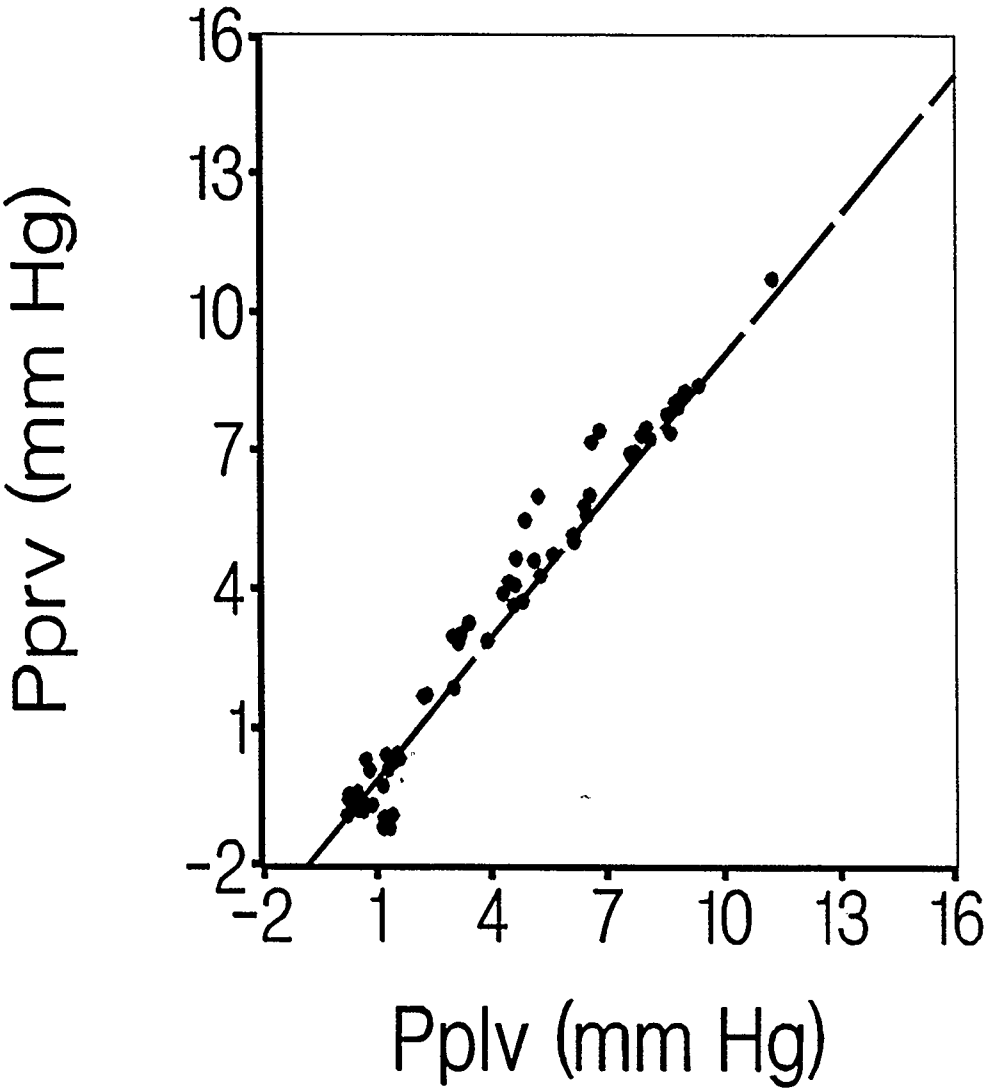

LV pericardial pressure is plotted against RV pericardial pressure over a range of central venous pressures for patient 2 (see table 1 for patient data). (slope = 1.034, intercept = -0.877, correlation coefficient = 0.986).

Figure 6.3 Pprv vs Pplv for Patient #3

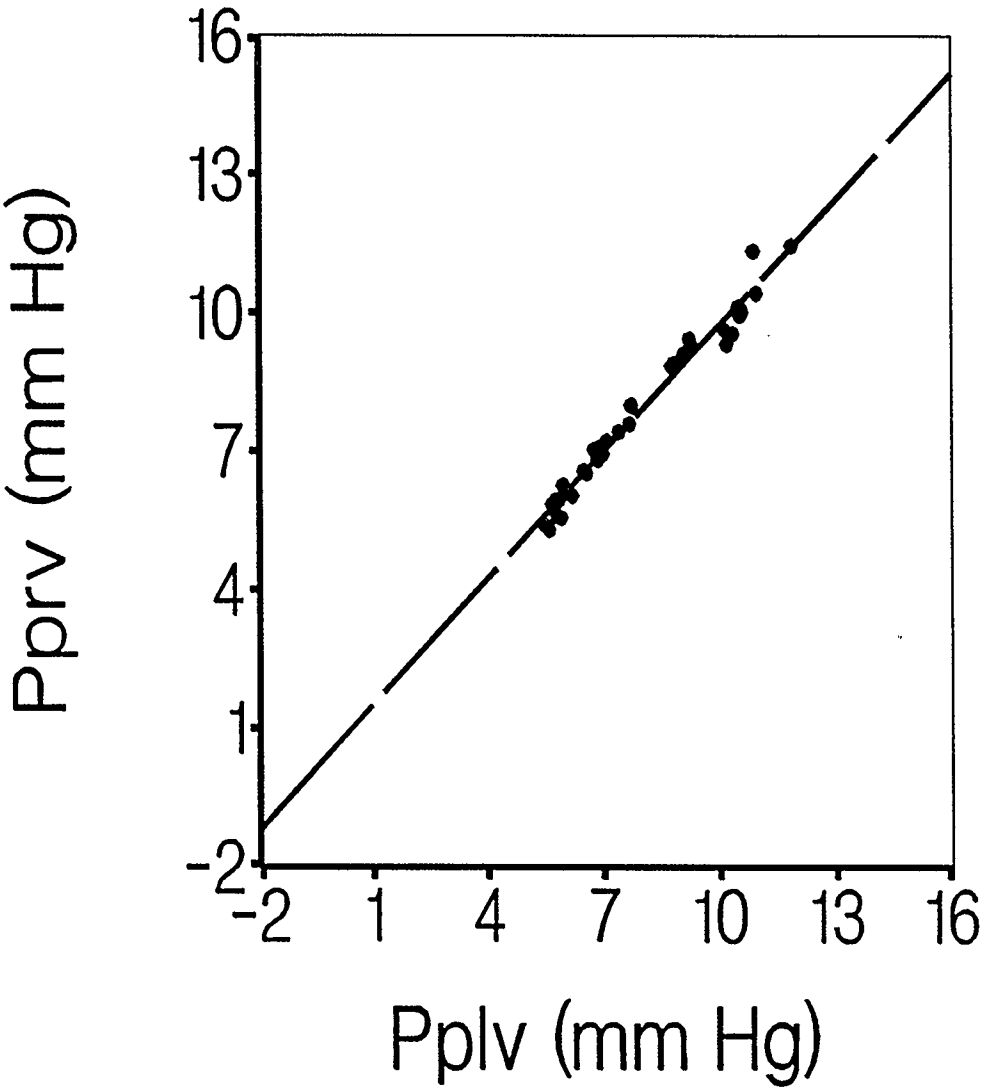

LV pericardial pressure is plotted against RV pericardial pressure over a range of central venous pressures for patient 3 (see table 1 for patient data). (slope = 0.904, intercept = 0.669, correlation coefficient = 0.995).

Figure 6.4 Pprv vs Pplv for Patient #4

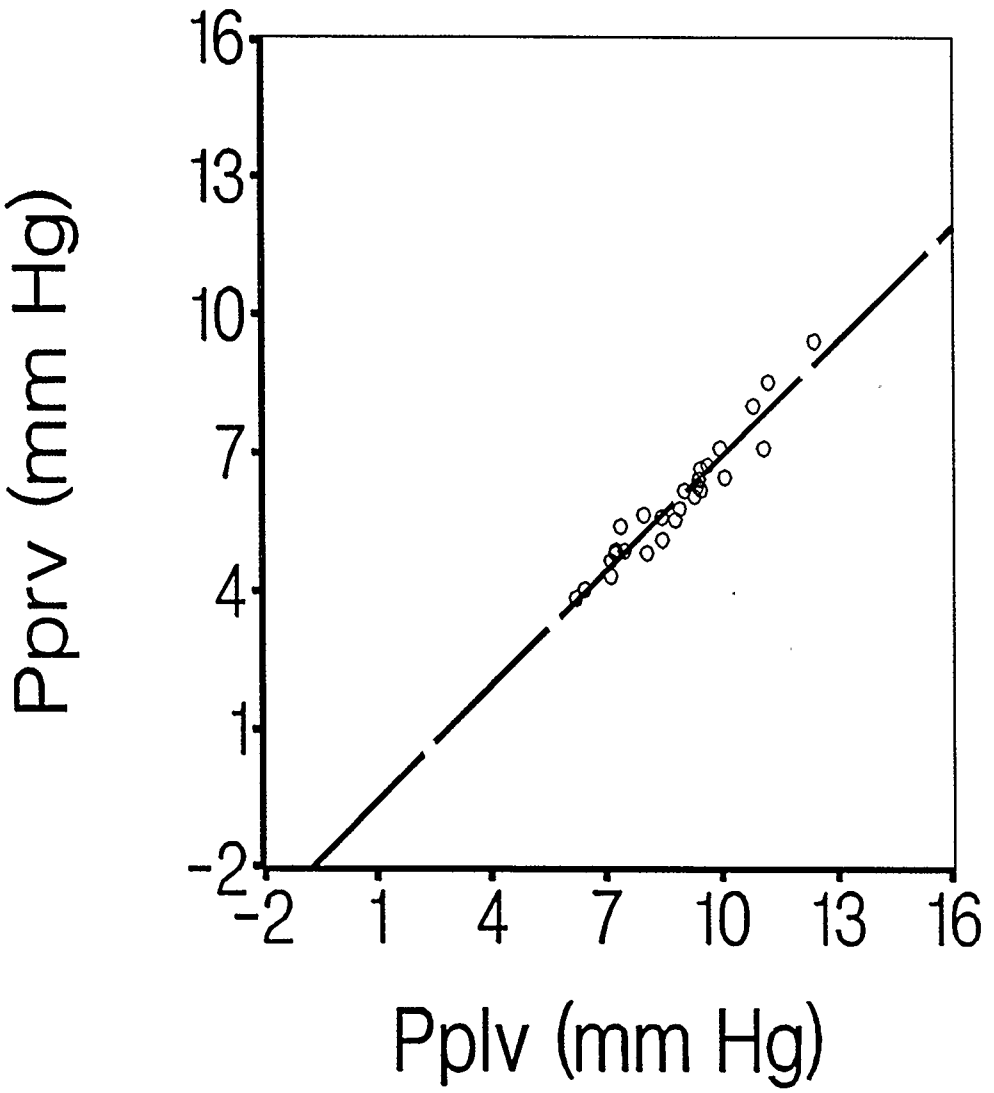

LV pericardial pressure is plotted against RV pericardial pressure over a range of central venous pressures for patient 4 (see table 1 for patient data). (slope = 0.831, intercept = -1.383, correlation coefficient = 0.966)

Figure 6.5 Pprv vs Pplv for Patient #5

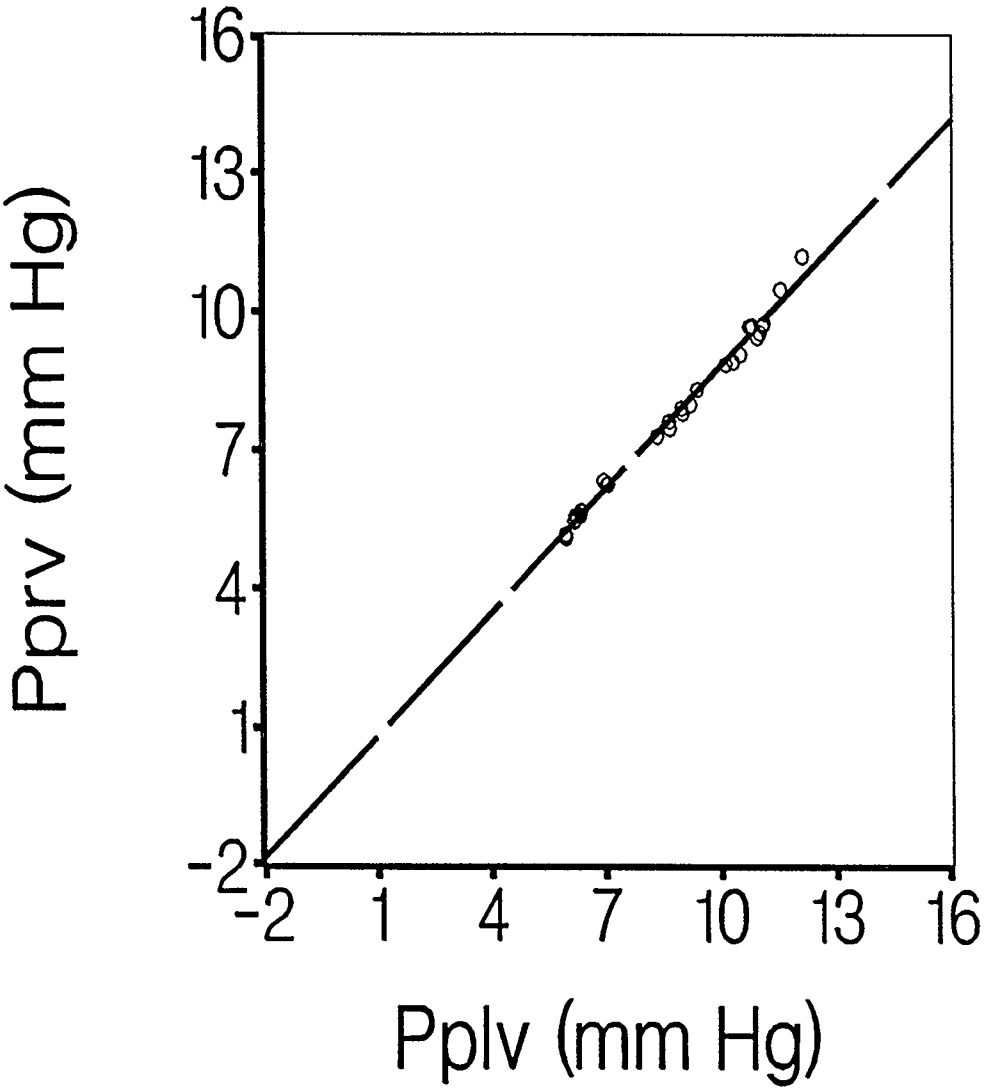

LV pericardial pressure is plotted against RV pericardial pressure over a range of central venous pressures for patient 5 (see table 1 for patient data). (slope = 0.891, intercept = -0.073, correlation coefficient = 0.996)

Figure 6.6 Pprv vs Pplv for Patient #6

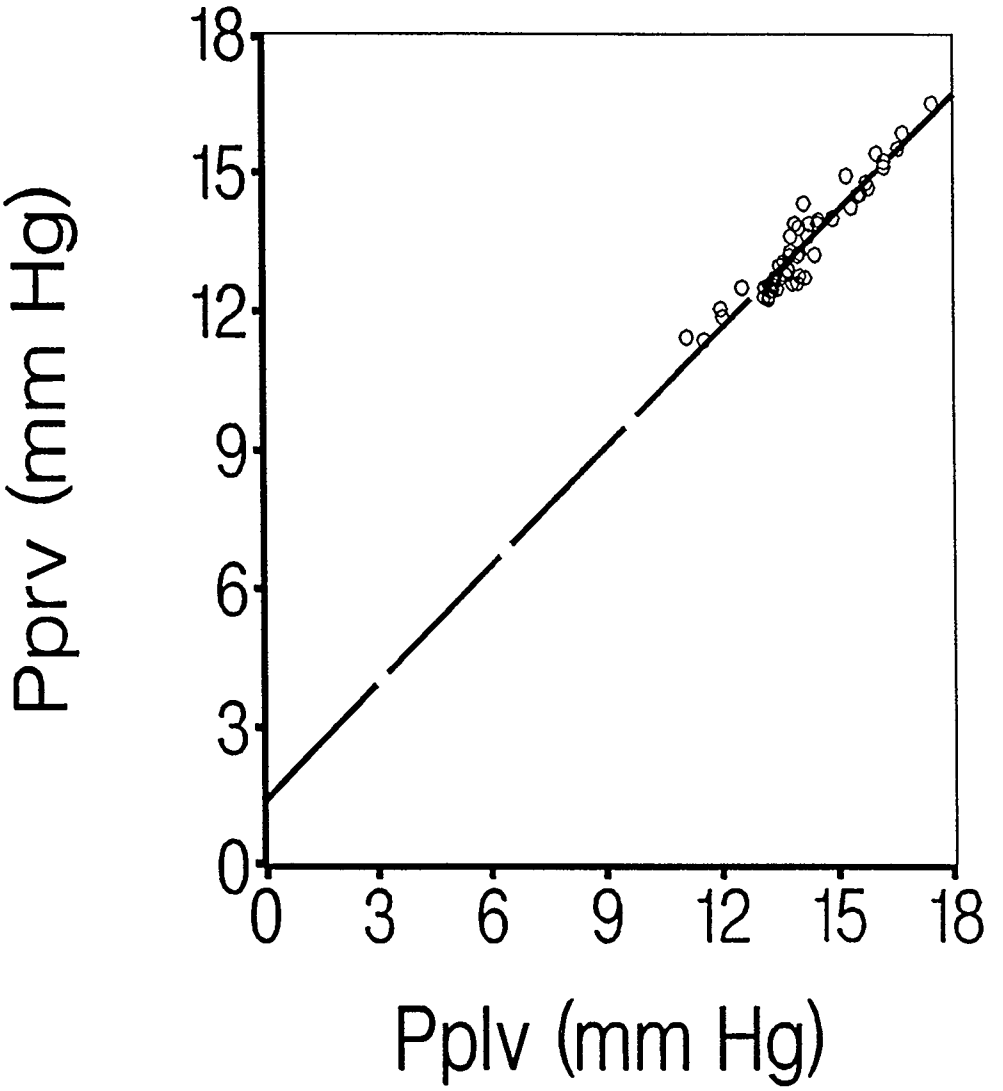

LV pericardial pressure is plotted against RV pericardial pressure over a range of central venous pressures for patient 6 (see table 1 for patient data). (slope = 0.850, intercept = 1.404, correlation coefficient = 0.954)

Figure 6.7 Pprv vs Pplv Pooled Data of all Patients

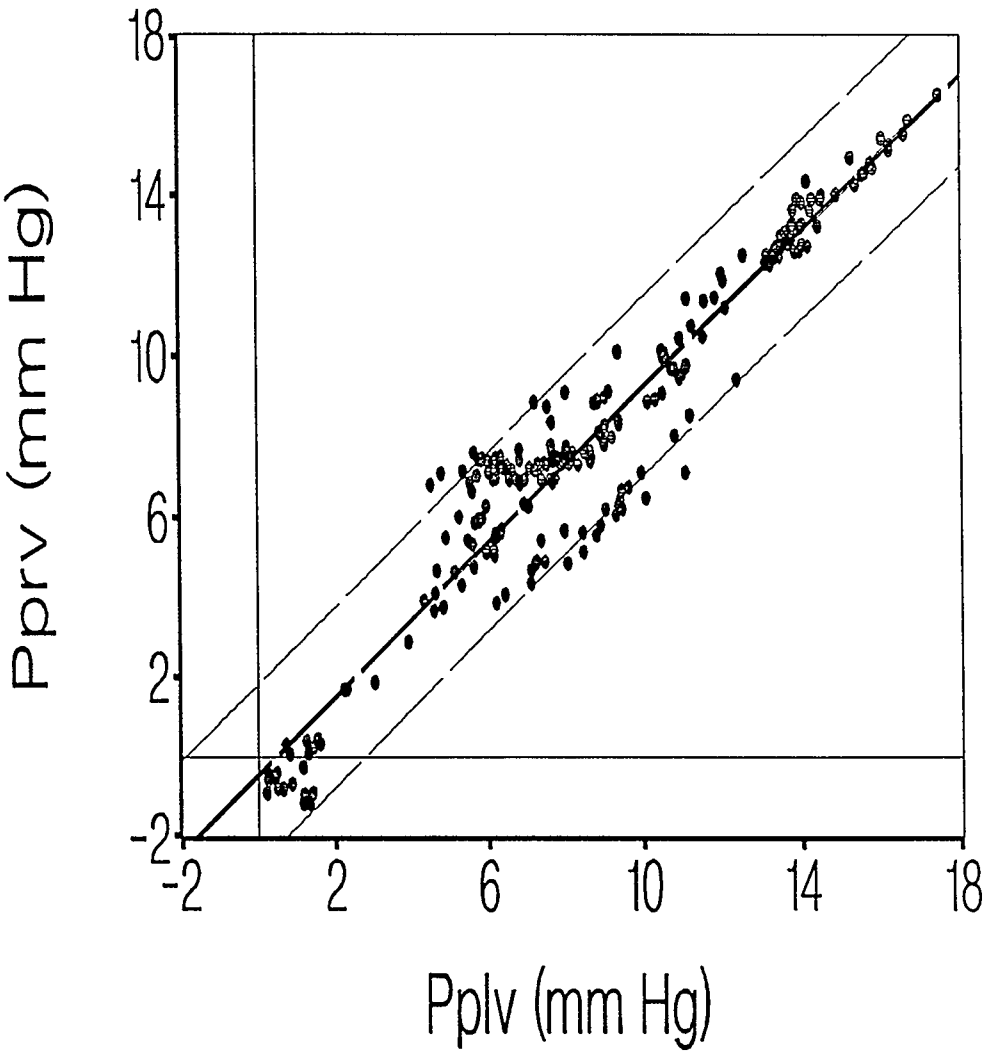

Linear regression using the pooled data of all six patients of RV pericardial pressure against LV pericardial pressure at end-diastole (slope = 0.968, intercept = -0.436 and correlation coefficient = 0.960; 95% confidence intervals are also plotted).

Figure 6.8 Pplv vs Prv Pooled Data of all Patients

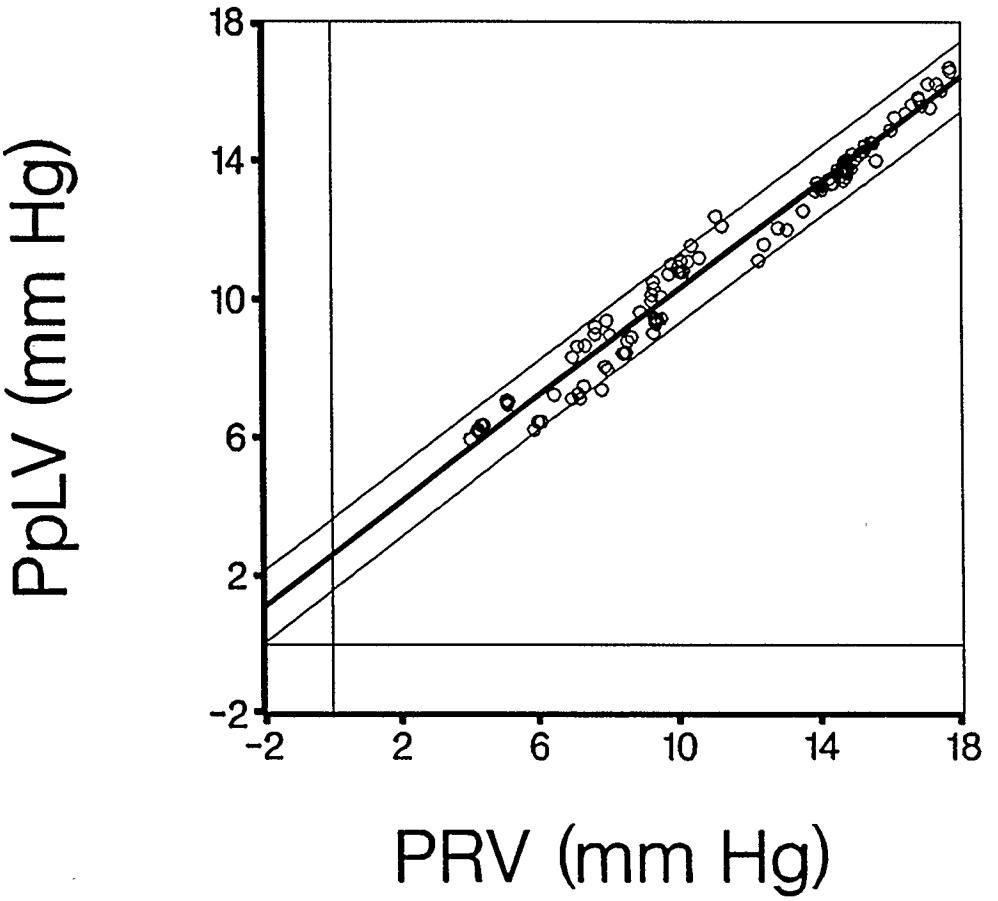

Linear regression using the pooled data of all six patients of RV cavitary pressure against LV pericardial pressure at end-diastole (slope = 0.767, intercept = 2.622 and correlation coefficient = 0.987; 95% confidence intervals are also plotted).

Chapter 7

CONCLUSIONS

It is the author's hope that this thesis has clarified some of the misconceptions regarding pericardial constraint and its effect on diastolic cardiac mechanics.

Results from Chapter 2 show that the linear static behaviour of the CVR pericardial balloon makes it ideal for the measurement of pericardial constraint at end diastole. The dynamic response of the CVR pericardial balloon was found to be limited only by the 2nd-order frequency response of the catheters used to connect it to an external strain-gauge pressure transducer. The CVR balloon accurately integrates nonhomogenously distributed loads to give the equivalent mean stress distributed over its active contact area. The CVR high-fidelity pericardial balloon has frequency-response characteristics which are superior to the standard CVR pericardial balloon. This new technology will allow the physiologist to measure systolic transmural pressure with an intact pericardium.

Chapter 3 uses the concepts of Chapter 2 to measure the transmural pressure of the right side of the heart. To determine the transmural pressure-dimension relationship of the right atrium (RA) and right ventricle (RV)

before and after pericardiectomy, six open-chest dogs were instrumented with liquid-containing pericardial balloons placed over the RA and RV free wall. RA appendage dimensions and RV free wall segment lengths were measured using sonomicrometry. Intact-pericardium RA and RV transmural pressure (P_{trans}) was calculated by subtracting the pericardial pressure (P_{peric}) measured with a balloon, from the cavitary pressure (P_{cav}) measured with micromanometer-tipped catheters. Pooled data of all six animals indicate that, at pericardium-intact RA and RV P_{cav} of 5, 10 and 15 mm Hg, the RV P_{peric} was 4.3 ± 0.3, 8.6 ± 1.0 and 13.3 ± 1.5 mm Hg and RA P_{peric} was 4.8 ± 0.3, 9.6 ± 0.6 and 14.6 ± 0.6, respectively (mean ± SD). Furthermore, we determined that, in the dog, RV strain would increase by 14% and RA by 68%, to maintain P_{cav}= 10 mm Hg upon pericardiectomy.

To compare animal with human data, RV (n=7) and RA (n=6) P_{trans} was measured using pericardial balloons intraoperatively in patients (age 19-76) undergoing cardiac surgery. The RA P_{trans} of was found to be 1.0 ± 1.5 mm Hg over central venous pressures ranging from 3 to 16 mm Hg. Also, at RV end-diastolic P_{cav} of 4.9 ± 0.7, 9.7 ± 0.9 and 14.5 ± 1.3 mm Hg, the RV P_{peric} were 3.9 ± 2.3, 7.7 ± 2.7, 11.3 ± 3.2, respectively. In conclusion, diastolic pericardial constraint accounts for: [1] 95% of the RA cavitary pressure in the dog and 89% in humans and [2] 85% of the RV cavitary pressure in the dog and 78% in humans.

Chapter 4 uses the recent advances in the CVR high-frequency

pericardial balloon technology to measure pericardial pressure over the right atrium and ventricle during the whole cardiac cycle. In contrast to the diastolic behaviour described in Chapter 3, Chapter 4 documents the nonuniform, regional behaviour of pericardial pressure over the right heart. During diastole, the pericardial pressure over the atrium seems to track its right ventricular counterpart from the bottom of the y-descent to the beginning of the A wave, describing a line of identity between the two pressures. However, during systole, between the bottom of the x-descent and the peak of the V-wave, these two pericardial pressures seem to be completely decoupled with RV pericardial pressure falling while RA pericardial pressure remains constant or increases. This systolic decoupling clearly indicates a considerable independence between the RA and the RV. That is, the systolic emptying of the RV lowers RA pericardial pressure but RA pericardial pressure continues to increase. This suggests that the relation of the pericardium to the RA must allow effective constraint even though the RV pericardium is momentarily slack.

Chapter 5 also exploits the advances in the CVR high-fidelity pericardial balloon technology which permit the measurement of pericardial pressure over the whole cardiac cycle. To determine the work performed on the right ventricular free-wall by the pericardium, 6 open-chest dogs were instrumented with a high-fidelity pericardial balloon over the RV free wall. RV free-wall segment lengths (L_{rv}) were measured using sonomicrometry. Work was calculated by integrating the loop area of pressure-segment length

relationships. Intact-pericardium RV transmural work (W_{trans}) was calculated by subtracting the RV pericardial work (W_{peric}) measured with a balloon from the RV cavitary work (W_{cav}). We determined that pericardium contributes to the W_{cav} significantly over mean right atrial pressures (mean P_{ra}) ranging from 5 to 15 mm Hg. Results from 6 dogs suggest that the left ventricle "contributes" to RV performance, via a pericardial mechanism. Results from Chapter 5 indicate that this mechanism contributes from 1/6 to 1/5 of the total work being imparted to the blood by the RV free wall under normal physiological conditions.

Chapter 6 describes the measurement of pericardial pressure over the RV and LV of humans. The object of the study was to test the hypothesis that the constraining effects of the normal human pericardium over the RV and LV are approximately equal over a physiological range of mean CVP. Accordingly, immediately after median sternotomy in 6 patients undergoing elective cardiac surgery, along with aortic pressure and CVP, the pericardial pressure over the RV and LV free walls were measured with standard CVR pericardial balloon transducers. CVP was increased using 1-2 litres of crystalloid solution and albumin. Results from the 6 patients confirm a linear relationship between right and left pericardial pressure (slope = 0.968, intercept = -0.436 and correlation coefficient = 0.996) over a range of CVP from 2 to 18 mm Hg. LV pericardial pressure was also found to track RV end-diastolic intracavitary pressure linearly and RV transmural pressure was

approximately 2 mm Hg for the range of CVPs previously mentioned. These results show that the RV end-diastolic cavitary pressure can be used as an approximate estimator of absolute and relative changes in LV pericardial pressure in the presence of a normal pericardium.

The standard CVR balloon has been used in animal and human research under sterile conditions with successful results. The easy use and accurate calibration makes it ideal for clinical use. The measurement of external cardiac constraint in patients undergoing coronary artery bypass surgery has been successfully investigated without any sequela. Patients which have marginal myocardial function after surgery, such that the embarrassment in preload by sternal closure causes them to 'crash', might benefit from delayed sternal closure. The CVR pericardial balloon might be employed to measure the magnitude of external constraint in these patient, helping the clinician decide when the patients heart might tolerate reapproximation of the sternum.

The development of the CVR high-fidelity balloon has opened up areas of physiology which, until now, have not been investigated with an intact pericardium. The CVR high-fidelity balloon might be employed to study the following areas:

1). The effect of negative thoracic pressure on the mechanisms of pulsus paradoxus. In particular, the direct measurement of

transmural systolic function.

2.) The diastolic and systolic effects of jet ventilation on the external constraint of the normal and failing heart.

3.) The measurement of systolic transmural function in a normal and infarcted myocardium with an intact pericardium. How well does the pericardium protect the infarcted heart wall during systole.

4.) The measurement of ventricular suction in normal and pathological states with an intact pericardium.

5.) The measurement of ventricular transmural relaxation with an intact pericardium.

6.) The measurement of diaphragmatic work over the respiratory cycle with normal and edematous lung pathology.

Bibliography

1. Spodick DH, Medical History of the Pericardium. Am J Cardiol 1970;26:447

2. Boyland JW, Founders of Experimental Physiology J.F. Lehmanns Verlag Publisher; 1971

3. Shabetai R: The pericardium and its diseases. in The Heart, eds. Hurst JW, Logue RB, Rackley CE, Schlant RC, Sonnenblick RC, Wallace AG and Wenger NK, McGraw-Hill Book Company, 1986;7:1249-1275

4. Barnard BL: The functions of the Pericardium. Pro Physiol Soc 1898;93-98

5. Katz LN: Analysis of several factors regulating the performance of the heart. Physiol Rev 1955;35:91-106

6. Kenner HM, Wood EH: Intrapericardial, intrapleural and intracardiac pressures during acute heart failure in dogs studied without thoracotomy. Circ Res 1966;19:1071-1079

7. Holt JP, Rhode EA, Kines H: Pericardial and ventricular pressure. Circ Res 1960;8:1171-1181

8. Morgan BC, Guntheroth WG, Dillard HD: Relationship of pericardial to pleural pressure during quiet respiration and cardiac tamponade. Circ Res 1965;16:493-498

9. Spodick DH: The normal and diseased pericardium: Current concepts of pericardial physiology, diagnosis and treatment. J Am Coll Cardiol 1983;1:1240-1251

10. Kingma I, Groves GH, Smith ER, Tyberg JV: Creep of the canine pericardium in vivo.Can J Physiol Pharmacol 1986;64: 892-896

11. Smiseth OA, Frais MA, Kingma I and Tyberg JV: Assessment of pericardial constraint in dogs. Circulation 1985;71:158

12. Lai-Fook SJ, Price CP, Staub NC: Liquid thickness vs. vertical pressure gradient in a model of the pleural space. J Appl Physiol 1987;62:1747-1754

13. Agostoni E, D'Angelo E, Roncoroni G: The thickness of the pleural liquid. Resp Physiol 1968;5:1-13

14. Agostoni E, D'Angelo E: Thickness and pressure of the pleural liquid at various heights and with various hydrothoraces. Resp Physiol 1968;6:330-342

15. Agostoni E, Miserocchi G, Bonanni V: Thickness and pressure of the pleural liquid in some mammals. Resp Physiol 1969;6:245-256

16. Lai-Fook SJ, Kaplowitz MR: Pleural space and thickness in situ by light microscopy in five mammalian species. J Appl Physiol 1985;59:603-610

17. Agostoni E, D'Angelo E: Comparative Features of the Transpulmonary Pressure. Resp Physiol 1970;11:76-83

18. Agostoni E: Mechanics of the Pleural Space. Physiol Rev 1972;52

19. Agostoni E: Mechanics of the Pleural Space. The Handbook of Physiology - The Respiratory System III, Chapter 30

20. Agostoni E, Mead J: Statics of the Respiratory System The Handbook of Physiology - The Respiratory System I, Chapter 13

21. Mead J, Agostoni E: Dynamics of breathing. In Handbook of Physiology. pp. 411-427

22. Miserocchi G, Agostoni E: Pleural liquid and surface pressures at various lung volumes. Resp Physiol 1980;39:315-326

23. Permutt S, Caldini P, Bane HN, Howard P, Riley RL: Liquid pressure versus surface pressure of the esophagus J. Appl. Phsyiol. 1967;23:927-933

24. Lai-Fook SJ, Beck KC, Southorn PA: Pleural liquid pressure measured by micropipettes in rabbits. J Appl Physiol 1984;56:1633-1639

25. Wiener-Kronish JP, Gropper MA, Lai-Fook SJ: Pleural liquid pressure in dogs measured using a rib capsule.

26. Olsen LE, Lai-Fook SJ: Pleural pressure measured with rib capsules in anesthetized ponies. J Appl Physiol 1988;64:102-107
J Appl Physiol 1985;59:597-602

27. Shabetai R: Pericardial and cardiac pressure.
Circulation 1988;77:1-5

28. Tyberg JV, Smith ER: On the interaction between the pericardium and the heart. In Mechanics of the Circulation. eds. HEDJ ter Keurs and JV Tyberg. Martinus Nijhoff Publishing, Dordrecht, Boston,1987.

29. Tyson GS Jr, Maier GW, Olsen CO, Davis JW, Rankin JS: Pericardial influences on ventricular filling in the conscious dog. An analysis based on pericardial pressure. Circ Res 1984;54:173-184

30. Freeman GL, LeWinter MM: Role of parietal pericardium in acute, severe mitral regurgitation in dogs. Am J Cardiol 1984;54:217-219

31. Freeman GL, LeWinter MM: Determinants of intrapericardial pressure in dogs. J Appl Physiol 1986;60:758-764

32. Smiseth OA, Frais MA, Kingma I, White AVM, Knudtson ML, Cohen JM, Manyari DE, Smith ER, Tyberg JV: Assessment of pericardial constraint: the relation between right ventricular filling pressure and pericardial pressure measured after pericardiocentesis.
J Am Coll Cardiol 1986;7:307-314

33. Smiseth OA, Scott-Douglas NW, Thompson CR, Smith ER and Tyberg JV: Non-uniformity of pericardial surface pressure in dogs. Circulation 1987;75:1229.

34. Janicki JS, Weber KT, Loscalzo J and Shroff S. Extracardiac pressure and ventricular haemodynamics.
Cardiovascular Res 1987;21:230-239

35. Butler J: The heart is in good hands. Circulation 1983;67:1163-1168

36. Holt JP: The normal pericardium. Am J Cardiol 1970;26:455-465

37. Duomarco J.L., Giambruno C.E., Duran C.A.: The pressure in the different zones of the pericardium . Acta Physiologica Latinoamerica 1959;7:267-272

38. Freeman GL, LeWinter MM: Pericardial adaptations during chronic cardiac dilation in dogs. Circ Res 1984;54:294-300

39. Glantz SA, Parmley WW: Factors which affect the diastolic pressure-volume curve. Circ Res 1978;42:171-180

40. Holt JP: Ventricular end-diastolic volume and transmural pressure. Cardiologia 1967;50:281-290

41. Janicki JS, Weber KT: The pericardium and ventricular interaction, distensibility, and function. Am J Physiol 1980;238:H494-H503

42. Junemann J, Smiseth OA, Refsum H, Sievers R, Lipton MJ, Carlsson E, Tyberg JV: Quantification of effect of pericardium on LV diastolic PV relation in dogs. Am J Physiol 1987;252:H963-H968

43. Kingma I, Smiseth OA, Belenkie I, Knudtson ML, MacDonald RPR, Tyberg JV, Smith ER: A mechanism for the nitroglycerin-induced downward shift of the left ventricular diastolic pressure-diameter relation. Am J Cardiol 1968;57:673-677

44. Kingma I, Smiseth OA, Frais MA, Smith ER, Tyberg JV: Left ventricular constraint: relationship between pericardial, pleural and esophageal pressure during positive end-expiratory pressure and volume loading in dogs. Annals of Biomed Eng 1987;15:331-346

45. LeWinter MM, Pavelec R: Influence of the pericardium on left ventricular end-diastolic pressure-segment relations during early and later stages of experimental chronic volume overload in dogs. Circ Res 1982;50:501-509

46. Shabetai R: Pericardial and Cardiac Pressure Circulation 1988;77:1-5

47. Smiseth OA, Scott-Douglas NW, Traboulsi M, Stone JA, Smith ER, TybergJV: The role of the pericardium: experimental aspects. Heart Failure 1987;3:6-12

48. Tyberg JV, Misbach GA, Parmley WW, Glantz SA: Effects of the pericardium on left ventricular performance. In Cardiac Dynamics. eds. J Baan, AC Arntzenius, EL Yellin. Martinus Nijhoff Publishers, The Hague, Boston, London, 1980:159-168.

49. Tyberg JV: Ventricular interaction and the pericardium. In The Ventricle: Basic and Clinical Aspects. Martinus Nijhoff Publishers, Dordrecht, Boston, Lancaster. 1985:171-184.

50. Tyberg JV, Scott-Douglas NW, Kingma I, Traboulsi M, Smith ER: Implications of pericardial pressure for the evaluation of diastolic dysfunction.

51. Tyberg JV, WJ Keon, EH Sonnenblick, CW Urschel. Mechanics of ventricular diastole. Cardiovasc Res 1970;4:423-428

52. Assanelli D, Lew WYW, Shabetai R, LeWinter MM: Influence of the pericardium on right and left ventricular filling in the dog. J Appl Physiol 1987;63:1025-1032

53. Hoit BD, Dalton N, Bhargava V, Shabetai R: Pericardial influences on right and left ventricular filling dynamics. Circ Res 1991;68:197-208

54. Applegate RJ, Santamore WP, Klopfenstein HS, Little WC: External pressure of the undisturbed left ventricle. Am J Physiol 1990;258 (Heart Circ. Physiol. 27):H1079-H1086

55. Goto Y, LeWinter: Nonuniform Regional Deformation of the Pericardium During the Cardiac Cycle in Dogs. Circ Res 1990;67:1107-1114

56. Slinker BK, Ditchey RV, Bell SP, and LeWinter MM: Right heart pressure does not equal pericardial pressure in the potassium chloride-arrested canine heart in situ. Circulation 1967;76:357-362

57. Mann D, Lew W, Ban-Hayashi E, Shabetai R, Waldman L, LeWinter MM: In vivo mechanical behavior of canine pericardium. Am J Physiol 1986;251:1449-1456

58. McMahon SM, Permutt S, Proctor DF: A model to evaluate pleural surface pressure measuring devices. J Appl Physiol 1969;27:886-891

59. Speirs AC, Blockman R: New implantable silicone rubbers: Plas Recon Surg 1963;31:166-75

60. Boyd IA, Pathak CL: The comparative toxicity of silicone rubber and plastic tubing. Scot Med J 1964;9:345-51

61. Shabetai R: Measuring pericardial constraint (editorial comment) J Am Coll Cardiol 1986;7:315-316

62. Banchero N, Schwartz PE, Tsakiris AG, Wood EH: Pleural and esophageal pressures in the upright body position. J Appl Physiol 1967;23:228-234

63. Masao T, Mitzner W, Robotham JL: Influences of the pericardium on ventricular loading during respiration. J Appl Physiol 1990;68:1640-1650

64. Smiseth OA, Frais MA, Kingma I, Smith ER, Tyberg JV: Assessment of pericardial constraint in dogs. Circulation 1985;71:158-164

65. Tyberg JV, Misbach GA, Glantz SA, Moores WY, Parmley WW: A mechanism for the shifts in the diastolic, left ventricular, pressure-volume curve: the role of the pericardium. European J Cardiol (Suppl) 1978;7:163-175

66. Traboulsi M, Scott-Douglas NW, Smith ER and Tyberg JV: Measurement of right ventricular transmural pressure. Clin Invest Med 1987;10:C33

67. Nagano T, Arakawa M, Tanaka T, Yamaguchi M, Takaya T, Noda T, Miwa H, Kagawa K, and Hirakawa S: Diastolic compliance of the left atrium in man: A determinant of preload of the left ventricle. Heart Vessels 1989;5:25-32

68. Hamilton DH, DeVries G, unpublished results.

69. Suga H, Yasumura Y, Nozawa T, Futaki S, Tanaka N: Pressure-volume relation around zero transmural pressure in excised cross-circulated dog left ventricle. Circ Res 1988;63:361-372.

70. Agostoni E, D'Angelo E, Roncoroni G: The thickness of the pleural liquid. Resp Physiol 1968;5:1-13

71. Permutt S, Caldini P, Bane HN, Howard P, Riley RL: Liquid pressure versus surface pressure of the esophagus. J Appl Physiol 1967;23:927-933

72. Smiseth OA, Refsum H, Tyberg JV: Pericardial pressure assessed by right atrial pressure: A basis for calculation of left ventricular transmural pressure Am Heart J 1984;108:603-608

73. Tyberg JV, Taichman GC, Smith ER, Scott-Douglas NW, Smiseth OA, Keon WJ: The relationship between pericardial pressure and right atrial pressure: an intraoperative study.
Circulation 1986;73:428-432

74. Raines RA, LeWinter MM, Covell JW. Regional shortening patterns in the canine right ventricle Am. J. Physiol. 1976;231:1395-1400.

76. Keith A. Fate of the bulbus cordis in the human heart.
Lancet 1924;2:1267-1273

75. Armour JA, Pace JB, Randall WC. Interrelationship of architecture and function of the right ventricle. Am. J. Physiol. 1970;218:174-179

77. Morris JJ, Pellom MS, Hamm DP, Everson CT, Wechsler AS. Dynamic right ventricular dimension.
J Thorac. Cardiovasc. Surg. 91:879-887, 1986

78. Arakawa M, Tanaka T, Hirakawa S: Pressure-volume relation of the left atrium in man. In Cardiac mechanics and function in the normal and diseased heart. eds. Hori M, Suga H, Baan J, and Yellin EL; Springer-Verlag Publishers 1989;150-154

79. Olsen CO, Rankin SJ, Arentzen CE, Ring WS, McHale PA and Anderson: The deformation characteristics of the left ventricle in the conscious dog. 1981;49:843-855, 1981

80. Boltwood CM, Skulsky A, Drinkwater DC, Lang S, Mulder DG, Shah PM: Intraoperative measurement of pericardial constraint : role in ventricular diastolic mechanics. J Am Coll Cardiol 1986;8:1289-1297

81. Mangano DT: The effect of the pericardium on ventricular systolic function in man. Circulation 1980;61:352-357

82. Mangano DT, Van Dyke DC, Ellis RJ: The effect of increasing preload on ventricular output and ejection in man. Limitations of the Frank-Starling mechanism. Circulation 1980;62:535-541

83. Mangano DT, Van Dyke DC, Hickey RF, Ellis RJ: Significance of the pericardium in human subjects: effects on left ventricular volume, pressure and ejection. J Am Coll Cardiol 1985;6:290-295

84. Bergel D.H: Measurement of blood pressure. Cardiovas Physiol 1983;P302:1-18

85. Falsetti HL, Mates RE, Carroll RJ, Gupta L, Bell AC: Analysis and correction of pressure wave distortion in fluid-filled catheter systems. Circulation 1974;49:165-172